U.S. DEPARTMENT OF ENERGY

PNNL-22886, RPT-DVZ-AFRI-019

Prepared for the U.S. Department of Energy
under Contract DE-AC05-76RL01830

System-Scale Model of Aquifer, Vadose Zone, and River Interactions for the Hanford 300 Area – Application to Uranium Reactive Transport

ML Rockhold
DH Bacon
VL Freedman
KR Parker
SW Waichler
MD Williams

October 2013

Pacific Northwest NATIONAL LABORATORY

Proudly Operated by Battelle *Since 1965*

DISCLAIMER

PACIFIC NORTHWEST NATIONAL LABORATORY
operated by
BATTELLE
for the
UNITED STATES DEPARTMENT OF ENERGY
under Contract DE-AC05-76RL01830

Printed in the United States of America

Available to DOE and DOE contractors from the
Office of Scientific and Technical Information,
P.O. Box 62, Oak Ridge, TN 37831-0062;
ph: (865) 576-8401
fax: (865) 576-5728
email: reports@adonis.osti.gov

Available to the public from the National Technical Information Service
5301 Shawnee Rd., Alexandria, VA 22312
ph: (800) 553-NTIS (6847)
email: orders@ntis.gov <http://www.ntis.gov/about/form.aspx>
Online ordering: http://www.ntis.gov

This document was printed on recycled paper.
(8/2010)

PNNL-22886, RPT-DVZ-AFRI-019

System-Scale Model of Aquifer, Vadose Zone, and River Interactions for the Hanford 300 Area – Application to Uranium Reactive Transport

ML Rockhold
DH Bacon
VL Freedman
KR Parker
SW Waichler
MD Williams

October 2013

Prepared for
the U.S. Department of Energy
under Contract DE-AC05-76RL01830

Pacific Northwest National Laboratory
Richland, Washington 99352

Summary

This report represents a synthesis and integration of basic and applied research into a system-scale model of the Hanford 300 Area groundwater uranium plume, supported by the U.S. Department of Energy (DOE) Richland Operations Office (RL). The report integrates research findings and data from DOE Office of Science (SC), Office of Environmental Management (EM), and DOE-RL projects, and from the site remediation and closure contractor, Washington Closure Hanford, LLC. The three-dimensional, system-scale model addresses water flow and reactive transport of uranium for the coupled vadose zone, unconfined aquifer, and Columbia River shoreline of the Hanford 300 Area.

The system-scale model of the 300 Area was developed to be a decision-support tool to evaluate processes of the total system affecting the groundwater uranium plume. The model can also be used to address "what if" questions regarding different remediation endpoints, and to assist in design and evaluation of field remediation efforts. For example, the proposed cleanup plan for the Hanford 300 Area includes removal, treatment, and disposal of contaminated sediments from known waste sites, enhanced attenuation of uranium hot spots in the vadose and periodically rewetted zone, and continued monitoring of groundwater with institutional controls. Illustrative simulations of polyphosphate infiltration were performed to demonstrate the ability of the system-scale model to address these types of questions. The use of this model in conjunction with continued field monitoring is expected to provide a rigorous basis for developing operational strategies for field remediation and for defining defensible remediation endpoints.

The system-scale flow and reactive transport model of the 300 Area subsurface was implemented using the simulator eSTOMP ("e" for extreme scale), developed recently by Pacific Northwest National Laboratory (PNNL) under the laboratory-directed research and development program's Extreme-Scale Computing Initiative. This is a parallel version of the STOMP (Subsurface Transport Over Multiple Phases) simulator that was developed specifically to allow for simulation with faster run times and/or for larger-scale subsurface flow and reactive transport problems. All model simulations with eSTOMP were performed on Olympus, a high-performance computing cluster supported by PNNL's institutional computing program.

Data from laboratory and field experiments performed for the Integrated Field Research Challenge (IFRC) project, supported by DOE-SC, and from other DOE-EM and DOE-RL projects, were used for model development and testing. A column experiment performed on an intact, uranium-contaminated core sample collected from the IFRC site was used as a small-scale validation test for a uranium surface complexation reaction network implemented with eSTOMP. Experimental data from this and other laboratory column experiments with 300 Area sediments were used to develop an alternative reaction network that also accounts for reactions associated with polyphosphate amendments. Experimental data from a field tracer and uranium desorption experiment performed in spring 2011 at the IFRC site, and water level data and chloride data from the 300 Area well monitoring network were used for calibration of the field-scale flow and tracer transport model.

Acknowledgments

This document was prepared by the Deep Vadose Zone- Applied Field Research Initiative at Pacific Northwest National Laboratory. Funding for this work was provided by the U.S. Department of Energy Richland Operations Office. The Pacific Northwest National Laboratory is operated by Battelle Memorial Institute for the Department of Energy (DOE) under Contract DE-AC05-76RL01830. The project benefitted from collaboration with and results produced by many others on several earlier projects. All people noted below are at PNNL unless indicated otherwise.

Field and laboratory characterization data and experimental results from the DOE Office of Science Hanford 300 Area Integrated Field Research Challenge (IFRC) project—John Zachara, Principal Investigator—were used for model testing and calibration. Vince Vermeul, Rob Mackley, Darrell Newcomer, and Brad Fritz were key contributors to the field aquifer characterization and tracer transport experiments that were performed at the IFRC site. Tom Wietsma and Mart Oostrom performed laboratory uranium mass transfer experiments used for testing surface complexation models and multistep outflow experiments that were used for estimating vadose zone hydraulic properties with columns of intact sediments from the IFRC site. Tom Resch performed analytical measurements of uranium and major ion chemistry for aqueous samples collected from both lab and field experiments on the IFRC project.

JoAnne Rieger (CH2M HILL Plateau Remediation Company) and Bob Peterson provided 300 Area sediment uranium and major ion aqueous chemistry data, respectively, from the Hanford Environmental Information System database. Chris Murray provided sediment uranium data from the IFRC site. Bill Perkins provided simulation results from the computational fluid dynamics model MASS1for Columbia River stage along the 300 Area. Jake Horner updated the EarthVision model of the 300 Area, which was originally produced by Paul Thorne, and also provided revised elevations of hydrogeologic unit contacts. Buddy Bentz (Washington Closure Hanford) provided civil survey results for ground surface elevations of liquid effluent and solid waste disposal sites in the 300 Area after excavation and prior to backfilling and re-vegetation of these sites. Jeff Serne provided data quality reviews and insightful comments on several portions of the document. Mark Freshley provided additional review comments.

Yilin Fang, Bruce Palmer, and Steve Yabusaki are acknowledged for the initial development of eSTOMP, a parallel version of the STOMP simulator. That work was supported by PNNL's laboratory-directed research and development program's Extreme Scale Computing Initiative. Yilin also implemented the multi-rate surface-complexation models in STOMP and eSTOMP and provided crucial debugging support. Kurt Glaesemann and Tim Carlson provided assistance with the Olympus computing cluster, supported by PNNL's institutional computing initiative. The availability of eSTOMP and Olympus were both critical to the successful completion of this project.

Finally, we thank Dawn Wellman for project management and oversight, and for sharing data and insights related to polyphosphate reactions and autunite formation in Hanford sediments. Previous work on polyphosphate was funded by DOE Environmental Management through the Columbia River Projects and by DOE Richland Operations.

Acronyms and Abbreviations

B.G.	burial ground
CHPRC	CH2M HILL Plateau Remediation Company
DOE	U.S. Department of Energy
EBF	electromagnetic borehole flow-meter
EM	Office of Environmental Management
EMSL	Environmental Molecular Sciences Laboratory
ERT	electrical resistivity tomography
HEIS	Hanford Environmental Information System
ICE-1	Intact Core Experiment 1
IFRC	Integrated Field Research Challenge
MAE	mean absolute error
MASS1	Modular Aquatic Simulation System 1D
MCL	maximum concentration limit
NQA-1	Nuclear Quality Assurance Level 1
PNNL	Pacific Northwest National Laboratory
PUF	pressurized unsaturated flow
PV	pore volumes
RL	Richland Operations Office
SA	surface area
SC	Office of Science
SFTEL	Subsurface Flow and Transport Experimental Laboratory
SpC	specific conductance
STOMP	Subsurface Transport Over Multiple Phases
USGS	U.S. Geological Survey
WCH	Washington Closure Hanford, LLC
WIDS	Waste Information Data System

Contents

Figures

Tables

1.0 Introduction

The primary purpose of this report is to describe a system-scale model of subsurface water flow and reactive species transport for the Hanford 300 Area. The system-scale model of the 300 Area was developed to be a decision-support tool that can be used to evaluate processes of the total system affecting the groundwater uranium plume. The model can also be used to address "what if" questions regarding different remediation endpoints,[1] and to assist in the design and evaluation of field remediation efforts.

The 300 Area, located in the southeast corner of the Hanford Site (Figure 1.1), has been the subject of a great deal of field characterization and scientific inquiry for more than two decades owing primarily to a persistent groundwater uranium plume (Peterson et al. 2008; Zachara et al. 2012). In addition to uranium, there are several other contaminants of concern in the 300 Area (Rockhold et al. 2012; Peterson 2005), some of which are described briefly at the end of this section. The system-scale model described herein represents a tool for integrating all available characterization and monitoring data with experimentally validated process models for contaminant transport and fate in the subsurface.

Activities performed for this project in FY13 included the following:

- Review and documentation of water level, temperature, and specific conductance data (2011 - 2012) from a network of monitoring wells, and sediment-associated uranium from previous core and grab sampling of 300 Area sediment, for quality assurance and consistency checks
- Update of the geologic framework model of the 300 Area to incorporate information from all recent well drilling activities
- Time-series analysis of well and river water level data and development of regression models to estimate water levels at selected wells from prior river stage and prior well water levels
- Development of software tools to facilitate model setup and calibration
- Independent estimation of sediment-associated contaminant uranium for use in field-scale modeling
- Calibration of the system-scale model of the 300 Area for water flow and tracer transport in the unconfined aquifer
- Implementation and testing of reaction networks for multi-rate uranium surface complexation and uranium-polyphosphate associated reactions
- Illustrative simulations of the reactive transport of uranium for a hypothetical remediation scenario involving infiltration of a polyphosphate solution over a hot spot near the southwest corner of the former South Process Pond
- Benchmark and quality assurance testing of eSTOMP

The report is organized as follows. Section 1 briefly summarizes the history of the uranium contamination problem for which the system-scale model was principally developed. This is followed by

[1] Lee, MH, MJ Truex, MD Freshley, DM Wellman, D Katzman, VV Vesselinov, ME Denham, A Bunn, C Eddy-Dilek, JG Morse, KM Thompson, EM Pierce, GH Chamberlain, and K Gerdes. 2013. Systems-Based Framework for Remediation Endpoints: U.S. Department of Energy, Soil and Groundwater Remediation Program, Draft, U.S. Department of Energy, Office of Environmental Management, Washington, DC.

maps showing the evolution of the uranium plume over time to illustrate plume persistence. A summary of remedial actions performed to date is then presented, followed by a brief review of previous modeling studies. Finally, other contaminants of concern are briefly discussed. Some of the information in Section 1 is from previous reports (Peterson et al. 2008; Zachara et al. 2012; Rockhold et al. 2012) but is reviewed here for completeness. Section 2 provides details on model development and inverse parameter estimation. Section 3 presents initial results from field-scale reactive transport simulations. Section 4 presents conclusions and recommendations. The appendices provide additional details on 300 Area hydrogeology and geochemistry, the 300 Area well monitoring network, and statistical models of water level responses in selected wells.

1.1 Summary of Waste Disposal Facility Operations

The 300 Area uranium plume is a result of past disposal practices in which liquid wastes from reactor fuel fabrication processes were disposed directly to unlined ponds and trenches located immediately adjacent to the Columbia River. The history of operations and chemistry of the waste streams are variable and complex, and not precisely known (Zachara et al. 2005; Zachara et al. 2007). Figure 1.2 shows a historical photograph of the ponds in operation. An estimated 47,306 kg of uranium was disposed of in the 300 Area (Peterson et al. 2008, Table 6.4; Simpson et al. 2006), primarily through three facilities: the South Process Pond (site 316-1), the North Process Pond (site 316-2), and the 300 Area Process Trenches (site 316-5). The named disposal ponds, trenches, and solid waste burial grounds (B.G.) in the 300 Area are shown in subsequent figures (Figure 1.3 through Figure 1.5).

Table 1.1 lists the operating periods for the key liquid waste disposal facilities in the 300 Area. Discharges of liquid effluent containing uranium started in the South Process Pond as early as 1943 and ended with the North Process Trenches in 1985. The North Process Pond and 307 Process Trenches operated in between these times. The North Process Trenches continued to receive non-hazardous liquid effluent through December 1994. In addition, uranium-contaminated materials and equipment were also disposed of in various solid waste burial grounds around the 300 Area (see Figure 1.3 through Figure 1.5).

1.2 Groundwater Monitoring

The maximum concentration limit (MCL) promulgated under Federal National Primary Drinking Water Regulations (40 CFR 141.66) for uranium in groundwater is 30 μg/L. Figure 1.3 through Figure 1.5 show the evolution of the 300 Area uranium plume from 1997-2012, with all contours shown being at or above the MCL. Sampled aqueous concentrations vary during the year, depending on whether a well is sampled during high or low water table conditions. Peterson et al. (2008) and Zachara et al. (2012) estimated the plume area, volume, and mass of uranium contained in the aqueous phase over time (Table 1.2). Variations in plume characteristics over time reflect year to year variations in peak water levels resulting from snowmelt in the Cascade Mountains and subsequent runoff, and perturbations from remediation activities.

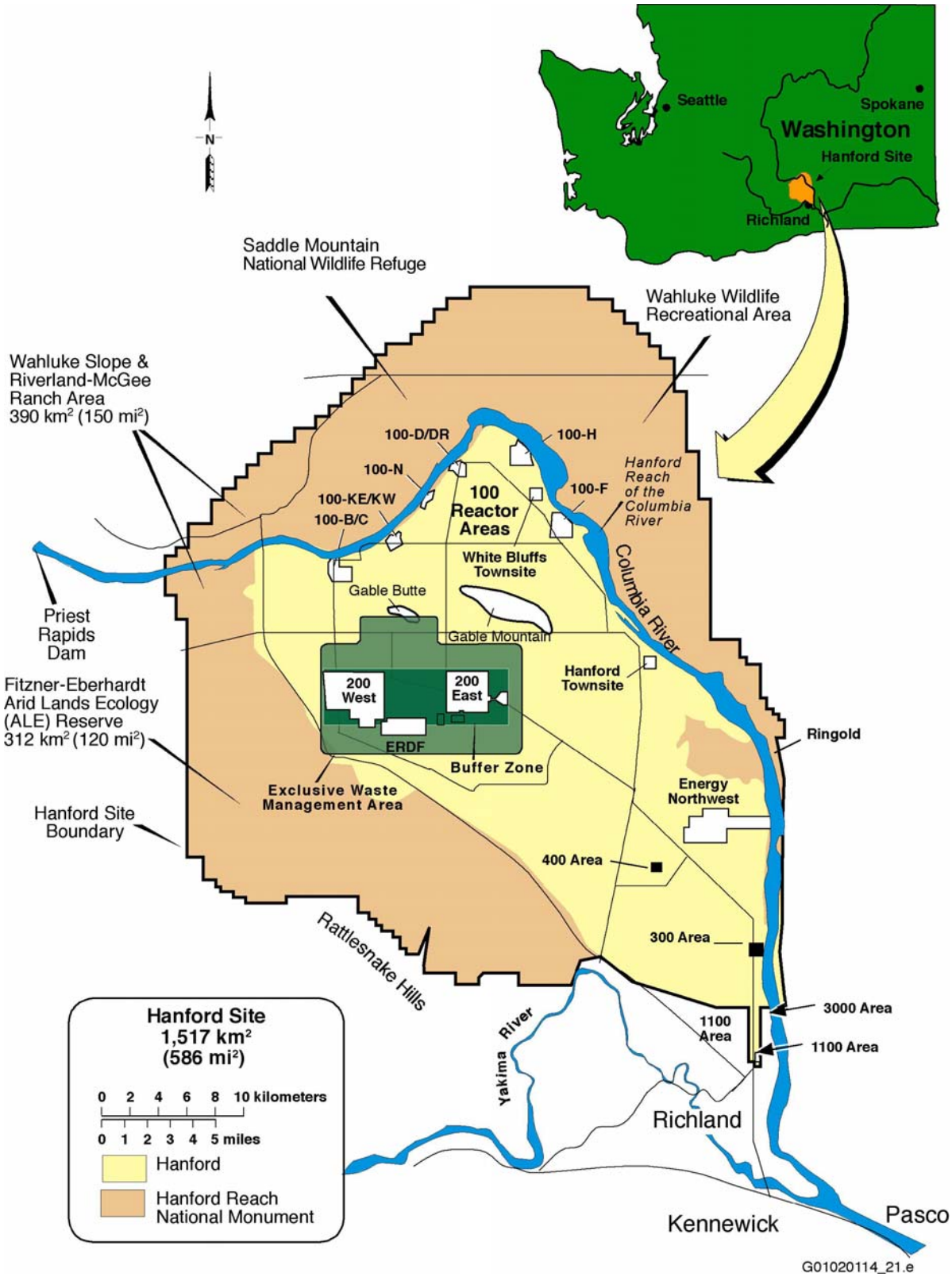

Figure 1.1. Map showing the location of the 300 Area in the southeast corner of the Hanford Site.

Figure 1.2. Early historical photo (date unknown) of the 300 Area showing the former North and South Process Ponds during operation or during high river stage.

The 300 Area uranium plume metrics reported in Table 1.2 are plotted in Figure 1.6. The linear regression line for uranium mass indicates that the calculated mass of uranium in groundwater has not changed appreciably over the past 15 years. Note that the calculations in Table 1.2 do not consider a new addition to the plume that resulted from mobilization of uranium during remediation of the 618-7 burial ground in 2008 (see Figure 1.4 and Figure 1.5).

Table 1.1. Operating periods for key liquid waste disposal facilities (after Peterson et al. 2008).

Disposal Facility	WIDS[a] Code	Period of Use for Effluent	Comments
South Process Pond	316-1	1943 to 1975	Estimates for uranium disposed to South and North Process Ponds range from 34,000 kg[b] to 45,500 kg.[c] Removal of contaminated soil was completed in 2000; excavation backfilled in 2004.
North Process Pond	316-2	1948 to 1974	Removal of contaminated soil completed in 1999; excavation backfilled in 2004.
307 Process Trenches	316-3	1953 to 1963	Taken out of service in 1965[b]; backfilled; buildings and pavement constructed over footprint; remedial action not yet undertaken.
300 Area Process Trenches	316-5	1975 to 1985; 1985 to 1994	Received non-hazardous liquid effluent after 1985 through December 1994. Expedited Response Action in 1991 to remove contaminated soil.
Treated Effluent Disposal Facility		1994 to present	Receives 300 Area effluents via the process sewer system.

(a) Waste Information Data System
(b) Young and Fruchter (1991)
(c) Simpson et al. (2006)
Source: *300-FF-1 Operable Unit Remedial Action Report* (DOE-RL 2005)

1.3 Remediation Actions

1.3.1 Excavation

Table 1.3 provides a summary of the remedial actions at the major liquid-waste disposal sites. Washington Closure Hanford, LLC (WCH) is responsible for decommissioning of former waste disposal sites and buildings in the 300 Area. The liquid effluent disposal sites listed in Table 1.3 and most of the solid waste burial grounds have been excavated. The excavated, contaminated material was sent to the Environmental Remediation Disposal Facility (ERDF), located on the Hanford Central Plateau (Figure 1.1). All excavated waste sites were then backfilled to grade with "clean" sediments and re-vegetated with native plants. Most of the planned 300 Area building decommissioning and demolition activities are now complete, with the exception of the 324 Building (Rockhold et al. 2012).

Civil survey elevation data for the excavated waste sites, prior to backfilling, were obtained from WCH. Figure 1.7 shows the calculated depths of excavation. Note that there are some artifacts shown in Figure 1.7 from interpolation in areas between the excavated sites. These interpolation artifacts have no impact on the model results that will be described later, since grid blocks for these areas, which should have had no contamination, were reset to background uranium concentrations.

Table 1.2. Calculated 300 Area groundwater uranium plume metrics (after Zachara et al. 2012).

Time Period Represented	>30 µg/L Portion of Plume: Area of Plume (km^2)	Volume of Water (m^3)	Mass of Uranium (kg)	>10 µg/L Portion of Plume: Area of Plume (km^2)	Volume of Water (m^3)	Mass of Uranium (kg)
June 2002	0.42	1,060,626	54.4	1.01	2,580,241	84.8
December 2002	0.43	901,216	78.0	0.86	1,794,192	95.8
June 2003	0.42	1,067,334	54.9	0.87	2,211,604	77.8
December 2003	0.32	673,342	40.7	0.87	1,808,715	63.4
June 2004	0.40	1,008,386	60.8	0.85	2,170,544	84.0
December 2004	0.40	836,520	52.3	0.95	1,979,449	75.2
June 2005	0.42	1,061,158	76.2	1.12	2,852,401	112.0
December 2005	0.41	846,596	63.0	0.96	1,988,448	85.9
June 2006 (EarthVision)	0.40 (0.41)	1,025,135 (994,158)	76.9 (71.8)	1.12 (1.11)	2,850,525 (2,835,993)	113.4 (105.2)
December 2006 (EarthVision)	0.48 (0.48)	1,003,316 (942,429)	78.8 (64.6)	0.74 (0.73)	1,536,019 (1,524,363)	89.4 (76.7)
June 2007 (EarthVision)	0.50 (0.50)	1,263,458 (1,280,611)	82.9 (77.9)	0.83 (0.84)	2,119,758 (2,206,019)	100.1 (95.6)
December 2007[a]	0.42	728,634	43.5	0.97	1,779,638	62.0
June 2008	0.54	1,202,220	57.4	1.12	2,510,294	80.0
December 2008[b]	0.43	753,077	45.8	1.00	1,831,501	66.5
June 2009	0.53	1,250,062	65.7	1.09	2,455,079	86.3
December 2009	0.50	946,647	49.8	0.93	1,740,837	66.9
June 2010	0.61	1,438,491	75.1	1.01	2,298,549	91.5
December 2010[c]						
June 2011	0.48	1,064,096	64.3	0.91	2,066,360	84.3
December 2011	0.57	1,064,833	71.7	0.92	1,715,957	84.2

(a) All estimates for post-June 2007 were derived using EarthVision and a revised spatial framework.
(b) Estimates do not include the new plume resulting from remedial action at the 618-7 Burial Ground.
(c) Incomplete data set for December 2010; partial set available for January 2011.

Assumptions for calculations prior to December 2007:

- Contaminated thickness: 9.8 m (June) and 8.0 m (December).
- Total porosity: 26%.
- Mass is estimated using mid-point concentration between map contours.

Assumptions for calculations starting in December 2007:

- Contaminated thickness uses EarthVision database, as updated by drilling in 2010.
- Estimates derived using EarthVision software at Pacific Northwest National Laboratory (PNNL) during September 2012.
- (Other assumptions remain the same as for pre-December 2007 calculations).

Source: Values for seasonal periods prior to December 2007 are from Peterson, 2008, Table 3.3.

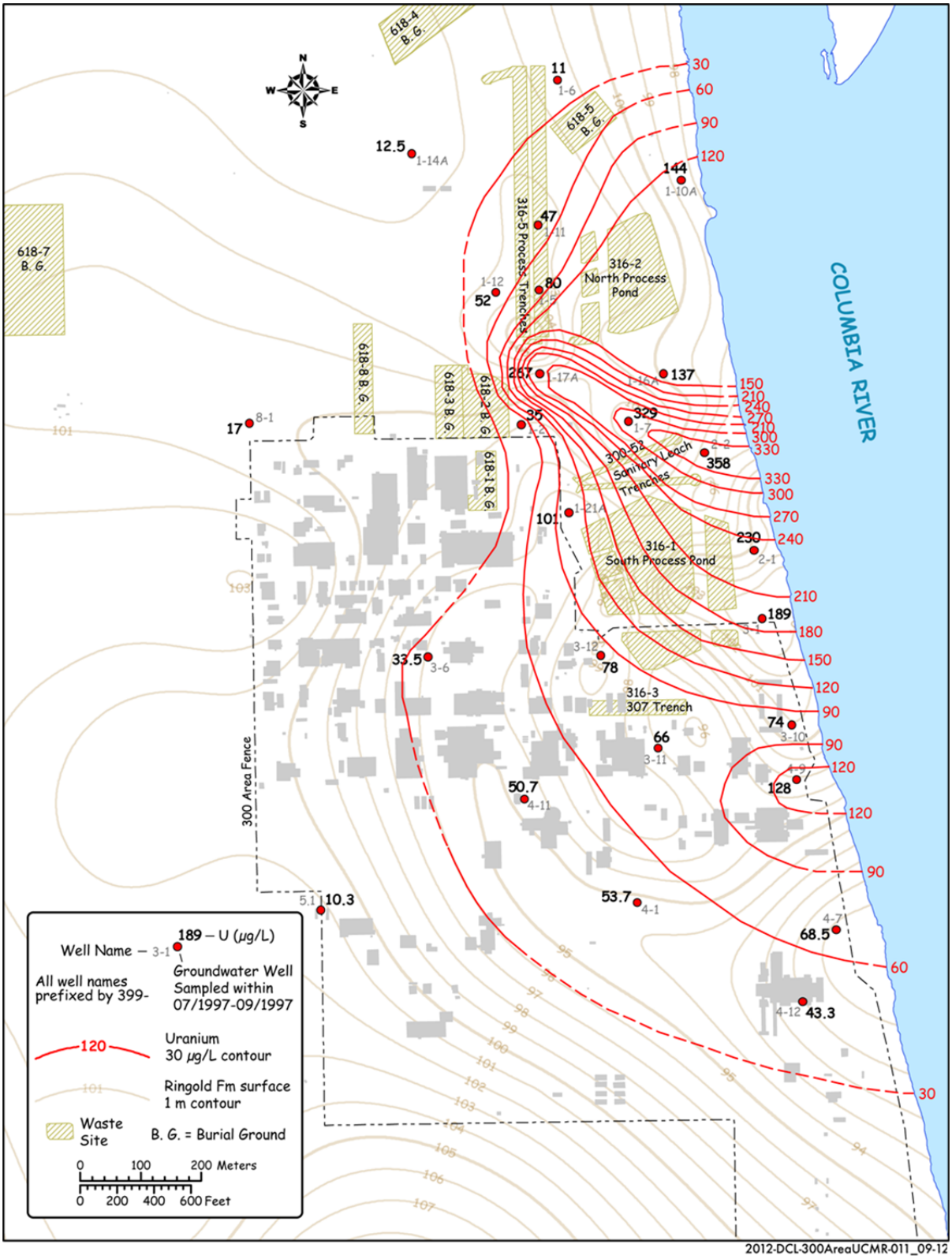

Figure 1.3. Maximum uranium concentration in groundwater during July - September 1997. (B.G. indicates burial ground.)

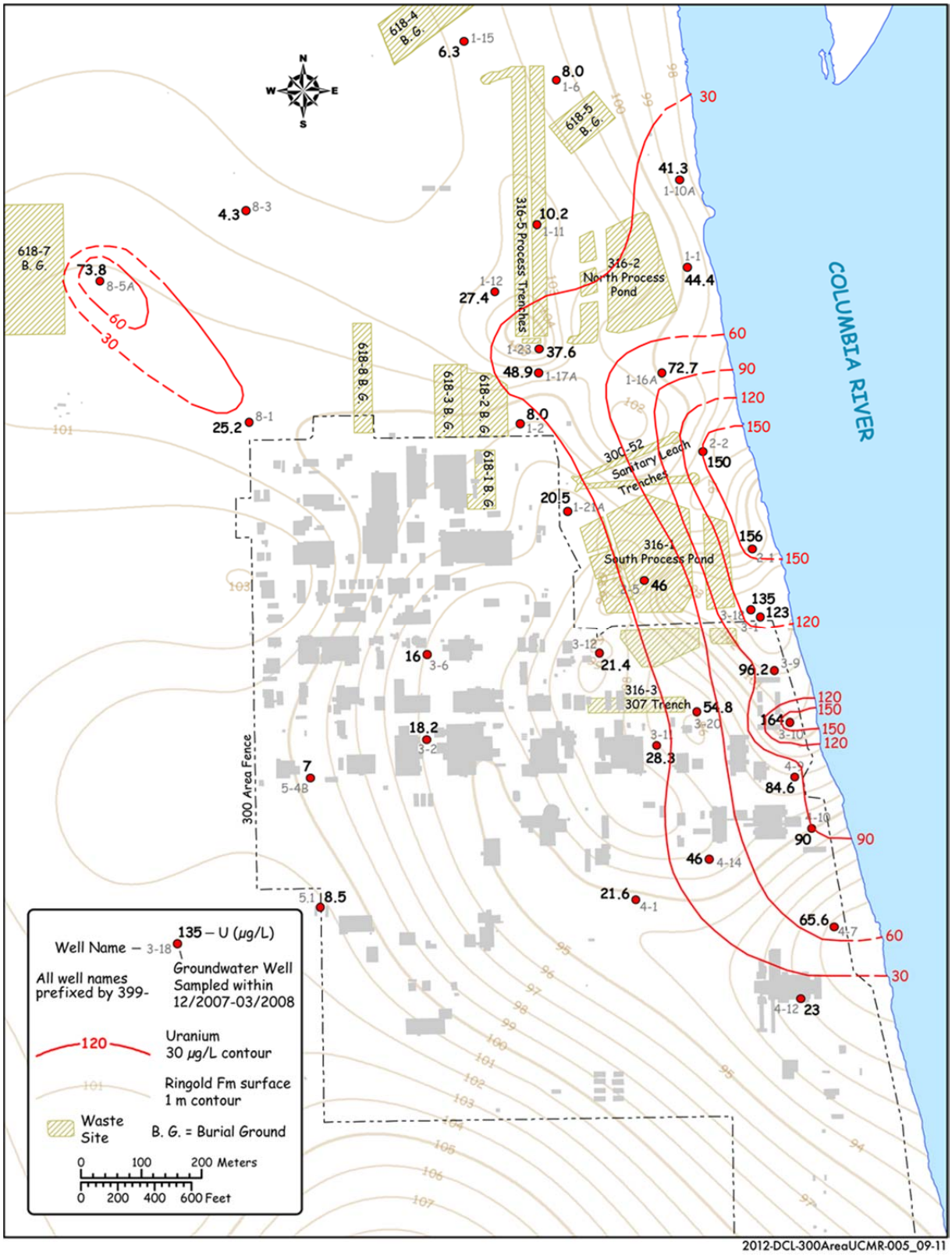

Figure 1.4. Maximum uranium concentrations in groundwater from December 2007 to March 2008.

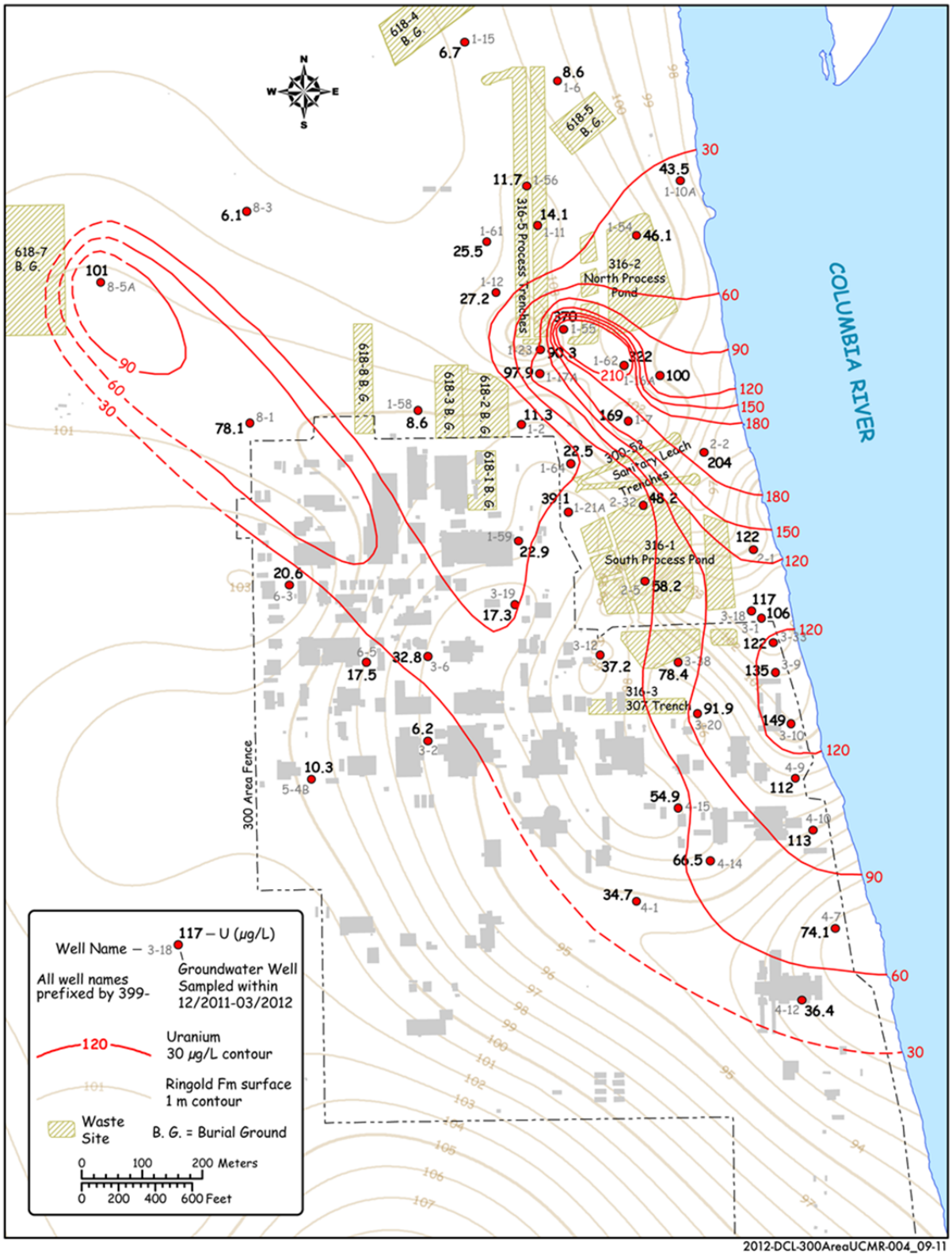

Figure 1.5. Maximum uranium concentrations in groundwater during December 2011 to March 2012.

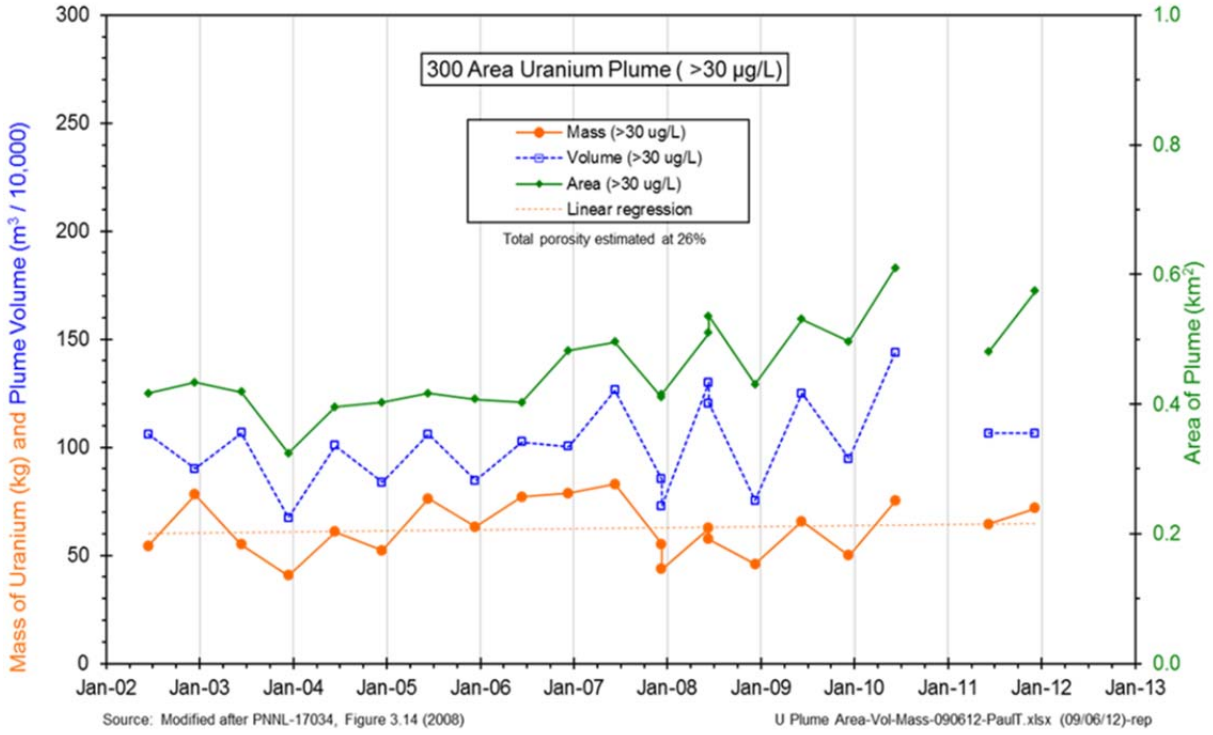

Figure 1.6. Plot showing calculated 300 Area groundwater plume metrics (after Zachara et al. 2012).

Table 1.3. Summary of remedial actions at major liquid waste disposal sites (after Peterson et al. 2008).

Disposal Facility	Excavation Dates	Backfill Date	Cleanup Verification Report	Comments
300 Area Process Trenches	1991	(Remained open)	DOE/RL-91-11 (DOE-RL 1992)	Scraped bottom of trenches and moved sediment to north end
300 Area Process Trenches	Jul 1997 to Feb 1998	2004	BHI-01164 (BHI 1998)	Additional excavation of sides and bottoms of trenches
North Process Pond	May 1998 to Jun 1999	2004	BHI-01298 (Lerch 1999)	Removed ~ 30,000 kg of uranium[(a)]
South Process Pond	Jun 1997 to Jun 2000	2004	CVP-2003-00002 (BHI 2003)	Removed ~ 40,000 kg of uranium[(b)]
307 Process Trenches	1965	1965	(Remedial action under the *Comprehensive Environmental Response, Compensation, and Liability Act* not yet undertaken)	Backfilled with scrapings from South Pond and fly ash[(c)]

(a) WIDS report for 316-2
(b) WIDS report for 316-1
(c) Young and Fruchter (1991)
Note: A comprehensive description of these remedial actions is presented in the *300-FF-1 Operable Unit Remedial Action Report* (DOE-RL 2005).

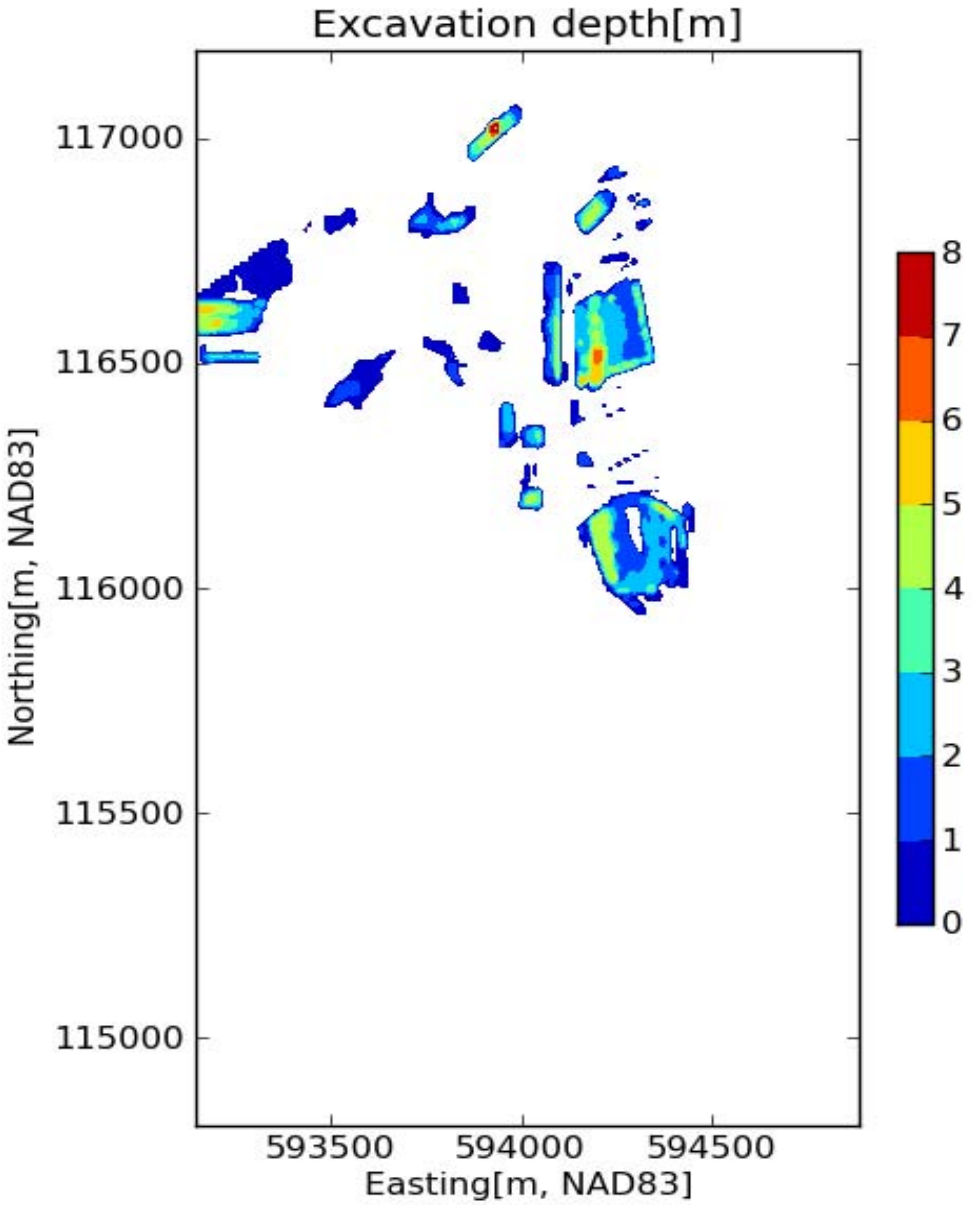

Figure 1.7. Calculated excavation depths for remediated liquid effluent disposal sites and solid waste burial grounds in the Hanford 300 Area.

Excavation and remediation of some of the former waste sites have led to additions to the groundwater uranium plume. Specifically, a new lobe developed on the west-northwest side of 300 Area uranium plume as a result of surface-applied water used for dust control during remediation activities at the 618-7 burial ground (Figure 1.4 and Figure 1.5). This resulted in the unplanned release of uranium contamination from vadose zone sediments and subsequent transport to groundwater. Soil fixatives containing $CaCl_2$ are often used with the water used for dust control (Lagos et al. 2007). Changes in

groundwater chemistry in monitoring wells downgradient of the 618-7 burial ground suggest that soil fixative may have been added to the water used for dust control at this site.

1.3.2 Polyphosphate Treatability Test

During fiscal year 2006, PNNL performed bench- and field-scale treatability testing designed to evaluate the efficacy of using polyphosphate injections to reduce uranium concentrations in the groundwater to meet drinking water standards (30 μg/L) in situ. This technology works by forming phosphate minerals (autunite and apatite) in the aquifer, which directly sequesters the existing aqueous uranium in autunite minerals and precipitates apatite minerals for sorption and long-term treatment of uranium migrating into the treatment zone, thus potentially reducing current and future aqueous uranium concentrations (Wellman et al. 2005, 2006).

Polyphosphate injection was selected for testing based on technology screening as part of the 300-FF-5 Phase III Feasibility Study for treatment of uranium in the 300 Area. The objective of the treatability test was to evaluate the efficacy of using polyphosphate injections to treat uranium-contaminated groundwater in situ. A test site consisting of an injection well and 15 monitoring wells was installed in the 300 Area near the process trenches that had previously received uranium-bearing effluents (Figure 1.8).

A complete description of the polyphosphate treatability test is provided in Vermeul et al. (2009). The stages of the test were installation of monitoring wells (the injection was installed as part of the 300 Area LFI – Well 399-1-23 [see Williams et al. 2007]), collecting baseline aqueous chemistry data at the site, hydraulic testing, conducting a bromide tracer injection test (December 2006), conducting the polyphosphate injection test, and post emplacement performance monitoring.

Numerical models of the transport of the injections at the site based on the tracer test were also developed and fit to the site data (described in Vermeul et al. 2009). One interesting result of the tracer test was the detection of bromide in down-gradient wells 399-1-32 and 399-1-7 (moving toward the southeast during the dropping river stage regime), located a significant distance from the injection site. The estimated ambient groundwater velocity based on these data was ~15 m/d (50 ft per day).

The polyphosphate injection test was performed over a 5-day period in June 2007. The injection design consisted of three separate injection phases; an initial phosphate solution injection was immediately followed by a calcium solution injection, which was immediately followed by a second phosphate solution injection. Each of the three solutions was premixed at a chemical plant and delivered to the field demonstration site in tanker trucks. Sodium bromide was included in the concentrated phosphate solutions to act as a conservative tracer during the polyphosphate injection phase (see Table 1.4 for rates, volumes, and durations). Good coverage of the solutions at the site occurred during the test based on measurements from the monitoring wells.

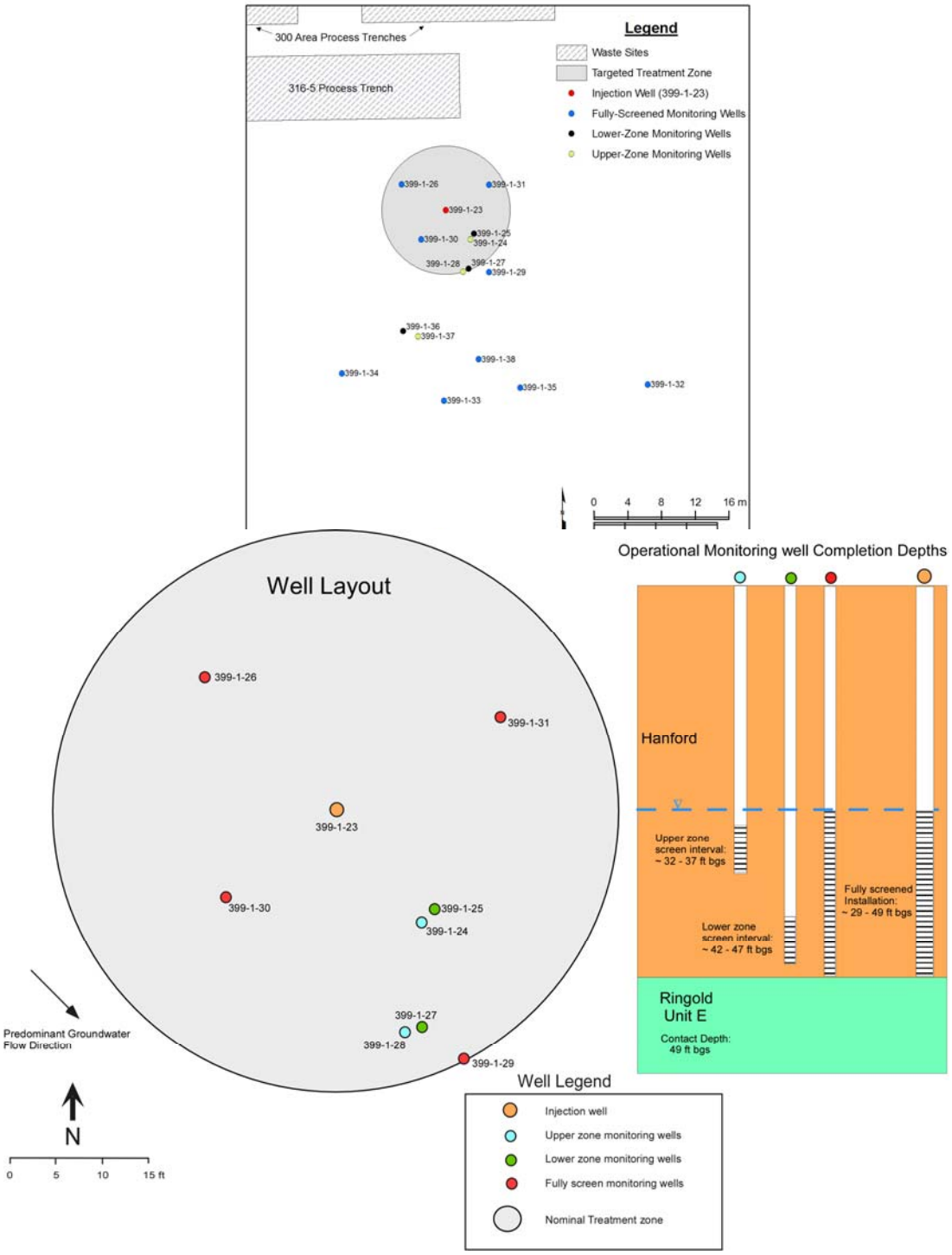

Figure 1.8. Initial well layout for polyphosphate treatability test site showing well-completion depths (from Vermeul et al. 2009). Inset figure above shows site location near 300 Area disposal sites.

Although initial post-treatment uranium concentrations decreased to below the drinking water standard of 30 µg/L, a significant rebound in uranium concentration was observed approximately 2 months after treatment. Hydrodynamic conditions in the aquifer at the site were unfavorable due to high groundwater velocities and low surface area of the coarse field sediments. Geochemical conditions at the site were also unfavorable due the effects of pH on the adsorption of uranium on apatite and the effects of uranium speciation. These and other factors that contributed to the poor performance of the treatment are discussed in detail in Wellman et al. (2008) and Vermeul et al. (2009).

Figure 1.9 shows measured concentrations of phosphate over time in the injection well (399-1-23) and in down-gradient monitoring wells. Although uranium concentrations have rebounded, phosphate concentrations at the injection well remain elevated more than 6 years after the treatability test was performed.

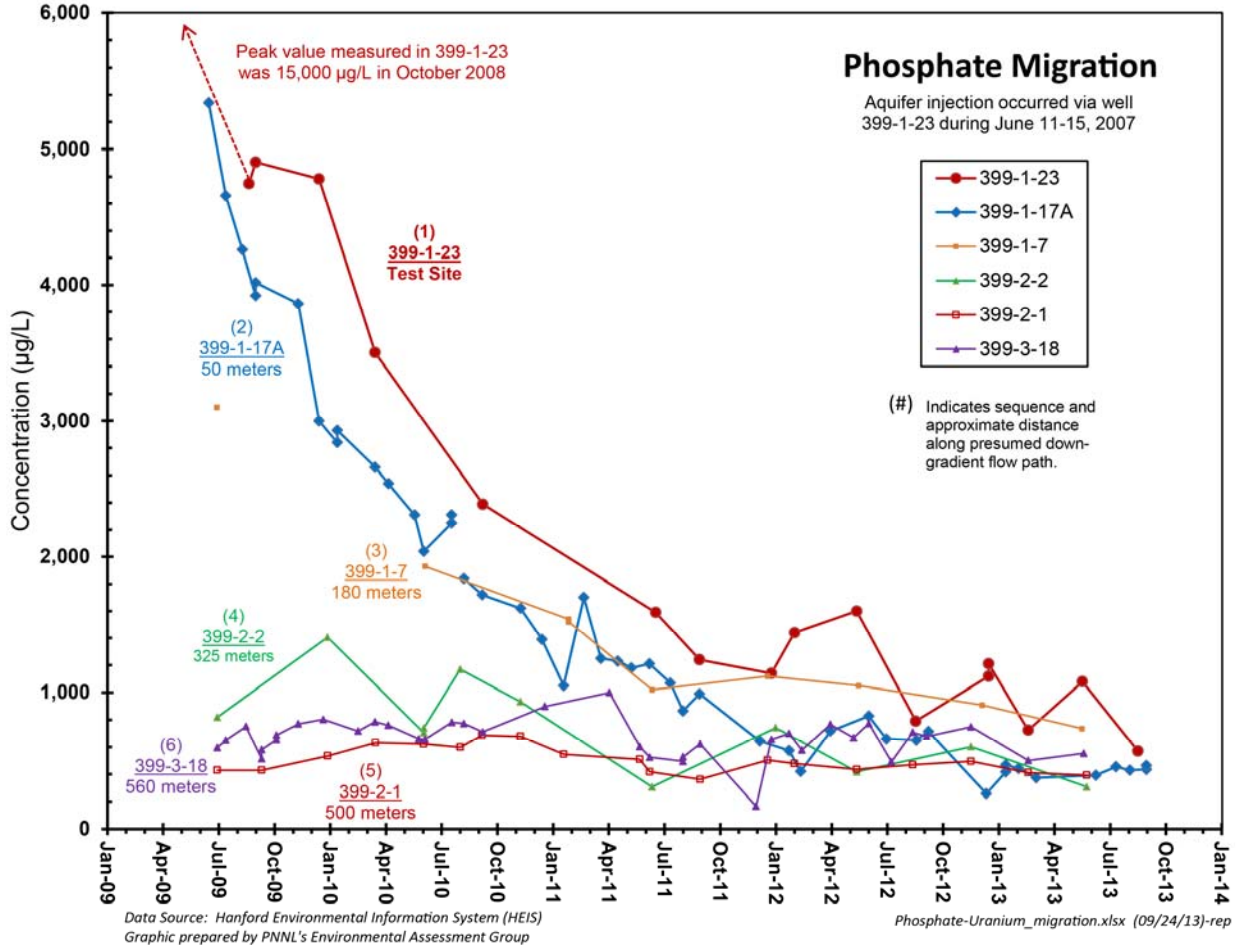

Figure 1.9. Measured phosphate concentrations in the polyphosphate treatability test well and down-gradient monitoring wells over time (modified after Fig. 4-98 from DOE/RL, 2013).

Additional laboratory studies performed since this field aquifer treatability test have indicated that the polyphosphate treatment technology may be useful for reducing (but not eliminating) the leaching rate of uranium from vadose zone sediments (Szecsody et al. 2012). This remains to be tested in the field. A preliminary reaction network for polyphosphate reactions with uranium was developed for the current study in anticipation of future field infiltration tests of this treatment technology. Results are presented later in this report.

Table 1.4. Summary of injection volumes, flow rates, and test durations for each phase of the polyphosphate treatability test

Injection	Tanker Solution Volume (gal)	Total Solution Volume (gal)	Injection Flow Rate (gal/min)	Duration (hr)
Phase 1	4,950	254,000	200	25
Phase 2	4,100	580,000	200	48
Phase 3	4,900	244,000	200	20

1.4 Previous Modeling Studies

Early modeling efforts included the use of 1D, 2D, and 3D models (Williams et al. 2008; Zachara et al. 2012). Many of the early modeling studies assumed that the source term for uranium had been completely removed by excavation of contaminated sediments from the former liquid effluent disposal sites, and they also typically used linear isotherm (a.k.a., K_d) models for uranium sorption (Lindberg and Bond 1979; DOE-RL 1994a, b; BHI 2002). Meyer et al. (2007a, b) developed a 3D model of the unconfined aquifer in the 300 Area to demonstrate a methodology for the combined evaluation of conceptual model, parameter, and scenario uncertainty. For computational efficiency, they also used a K_d sorption model, albeit with spatially variable K_d values developed using a surface complexation model (Davis and Kent 1990) with aqueous chemistry data from 300 Area groundwater. Relatively coarse spatial discretization was used for the model grid, and monthly average river stages were used for boundary conditions. The multiple conceptual models that were utilized by Meyer et al. (2007a) all assumed no residual uranium contamination on the sediments, aside from that which was in equilibrium with groundwater.

Projections from early models of flow and uranium transport for the 300 Area have tended to underestimate the time required for groundwater uranium concentrations to fall below the MCL (DOE-RL 1994a, b). Inaccuracies in these forecasts have been attributed primarily to the lack of accounting for residual contaminant uranium in the vadose zone, and to the use of the simplistic K_d models (Bethke and Brady 2000).

Recent modeling efforts have utilized more rigorous, multi-component reactive transport modeling with either equilibrium (Hammond and Lichtner 2010; Hammond et al. 2011) or multi-rate uranium surface complexation reactions (Yabusaki et al. 2008; Ma et al. 2010; Greskowiack et al. 2011) instead of the linear K_d approach. With the exception of the papers by Hammond and colleagues, all published applications of surface complexation models applied to the 300 Area to date have used 2D vertical cross section models. Although Hammond et al. (2011) used a 3D model, their domain did not include the

whole extent of the 300 Area groundwater uranium plume. Also, instead of using measured sediment-associated uranium data, they used a hypothetical mineral source of uranium in the South Process Pond to resupply the simulated groundwater plume. No efforts have been made to date to apply multi-component reactive transport models with uranium surface complexation reactions and actual field data for sediment-associated uranium to model the entire 300 Area uranium plume in 3D.

Recently, new projections were made of the time required for uranium concentrations to fall below the MCL for selected 300 Area wells (Nichols 2012). These forecasts were made using simplified models (two idealized 2D vertical cross-sections and K_d-based), but with better accounting for the remaining inventory of uranium in the subsurface than has been used in the past. These recent results suggest that for three wells (399-1-17A, 399-1-7, and 399-2-2) for which calculations were made (see Figure 1.3 through Figure 1.5 for well locations), the time required for concentrations to fall below the MCL could range from 34 years to more than 200 years for a no action alternative (depending on the assumed sorption model), and from 1 year to more than 180 years for scenarios involving removal of uranium sources and reducing infiltration rates. The continuing use of 2D vertical cross section models with K_d-based uranium sorption appears to be due in part to the reduced computational demands and fewer data requirements for these simplified models.

1.5 Recent Scientific Investigations

In spite of significant remediation efforts, and projections from earlier simplified models that the 300 Area uranium plume would have dissipated to below the MCL before now, the plume has remained largely unchanged in mass and volume over the past 15 years (Figure 1.6 and Table 1.2). This prompted the U.S. Department of Energy (DOE) Office of Science (SC) to support an Integrated Field Research Challenge (IFRC) project in the 300 Area, which ran from 2008 - 2012, to develop an improved understanding of mass transfer processes that may be responsible for long-term persistence of the uranium plume. An experimental field site was established for the IFRC project within the footprint of the former South Process Pond (Bjornstad et al. 2009). Detailed site characterization studies and laboratory and field experiments were performed for this project. Some of these data from the IFRC project were used in the current study.

The IFRC well field originally consisted of 35 wells located within a relatively small triangular array, 60 m on a side. Additional wells were added within and outside of the original IFRC well field in 2010. The original IFRC well field is about 1800 m^2 in area. The 300 Area groundwater uranium (VI) plume has an area of approximately 2.2 km^2 (Peterson et al. 2008). In spite of its small size relative to the 300 Area uranium plume, experiments performed at the IFRC site unequivocally point to a vadose zone resupply mechanism (a continuing source of uranium) as being primarily responsible for plume persistence (Zachara et al. 2012).

This resupply mechanism can be briefly summarized as follows. Residual uranium left in the vadose zone and capillary fringe region (below the depth of remedial excavations) is periodically accessed by the rising water table during high river stage. Uranium in this region is then desorbed, resulting in increased uranium concentrations in the aquifer. Interpretations of uranium mass transfer behavior are confounded by complex geochemical processes, with dilute river water favoring stronger sorption of uranium to the sediments relative to groundwater (Stoliker et al. 2011), and by wellbore flow effects (Vermeul et al. 2011).

Wellbore flow effects occur in wells that are screened over the full saturated thickness of the unconfined aquifer, resulting in different portions of the aquifer (upper or lower) being preferentially sampled, depending on whether the water table is rising or falling. When the water table is falling after a period of elevated water table conditions, concentrations measured in samples from the fully screened wells are usually higher and are more representative of residual contamination from the capillary fringe and lower vadose zone. When the water table is rising, concentrations measured in samples from the fully screened wells are more representative of the lower part of the unconfined aquifer, which tends to have much lower uranium concentrations relative to the overlying capillary fringe region and lower vadose zone. The extent to which wellbore flow influences uranium concentrations measured in a well is dependent on the degree of local stratification of the aquifer, and the time of year and water table conditions during sampling. The presence of wellbore flow effects does not negate any of the long-term aqueous uranium concentration monitoring data. Wellbore flow effects simply make the interpretation of these data more difficult.

Field experiments performed at the IFRC site have been simulated using 3D models (Murakami et al. 2010; Chen et al. 2013). These modeling efforts have focused primarily on modeling flow and tracer transport rather than uranium mass transfer. However, efforts to model observed uranium mass transfer behavior from the field experiments are ongoing.

1.6 Other Contaminants of Concern

Peterson et al. (2005) describe other contaminants of concern in the 300 Area that were known at that time based primarily on groundwater monitoring data (DOE-RL 2013b). Since then, WCH has excavated most of the known former waste disposal sites and has decommissioned and demolished most of the buildings in the 300 Area. One exception is the 324 Building, which still stands.

A highly radioactive waste stream containing ^{90}Sr and ^{137}Cs was spilled in the B-cell of the 324 Building in 1986. Prior to decommissioning of the building, WCH installed Geoprobe access tubes under the building in 2010 and measured exposure rates, water contents, and temperatures. Elevated temperatures of up to 61 ºC (142 ºF) and exposure rates of up to 8,900 R/hr were detected. This resulted in suspended deactivation of the 324 Building to evaluate the need for additional building safety systems and further site characterization.

Limited sediment characterization and subsurface flow and transport modeling were performed to assess the possible extent of contamination (Rockhold et al. 2012). Measurements and modeling suggest that the spilled contaminants are still located relatively high in the sediment profile such that there appears to be no immediate risk for contamination of groundwater. The contaminants remain in place under the B-cell, pending a decision on how best to deal with them. Although there is no immediate need for additional modeling of that spill event or subsequent contaminant transport, the 324 Building lies within the spatial extent of the system-scale model of the 300 Area described herein. Therefore, the system-scale model could potentially be used to address future issues associated with this or other contaminants in the 300 Area, as needed.

2.0 System-Scale Model of Flow and Reactive Transport

The system-scale flow and reactive transport model of the 300 Area represents an update and modification to the large-scale groundwater model of the 300 Area developed previously by Williams et al. (2008). Modifications include changes to the spatial extent of the model domain, updating of unit interfaces defining the elevations of the contact between the Hanford fm and the underlying Ringold Fm, and the addition of reaction networks for uranium surface complexation, aqueous speciation, and mineral reactions associated with the addition of polyphosphate amendments. In addition, a more realistic representation of boundary conditions along the river shoreline was developed based on output from the MASS1[1] computational fluid dynamics model of the Columbia River. Further details are provided below.

2.1 Update of Geologic Framework Model

The shape of the interface between the Hanford and Ringold units is a very important feature of the 300 Area hydrogeologic system. This interface was produced by scouring away of Ringold Fm sediments during multiple cataclysmic flood events, resulting in the formation of incised channel features (Bjornstad et al. 2009). The interface between the Hanford fm and undifferentiated Ringold Fms was defined using all available borehole and geophysical wire-line log data to define so-called unit "picks" or "tops" at each borehole location, as described previously by Williams et al. (2008). These interface elevations, which were previously contoured by hand (by Bruce Bjornstad, PNNL), were updated based on all data available as of January 2012, including 11 new remedial investigation / feasibility study (RI/FS) boreholes and approximately 39 IFRC wells. The revised unit picks were used in conjunction with added control points to allow for reproduction of hand-drawn contour maps as faithfully as possible using EarthVision. A map of the elevation of the surface of the Hanford/Ringold Fm contact is shown in Figure 2.1. The revised geologic framework model was queried to produce unit picks at selected x-y locations for use in the flow and transport model. Additional details on site hydrogeology are provided in Appendix A.

2.2 Extent of Model Domain

The extent of the modeled domain for the updated flow and transport model was changed from that used previously by Williams et al. (2008) for several reasons. First, water level data from some wells that were previously used to define boundary conditions in the earlier work, based on measurements from the early 1990s, were not available for the current time period of interest. Second, new wells have been added in the 300 Area for both site characterization and monitoring. Data from these newer wells were used to update the geologic framework model of the site and to inform initial and boundary conditions used in the current model. New model setup routines were also developed to provide more flexibility in adapting to future changes in the configuration of the well monitoring network and/or to changes in the spatial discretization of the model grid. Finally, the older model of the 300 Area only considered water flow and transport of a conservative solute while the new model also considers the reactive transport of uranium and polyphosphate reactions. Related to this, as noted previously, a new lobe developed on the west side of the 300 Area groundwater uranium plume, starting in 2008 following remediation/excavation activities at the 618-7 burial ground (see Figure 1.4 and Figure 1.5). The current model domain, shown in

[1] Modular Aquatic Simulation System 1D

Figure 2.2, was extended to the west so that the new source area around well 399-8-5A could be included within the model domain (see Figure 1.4 and Figure 1.5).

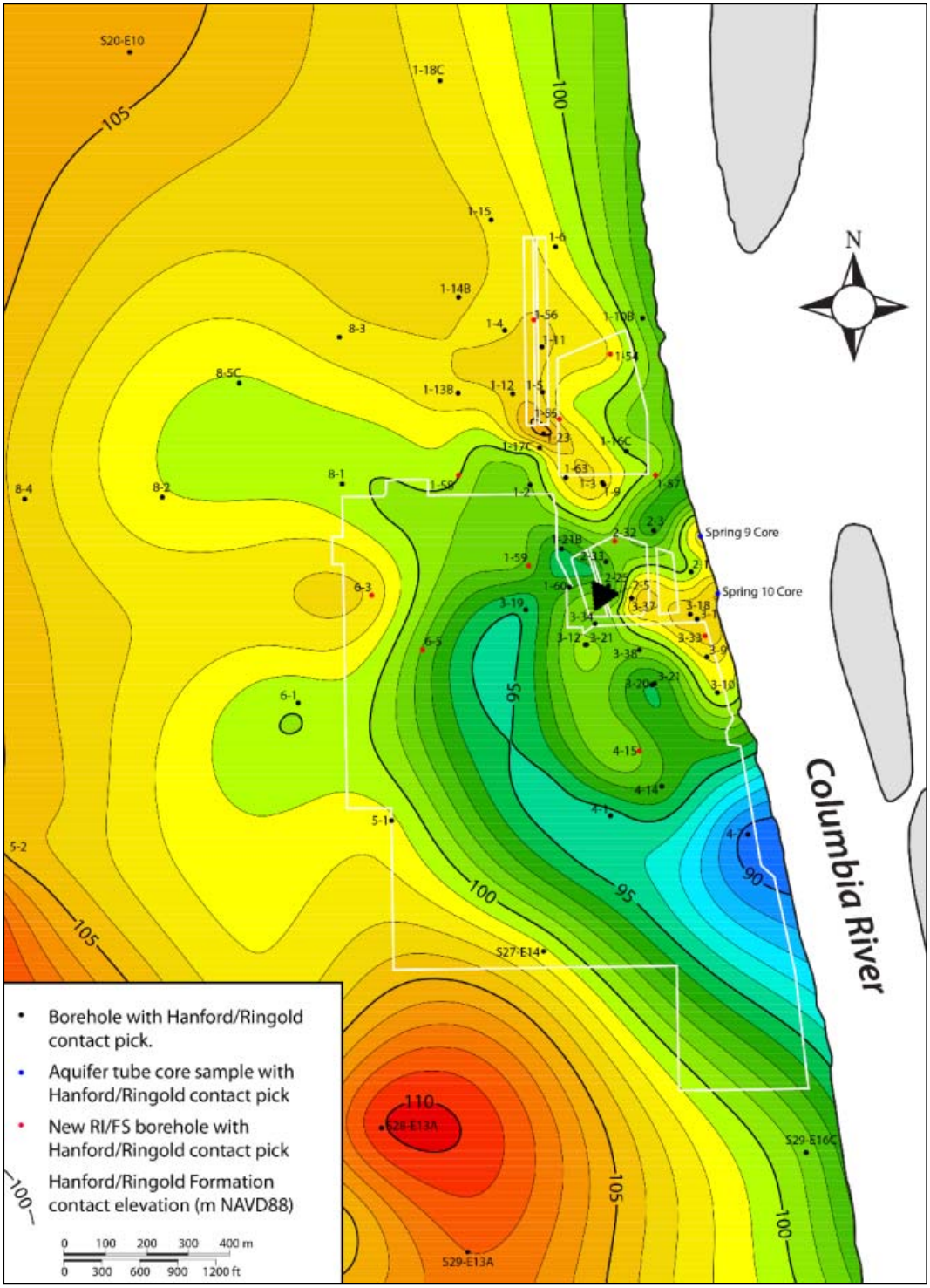

Figure 2.1. Map showing elevation of the top of the Hanford/Ringold Fm contact in the 300 Area. The IFRC site is shown as the small black triangle near the center of the figure.

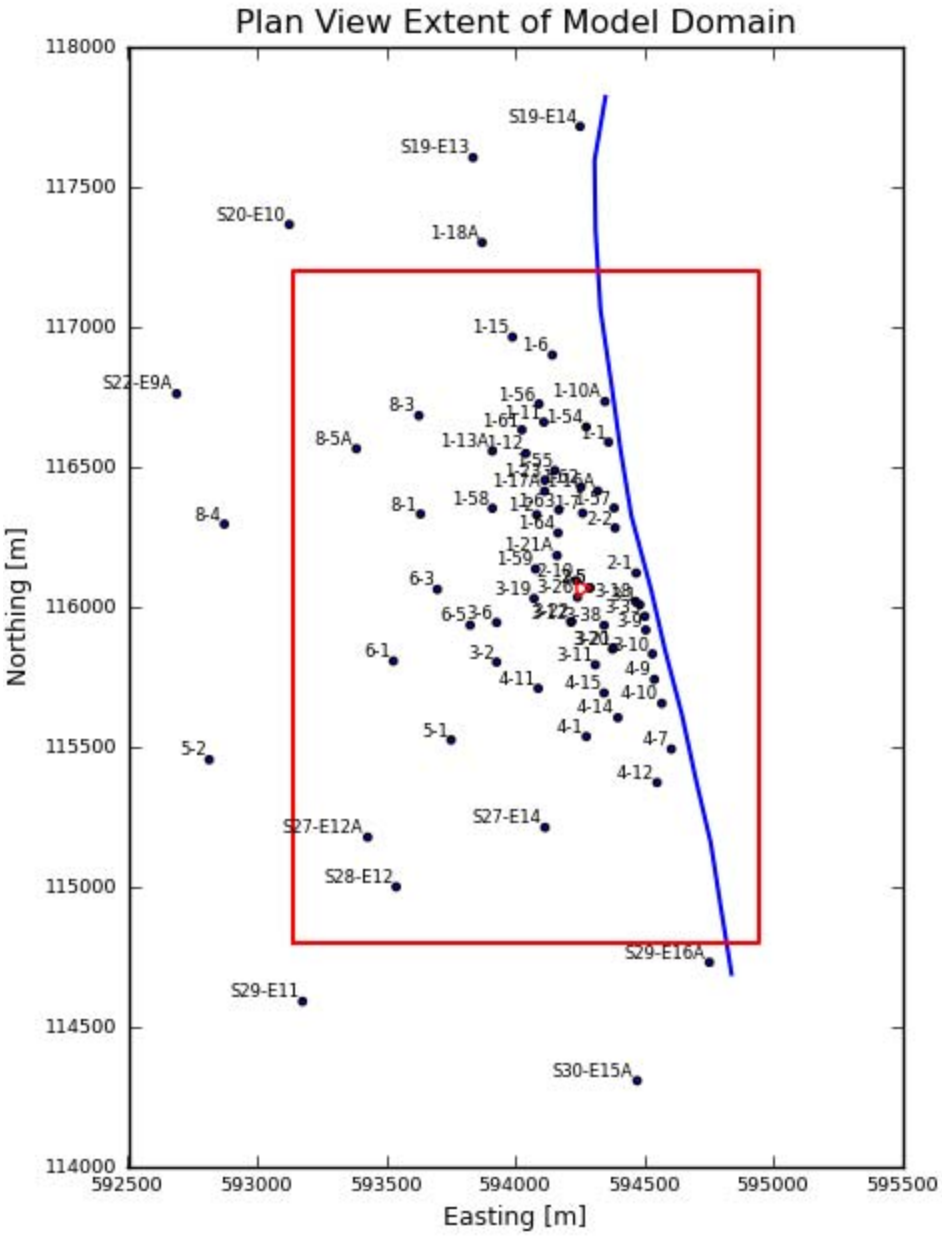

Figure 2.2. Plan view extent of model domain (red rectangle) showing locations of some monitoring wells. The blue line represents the Columbia River shoreline and the red triangle near the center of the figure represents the IFRC site.

The source area for the new portion of the groundwater uranium plume is outside of the domain of the earlier 300 Area groundwater flow and tracer transport model developed by Williams et al. (2008).

The domain of the new model spans 2400 m in the x- (N-S) direction, 1750 m in the y- (E-W) direction, and 28 m in the z- (vertical) direction. Uniform 10-m grid spacing was used the both the x- and y-directions, and uniform 1-m grid spacing was used in the vertical direction, for a total of 175, 240, and

28 grid cells in the x-, y-, and z-directions, respectively. This results in a total of 1,176,000 model grid blocks. Cells lying above the ground surface or east of the main river channel were defined as inactive.

2.3 Specification of Initial and Boundary Conditions

2.3.1 Initial Conditions

Initial pressures were first specified by assuming a uniform water level of 105.2 m and hydrostatic conditions. The flow model was then run to steady state using a constant recharge rate on the upper boundary, and fixed pressures on the boundaries interpolated from water level measurements on Jan. 1, 2011, 00:00. The resulting steady state pressure distribution was used for initial conditions in all subsequent transient model simulations.

Initial concentrations for solute and aqueous species were calculated from interpolated values of the major ions measured in groundwater. For reactive transport of uranium, the initial sorbed uranium concentrations were calculated from measured sediment-associate uranium data interpolated to the model grid. For surface complexation, the total sorbed uranium was partitioned over the sorption sites based on the surface complexation reactions and their specified conditional stability constants, as described in more detail in Appendix A. Further details on sediment-associated contaminant uranium are now discussed.

2.3.1.1 Sediment-Associated Contaminant Uranium

Sediment-associated uranium data used in this report were obtained from three primary sources: 1) the Hanford Environmental Information System (HEIS) database, 2) data from PNNL (not in HEIS) that were obtained using several different methods, and 3) measurements of labile uranium for the <2 mm size fraction for sediment samples from the IFRC site (Murray et al. 2012).

Laboratories currently contracted by CH2M HILL Plateau Remediation Company (CHPRC), which is responsible for data in HEIS, typically use the U.S. Environmental Protection Agency 3050b protocol for preparation of sediment samples for analysis of uranium by inductively coupled plasma mass spectrometry (private communication with Steve Trent, CHPRC, September 2013). This is a nitric and hydrochloric acid-based extraction technique for metals. In the field, samples are biased toward finer-grained material because the samplers typically attempt to remove pebble and larger sized material before packaging the samples for submittal to the laboratory. Additional sorting may be done by the laboratory to avoid coarser materials when forming sample aliquots. However, there is no distinct size separation (sieving) step, unless specifically requested by project personnel. Therefore, the grain size fractions used for determining the sediment-associated uranium data reported in HEIS are essentially unknown. For our purposes, we assume that all sediment-associated uranium data available in HEIS represent *total* uranium measured on the <2 mm size fraction.

Murray et al. (2012) used the bicarbonate extraction method to determined labile U on the <2 mm size fraction. The mass fraction <2 mm was also measured, so estimates of the labile U on the bulk sediment were also made by Murray et al. (2012) using the typical gravel dilution method, multiplying the labile U measured on <2 mm size fraction by the mass fraction <2 mm. This calculation implicitly assumes that the gravel fraction is inert, such that uranium does not adsorb to or desorb from particles

greater than 2 mm in diameter. This common assumption has recently been shown to be untrue (Stoliker et al. 2013; Shang et al. 2014).

Similar to the HEIS data set, other PNNL data sources (Wang et al. 2012; Williams et al. 2007) have typically reported measurements of total U, but made by several different methods. Sometimes the <2 mm size fraction has been reported and sometimes not. Therefore, for the most part, these data were assumed to represent total U measured on the <2 mm size fraction, unless reported otherwise.

The data from these three sources were pooled to produce a set of measurements for 816 sample locations that were converted to consistent units and then interpolated to the model grid used for numerical simulations. Conversions from adsorbed (a.k.a. labile) to total uranium, or vice versa, were done using the linear regression relationship shown in Appendix A, Figure A.7 based on the PNNL data. After interpolation to the model grid, the concentration values for grid blocks lying within areas that were known to have been excavated and backfilled with clean sediment (see Figure 1.7) were reset to values below the assumed background value for total soil uranium concentration (<3 μg/g). Spatial interpolation of the sediment-associated uranium data over the system-scale model grid was performed using the "linear" method in the *griddata* function of the Python-based Scipy library (http://docs.scipy.org/doc/scipy/reference/generated/scipy.interpolate.griddata.html, last referenced Aug. 22, 2013). This is a natural neighbor interpolation scheme that uses Delaunay triangulation over the convex hull of the data.

Figure 2.3 shows iso-surfaces of *total* sediment-associated uranium concentrations for the <2 mm size fraction within the domain of the 300 Area system-scale model. Total sediment uranium concentrations <3 ug/g are considered to be background, or uncontaminated (DOE-RL 2013a), so the regions within the depicted iso-surfaces can be considered as areas of contamination by process uranium. In Figure 2.3, one area located between the southern end of the former Process Trenches and the southwest corner of North Process Pond stands out as having elevated concentrations. The centroid of this "hot spot" appears to lie approximately at the coordinates: easting [m] = 594150, northing [m] = 116520, and elevation [m] = 107. This elevation is just above the average elevation of the water table in this area. Targeted remediation at this location, to reduce the mobility or mass of uranium, would likely lead to significantly faster dissipation of the 300 Area groundwater uranium plume than would occur otherwise under a no-action alternative. Preliminary results to evaluate an enhanced plume attenuation scenario involving polyphosphate infiltration over this hot spot are presented in a later section of this report.

We focus now on the total calculated mass of uranium remaining in the system. All measured sediment-associated uranium concentration data (816 sample points) were interpolated to the system-scale model grid. The interpolated results were screened to exclude locations with concentrations below 3 ug/g total uranium, which has been deemed the background concentration. The calculated results for total uranium on the <2 mm size fraction were scaled to the bulk sediment using the standard gravel dilution approach, with an assumed gravel mass fraction of 70%. Average values of particle density and porosity of 2.72 g/cm^3 and 0.23, respectively, were assumed. Table 2.1 shows the calculated results.

The total calculated mass of contaminant uranium remaining for <2 mm size fraction sediments is 319 kg. After scaling to the bulk sediment, this value is reduced to ~96 kg. This value is similar to but greater than the long-term average mass of uranium in groundwater (~60 kg) calculated from measured groundwater concentrations above the MCL (Table 1.2). Calculations suggest that ~72% of the remaining sediment-associated uranium inventory is located above an elevation of 106 m. It should be

emphasized that the calculated mass removed from grid blocks located within excavated regions is not an estimate of what was actually removed in the field. The estimated mass of sediment and associated uranium removed in the field is documented in the closure verification packages for each waste site (DOE-RL 2005).

Table 2.1. Calculated mass of sediment-associated contaminant uranium within system-scale model domain based on measured and interpolated total sediment uranium data for <2mm size fraction. Porosity and particle density of 0.23 and 2.72 g/cm^3, respectively, were assumed.

Category	Mass U, <2 mm size fraction (kg)	Mass U, scaled to bulk sediment (kg)
Total calculated mass of sediment-associated contaminant uranium in system-scale model domain	398	119
Calculated mass of uranium removed from model grid blocks located within excavated regions	79†	24
Calculated mass of uranium remaining	319	96
Calculated mass of remaining contaminant uranium located at elevations >106 m	229	69
Calculated mass of remaining contaminant uranium located at elevations ≤106 m	90	27

†This is not an estimate of what was actually excavated and removed from the field, which is documented in the closure verification packages for each waste site (DOE-RL 2005). This calculated value represents interpolated mass located in excavated regions, and is based mostly on data collected after field remediation efforts.

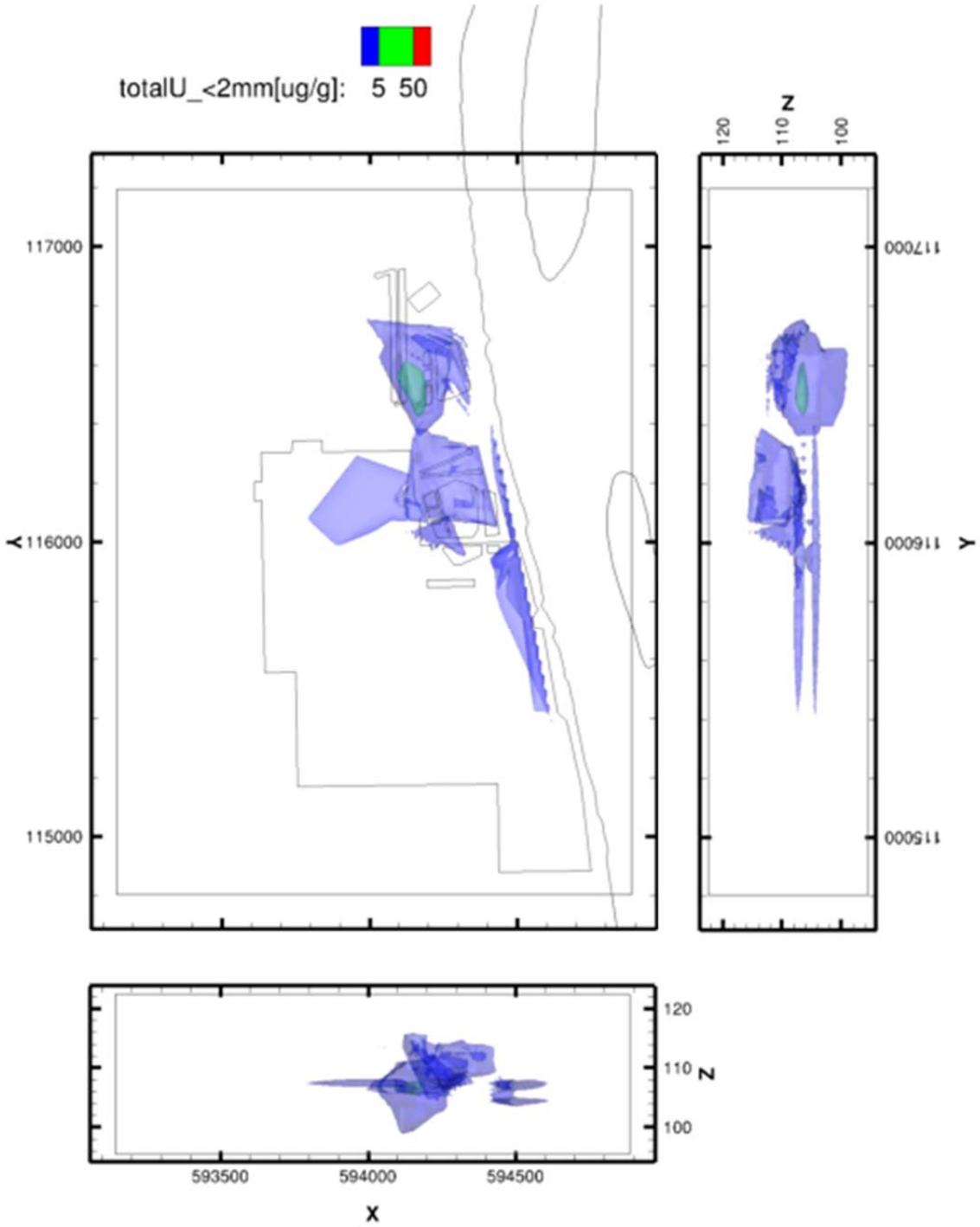

Figure 2.3. Iso-surfaces showing the distribution of total sediment-associated contaminant uranium in the subsurface of the 300 Area. This figure is based on interpolation of measured data from 816 sample locations. Total sediment uranium <3 ug/g is considered to be background, or uncontaminated, so the iso-surfaces shown represent areas where concentrations are above background.

2.3.2 Boundary Conditions

The lower boundary of the model domain was specified as a zero flux or no-flow boundary condition for water, solutes, and reactive species. The upper boundary was assigned a Neumann or constant flux condition of 0.06 m/yr for water, based on the long-term average recharge rate for a 300 Area lysimeter (Rockhold et al. 2009), and fixed concentrations corresponding to average groundwater concentrations for solute or reactive species. All lateral boundary conditions were specified as linked-list seepage face boundaries for water flow, and inflow-outflow boundaries for solutes or aqueous species. Multiple linked lists were used for each boundary. Solute or aqueous species concentrations on the lateral boundaries were specified as the average groundwater concentrations for the northern, southern, and western boundaries, and as the average river water concentrations for the eastern boundary bordering the Columbia River. Further details will be provided about river boundary specifications.

Seepage face boundaries for water flow are essentially Dirichlet-type boundary conditions corresponding to specified aqueous pressures for nodes that are saturated, and Neumann-type zero-flux boundary conditions for nodes that are unsaturated (in the vadose zone). The boundary type is updated dynamically by the code during the course of a simulation by evaluating the pressures and saturations of the nodes that have specified seepage face boundaries. A time-series of aqueous pressures, corresponding to measured water levels in wells or in the river, or interpolated values based on measurements, are specified for the first location in each linked list. Gradients are also specified and the pressures of all cell faces in each linked list are calculated internally by the code from the specified pressure for the first location, the gradient, and the Euclidean distance between the first cell face, and each subsequent cell face in the linked list.

Special considerations were required for the eastern boundary of the domain bordering the Columbia River. As described in Appendix C, river stage is measured at one location along the 300 Area, known as SWS-1. However, it is well known that there is a gradient in river stage along the Hanford Reach. A computational fluid dynamics model of the Columbia River has been developed by PNNL using the code MASS1 (Richmond and Perkins 2009). This model used LiDAR data (Coleman et al. 2010) to map the bathymetry of the river channel, and uses outflow data from the upstream Priest Rapids Dam and forebay river stage data for the downstream McNary Dam to define boundary conditions for modeling flow through the Hanford Reach.

Figure 2.4 shows cross sections through the Columbia River along the 300 Area, for which MASS1 model results were extracted. Figure 2.5 shows calculated water levels for these cross sections at different times. Based on these results, and the measured water levels from the river gauging station SWS-1, the eastern boundary of the system-scale subsurface flow and transport model for the 300 Area was divided into four linked lists of boundary cells representing the river channel and shoreline. The calculated, time-varying water levels for MASS1 locations 328, 323, 321, and 319 were used to define the base pressures for each of the four linked lists. The gradients for these four linked lists were defined by the water levels and distances between the paired locations: 328-323, 323-321, 321-319, and 319-317. Interestingly, the changes in the river elevation gradients depicted in Figure 2.5 are also evident from the riffles shown in the aerial photograph in Figure 2.4. The MASS1 results essentially show a series of “pools” and “drops” along the Hanford Reach that are characteristic of many rivers.

Figure 2.4. Aerial photograph of the 300 Area with red lines representing cross sections through the Columbia River. MASS1 model results for these cross section locations were extracted for use in developing boundary conditions for the 300 Area system-scale subsurface flow and transport model. The decimal numbers are river miles.

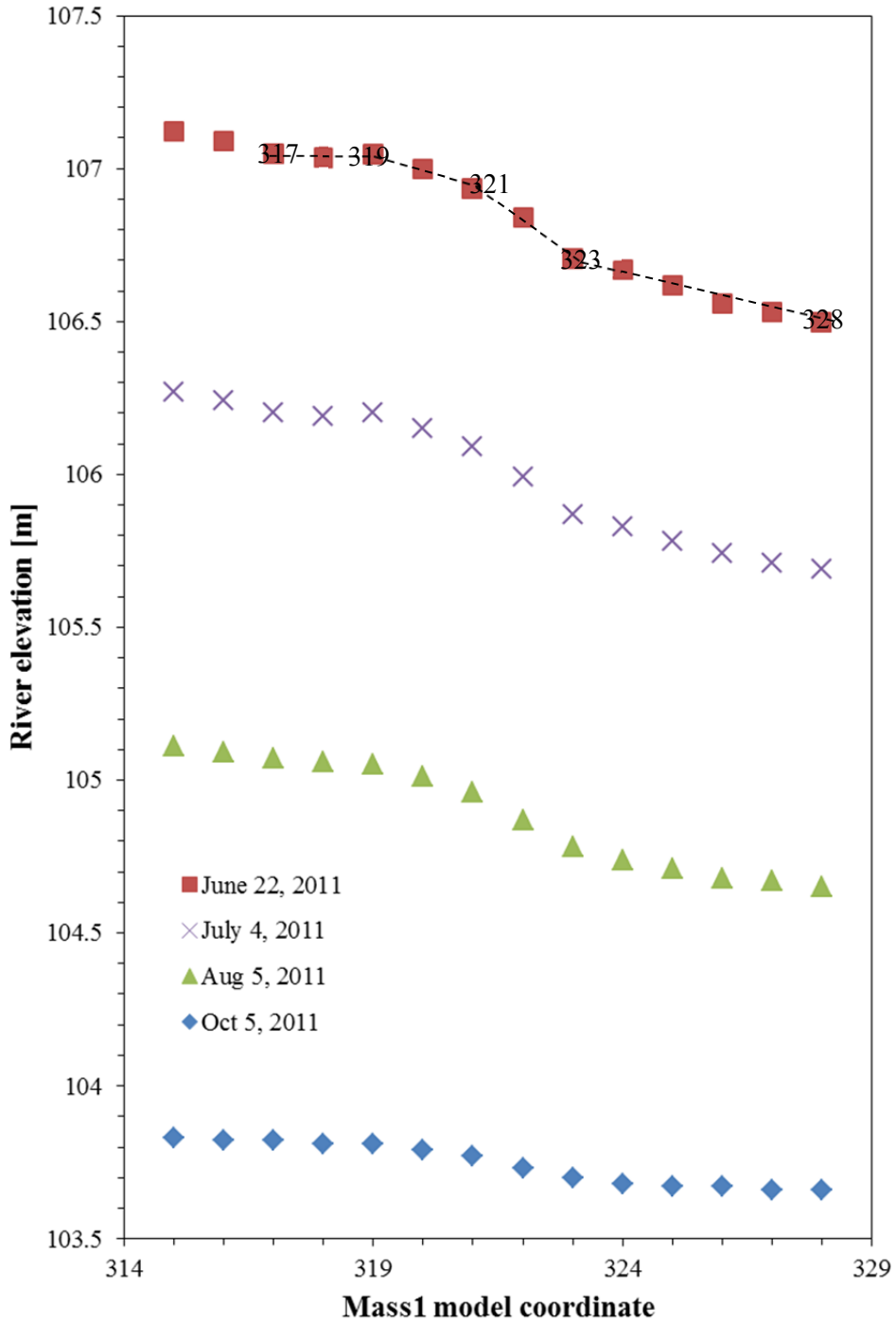

Figure 2.5. River elevation along 300 Area shoreline calculated using calibrated MASS1 model. Data from gauging station at SWS-1 (see Appendix C) and MASS1 model results were used to compute water levels and gradients used for eSTOMP model boundary conditions for four segments: 317-319; 319-321, 321-323, and 323-328.

2.4 Inverse Parameter Estimation

Williams et al. (2008) previously developed both zoned representations and multiple, geostatistically generated realizations of the hydrogeologic units and their properties underlying the 300 Area. Both approaches produce valid alternative conceptual models of the hydrogeologic system. For the zoned models, Williams et al. (2008) split the Hanford fm into lower and higher K zones, which were located in the northern and southern regions of the model domain, respectively. In addition, they included a river alluvium material along the entire length of the river corridor to account for the dampened response of wells close to the river and measurements made in the river sediments that showed these sediments to have lower K values. The zonation pattern and parameter estimates for the zones used by Williams et al. (2008) were adjusted manually to improve correspondence between simulated and observed water levels for selected 300 Area wells. The geostatistically generated realizations used gamma log data, grain-size gamma log correlation functions, and the Kozeny-Carmen equation to estimate K values. No attempt was made to calibrate the parameters for the geostatistical realizations.

For the current model, we adopted a different strategy. The subsurface domain was grouped into the two primary hydrogeologic units, the Hanford fm, with spatially variable properties, and an underlying, undifferentiated Ringold Fm, with uniform properties (instead of multiple Ringold subunits). This simplification for the Ringold Fm is motivated by the fact that the hydraulic conductivity of the Hanford fm is 2-3 orders of magnitude or more lower than any of the Ringold Fm subunits. Although there are some differences in density, porosity, and other properties for the Ringold subunits (Williams et al. 2008), the reduced hydraulic conductivity of the overall Ringold Fm relative to the Hanford fm is the dominant feature of importance to this system. The properties of the Ringold Fm were assumed to be known, while spatially variable hydraulic conductivities for the Hanford fm were estimated by inverse modeling. The porosity of the Hanford fm was assumed to be a constant value of 0.23 based on measurements on intact core samples from the IFRC site.

Spatially variable depth-averaged hydraulic conductivities for the region representing the Hanford fm were estimated using a pilot point methodology with regularization constraints using parallel PEST (Doherty and Hunt 2010). Spatial interpolation between pilot point locations and the centroids of model grid blocks was also performed using the "linear" method in the *griddata* function of the Python-based Scipy library. To reduce computational effort, a relatively small number of pilot points (20) were used, and the vertical extent of the domain was reduced by one-half, relative to the full model that extends up to ground surface. The vertical extent of the calibrated model thus ranged from 95-109 m, instead of from 95-123 m as was used for the full model. There are no observational data from the vadose zone to inform the inverse modeling, so including the upper vadose zone for inverse modeling provides no benefit and significantly increases the computational cost. Therefore, the truncated domain was used for all inverse modeling. The final parameter estimates from the inverse modeling were projected upward into the overlying domain that represents the upper vadose zone for subsequent use in infiltration and reactive transport modeling.

The pilot points were distributed as shown in Figure 2.6. A number of pilot points were located in the areas that represent the river channel in order to potentially capture the properties of river alluvium, noted previously by Williams et al. (2008). Regularization constraints were imposed via 46 prior information equations. First, a preferred state of the system was defined by specifying a depth-averaged hydraulic conductivity of 7000 m/d for the Hanford fm at a pilot point located in the center of the IFRC well field.

This is the average value of hydraulic conductivity determined from analysis of short-duration constant-rate injection tests performed at the IFRC site (see Figure 2.7). Second, the differences between the estimated value of hydraulic conductivity at any pilot point location and the values at all adjacent pilot point locations linked to it were taken to be zero. These specifications impose both a preferred value constraint on the hydraulic conductivity of the Hanford fm, based on aquifer test results, and a smoothness constraint on the overall system. A two-part objective function is minimized by PEST in which parameters are adjusted to minimize the weighted differences between simulation results and observed data, subject to a penalty for deviation of parameter values from those favored by the regularization constraints.

The observational data to which simulation results were compared consisted of selected measurements of hourly water level data in 2011 from 24 wells in the 300A monitoring network (see Appendix C), and quarterly measurements of chloride data obtained from HEIS for 21 wells. In addition, daily measurements of chloride data obtained from one well during a tracer test performed at the IFRC well field in spring 2011 were used for model calibration. Although specific conductance data are more prevalent from the network of automated sensors and data loggers in the 300 Area well monitoring network, chloride data were used here in order to capitalize on the tracer test that was performed at the IFRC site.

The spring 2011 IFRC tracer test consisted of an injection of 220,000 gal of water containing 210 mg/L Cl- into well 399-2-34, which is located near the northern apex of the IFRC well-field triangle (Figure 2.7). The injection started on March 25, 2011, 14:14, and ended on April 9, 2011, 07:15, for a total injection period of 353 hours at a rate of 10 gallons per minute. All wells in the IFRC well field were sampled daily. Measurements from one well, 399-3-28, located ~42 m down-gradient from the injection well, were used as observations for the inverse modeling.

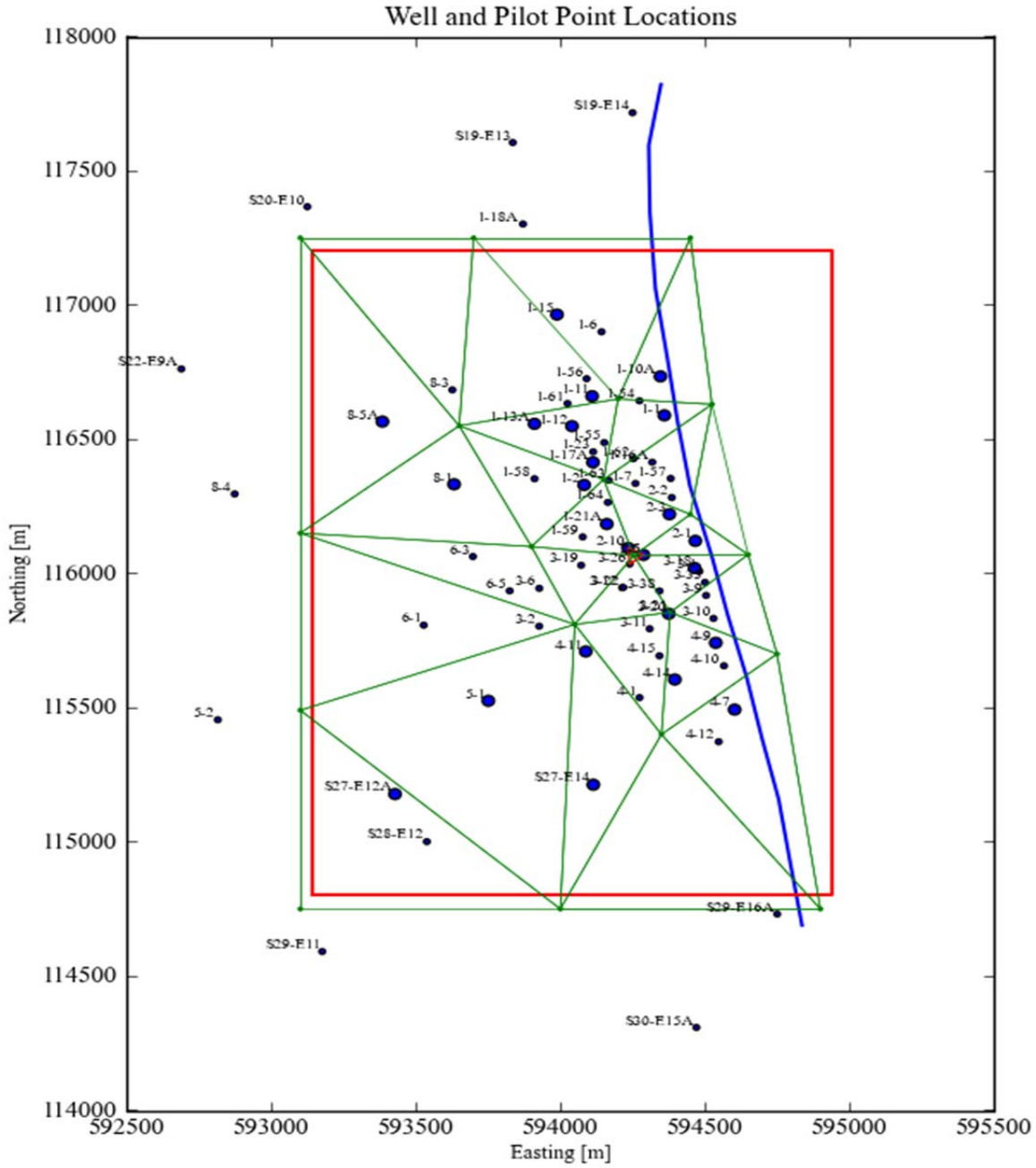

Figure 2.6. Map showing plan view of model domain and well and pilot point locations. The red rectangle is the outline of the model domain, the blue line is the river, the connected green points are pilot point locations, and the labeled points are monitoring wells. The larger blue points are wells used for water level observation data in inverse modeling. The small red triangle in the middle of the figure is the IFRC site.

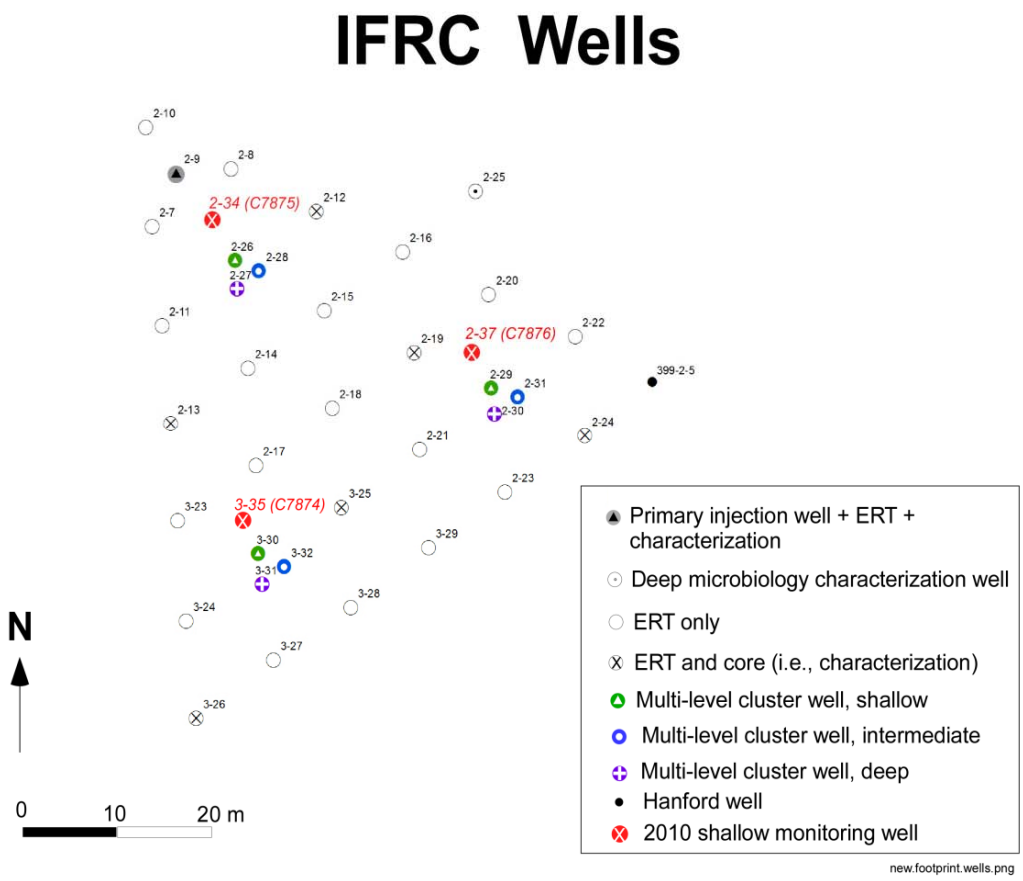

Figure 2.7. Layout of IFRC well field showing location of injection well (2-34) and monitoring well (3-28) from which chloride data were used for inverse modeling.

The weights that were applied to water level measurements were proportional to the inverse of the estimated water level observation errors. According to Hill (1998), given a measurement accuracy, a_h, so that h-a_h <= h* <= h + a_h (with h* and h being the "true" and measured water levels), the standard deviation of observation error is $\sigma_h = a_h/1.96$. This assumes that water level observation error follows a normal distribution with zero mean and 1.96 is determined from the 95% confidence interval. The weights associated with head observations can thus be estimated via

$$w_h = \frac{1}{\sigma_h} = \frac{1}{a_h / 1.96} = \frac{1.96}{a_h} \qquad h - a_h \le h^* \le h + a_h \tag{2.1}$$

Meyer et al. (2007a) considered a number of different potential error components (e.g., well altitude error, well location error, non-simulated transient error, and measurement error) and assumed that water level observation error for 300 Area wells was $a_h = 0.06$ m. This gives a uniform weight of 32.667 for each water level observation. We used the same water level observation weights. However, one key difference is that the water levels used in the current work are from automated measurements obtained with dedicated pressure transducers and data loggers for each well, whereas Meyer et al. (2007a) used

manual “e-tape” measurements reported in HEIS, which likely have larger errors. Thus, we may be overestimating water level observation errors.

Chloride data were weighted as follows. An average value for Cl- in river water of 1.212 mg/L was obtained from USGS monitoring data (Appendix A, Figure A.15). This average value was applied as a fixed concentration on the river boundary cell faces. The standard deviation of the river Cl- measurements was 0.191. The river Cl- concentrations actually vary in time, instead of being constant as applied for the linked list river boundary conditions specified in the model, so the reciprocal of the standard deviation of these time-varying river Cl- measurements (5.23) was used as the weight for each Cl- observation from the monitoring wells. It should be noted, however, that significantly more water level data than chloride data were used, so the water level data dominate the parameter estimation process.

Figure 2.8 shows observed water levels versus time and simulation results from the calibrated model for selected wells. Overall the correspondence between simulated and observed water levels for these and other wells (not shown) is considered to be good.

Figure 2.9 shows a 1:1 plot of observed and simulated water level results, and residuals (simulated – observed) over time. There appears to be a slight bias in the simulation results, with simulated water levels being slightly higher than the observed water levels. The cause for this bias is unknown at this time, but this bias is not expected to have a significant impact on other applications of the calibrated model.

Figure 2.10 shows observed and simulated chloride concentrations. As noted previously, chloride data were used instead of the more prevalent specific conductance data in order to utilize field experimental results for the IFRC site. The results shown in Figure 2.10 for well 399-3-28 indicate very good correspondence between simulated and observed results for that experiment. The spring 2011 experiment at the IFRC site also evaluated U(VI) desorption and re-adsorption. Those results for U(VI) mass transfer may be evaluated in a future modeling effort.

Figure 2.11 shows a 1:1 plot of observed and simulated chloride results and residuals (simulated-observed). Overall, the correspondence between the simulated and observed chloride transport results is considered to be good. Preliminary exploratory analysis indicates that improvements in model fit can be obtained using more pilot points placed strategically near wells showing the largest mismatches between simulated and observed data, and by using weights of unity for the water level data so that the concentration data have relatively more weight in the parameter estimation process.

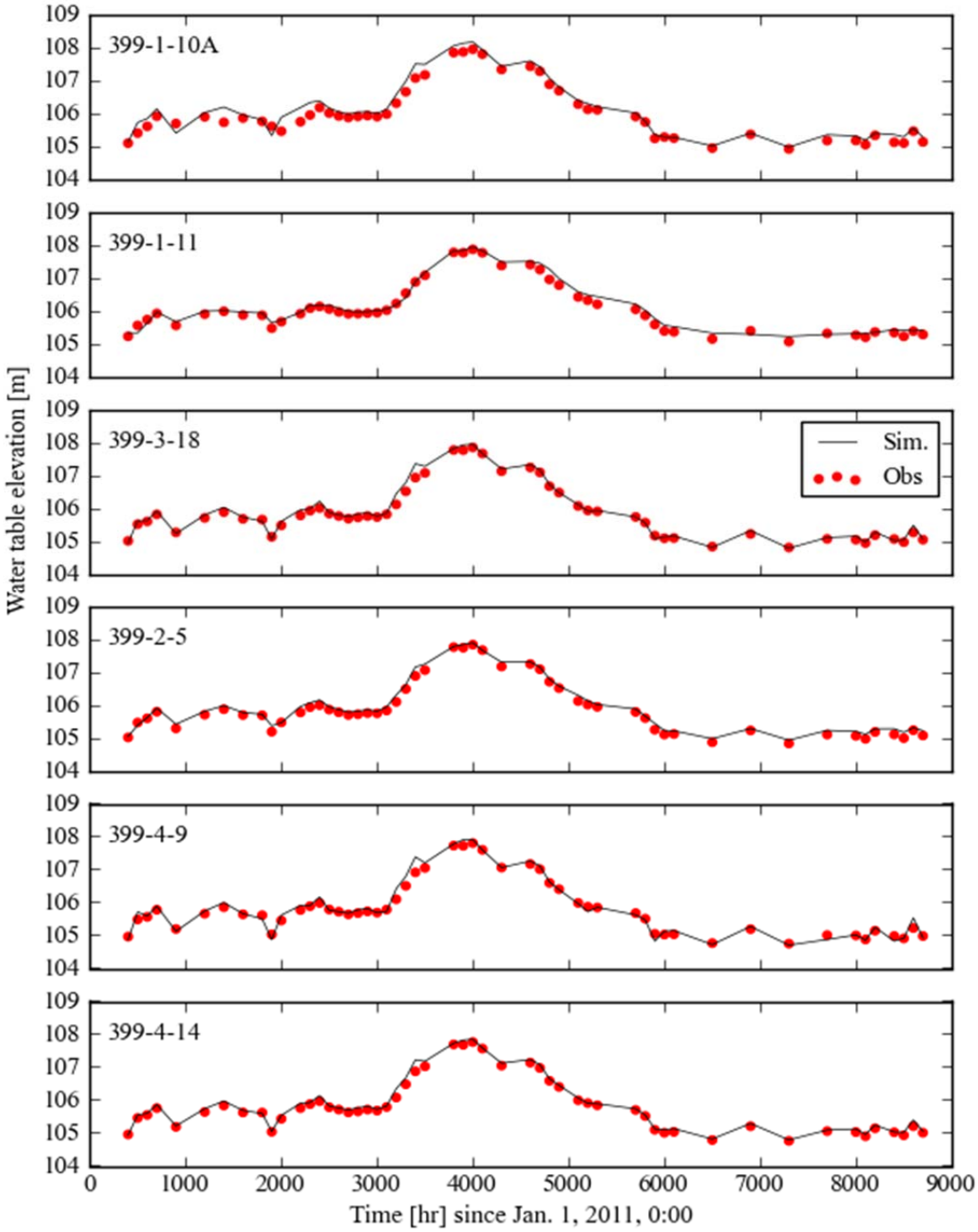

Figure 2.8. Observed and simulated water levels for selected wells after pilot point optimization.

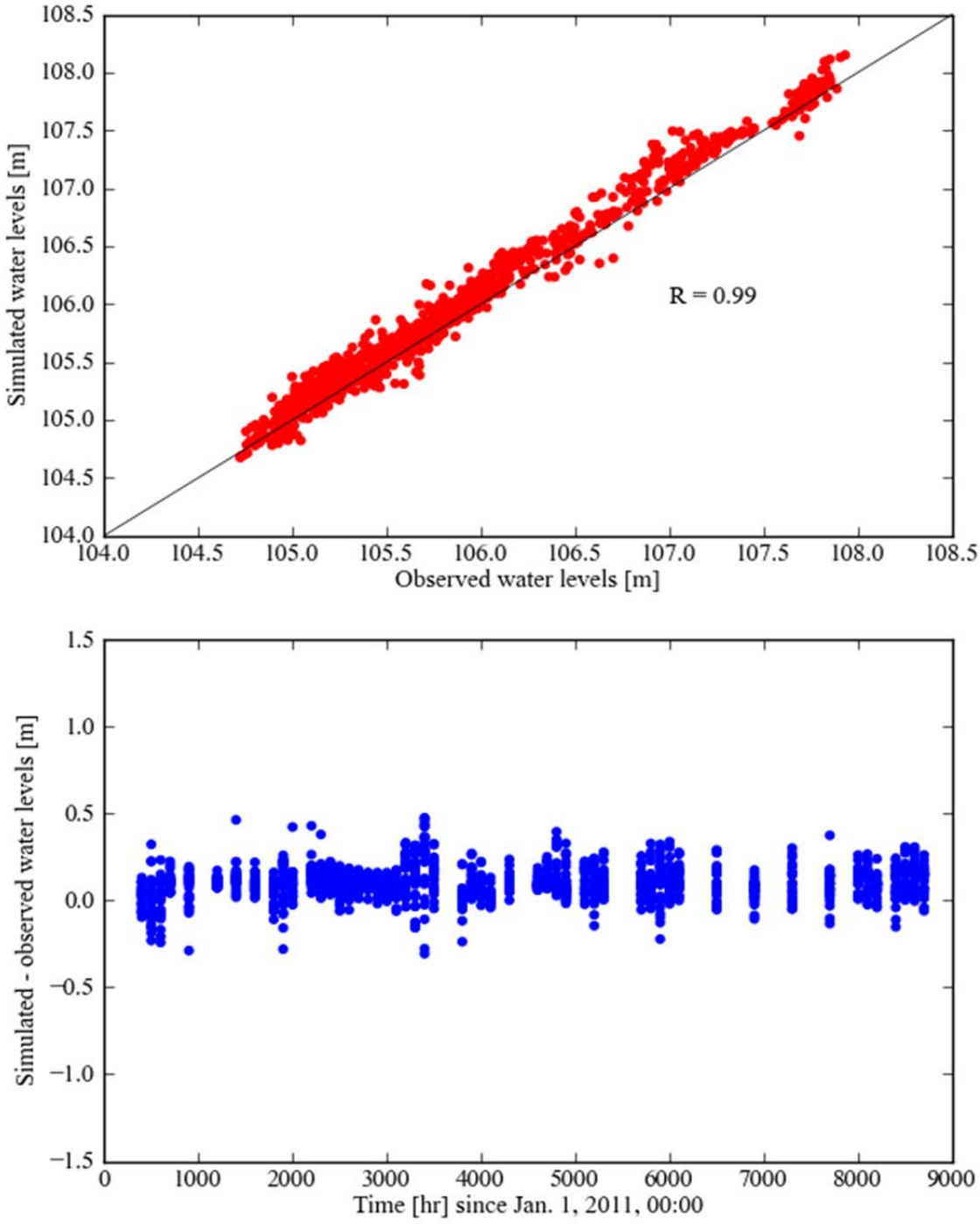

Figure 2.9. Observed versus simulated water levels and residual (simulated-observed) plots.

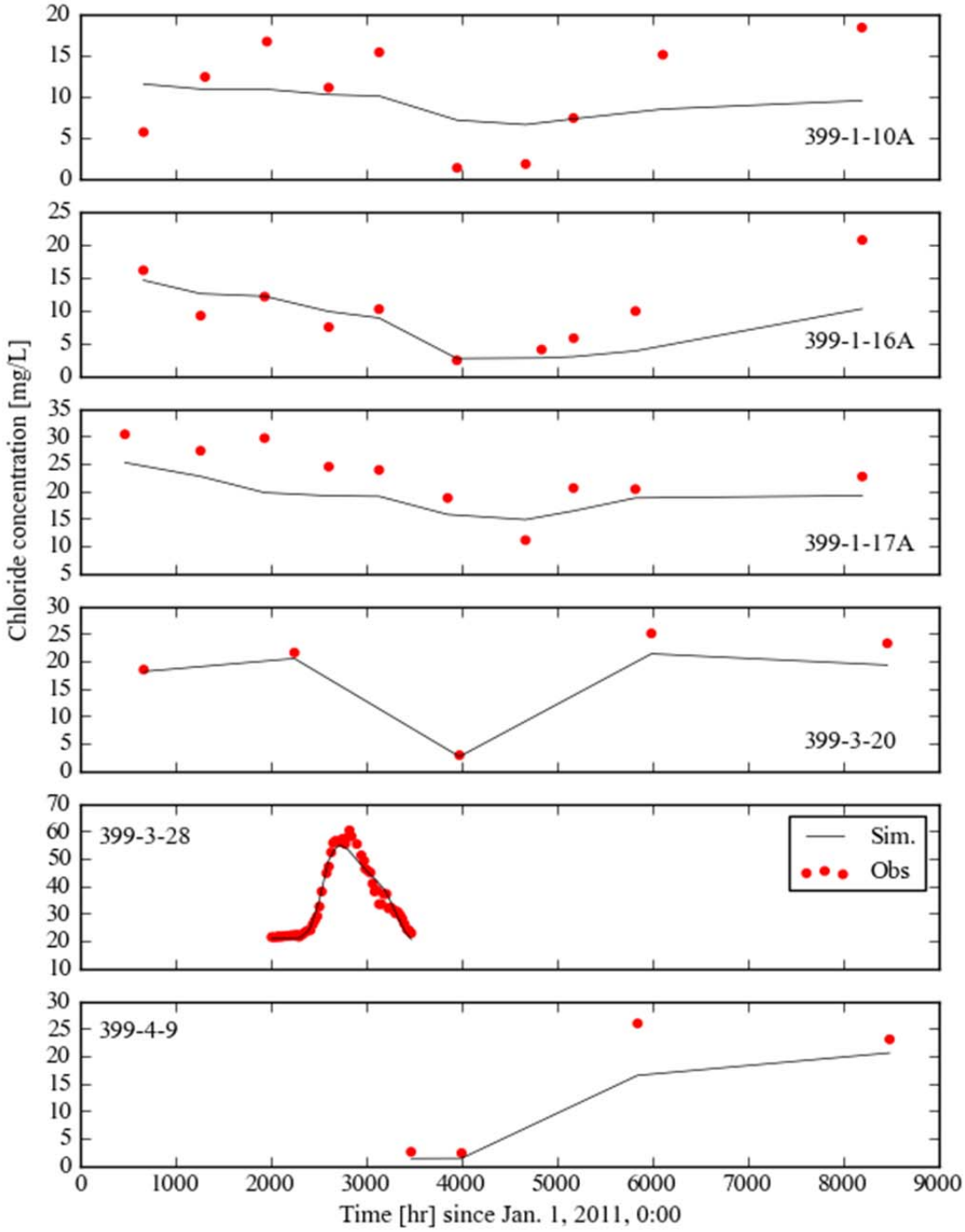

Figure 2.10. Observed and simulated chloride concentrations. Data for well 399-3-28 represent a tracer test at the IFRC well field.

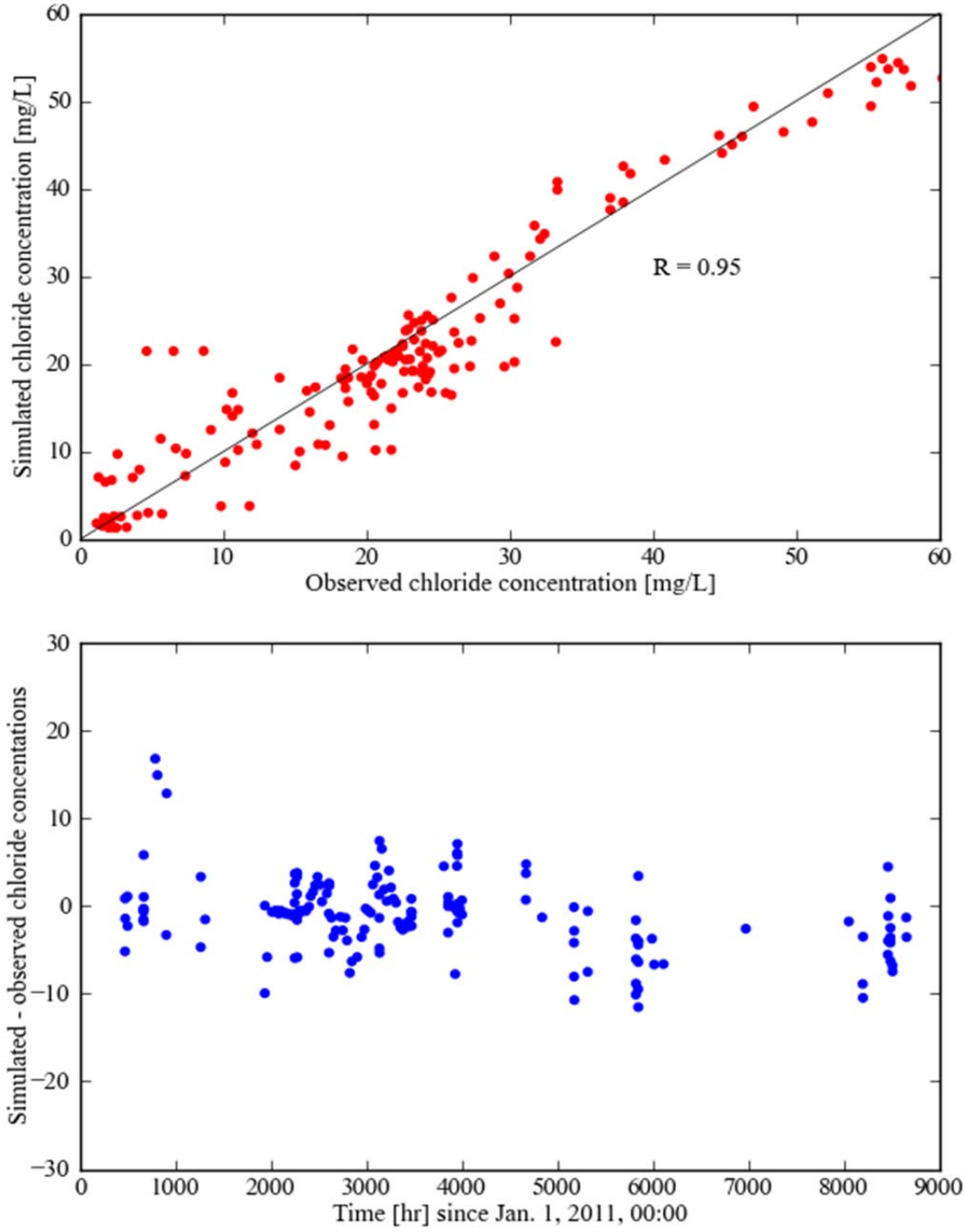

Figure 2.11. Observed versus simulated chloride concentrations and residuals (simulated-observed).

Figure 2.12 and Figure 2.13 show the permeability distribution resulting from the inverse modeling for four horizontal slices through the model domain, at elevations of 104, 102, 100, and 98 m. These permeability distributions appear to reveal a large-scale channel feature that runs from the north-central to the southeast portion of the model domain. These figures also reveal additional smaller-scale channel features in the surface of the Ringold Fm that are normal to the larger-scale feature.

In summary, although these results are preliminary, this application of the pilot point method with regularization constraints to estimating spatially distributed permeabilities for the 300 Area appears to have been effective. Further details regarding finer-scale structure of heterogeneities, including stratification, could be revealed by using more pilot points and observational data from more wells. Use of specific conductance data, for which higher temporal and spatial resolution data are available, instead of chloride, could potentially also lead to some improvements, including the possibility of joint estimation of permeability and porosity. The inverse results obtained in this initial modeling effort were used in subsequent transport modeling, described next.

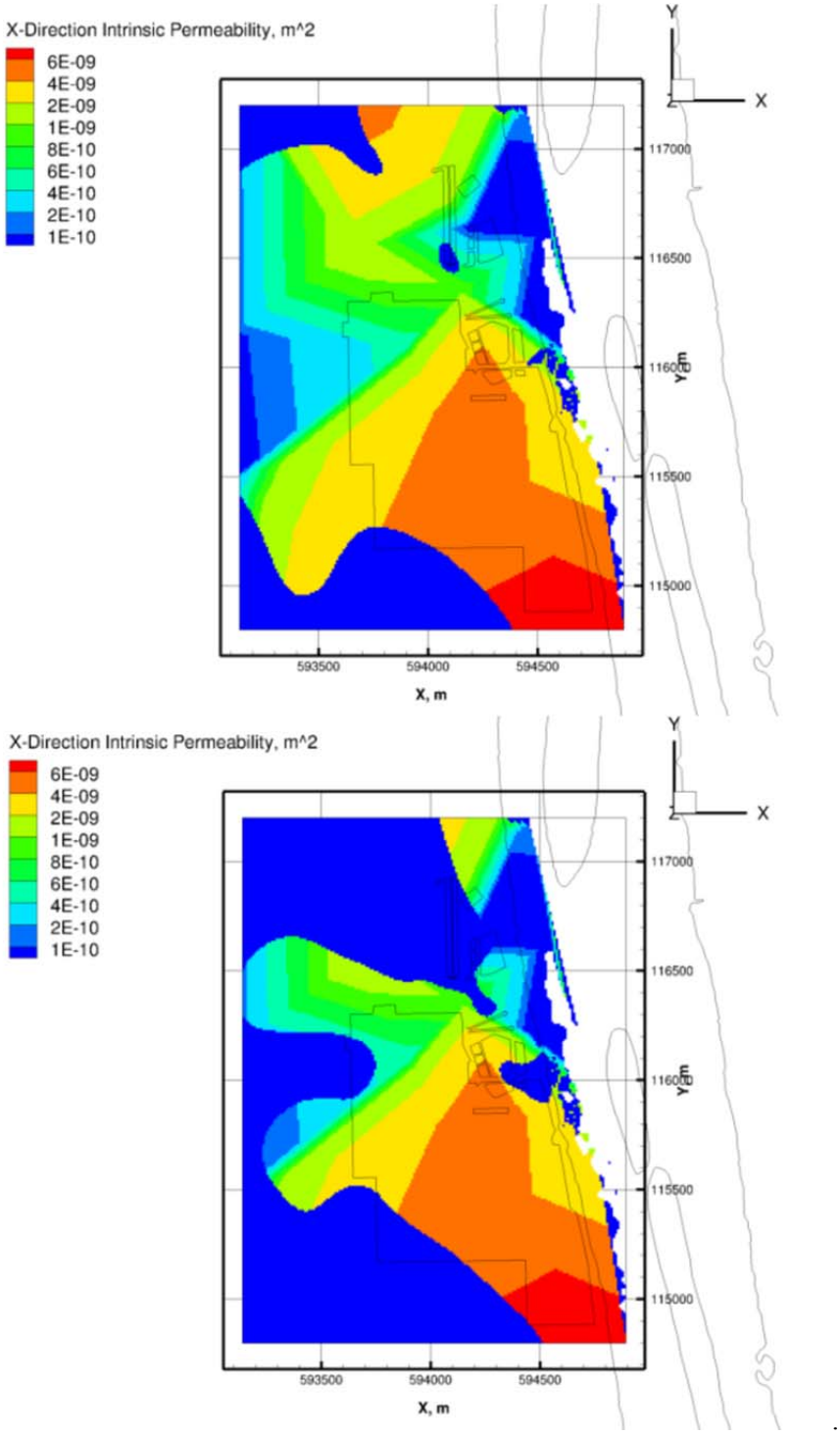

Figure 2.12. Permeability distributions at elevation, z = 104 m (top figure) and z = 102 m (bottom figure) for the calibrated groundwater flow and tracer transport model.

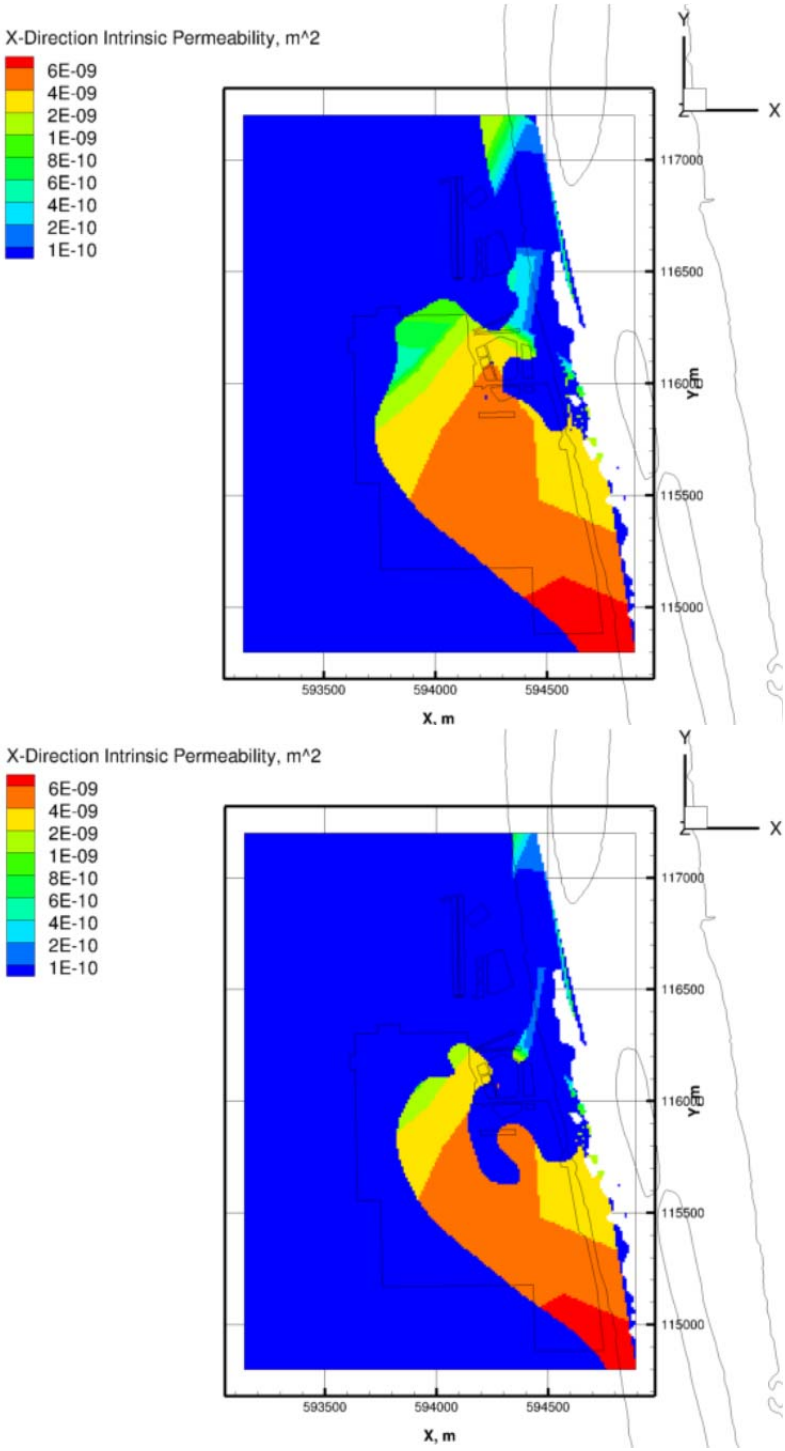

Figure 2.13. Permeability distributions at elevation, z = 100 m (top figure) and z = 98 m (bottom figure) for the calibrated groundwater flow and tracer transport model.

2.5 Reactive Transport Models

Two primary approaches have been applied to modeling transport and sorption processes associated with uranium in 300 Area sediments: the linear equilibrium adsorption or K_d approach (Meyer et al. 2007a; Nichols 2012), and surface complexation modeling (Davis and Kent 1990; Liu et al. 2008, 2009; Ma et al. 2010; Stoliker et al. 2013). Surface complexation modeling can be further subdivided into equilibrium and kinetic approaches. Zachara et al. (2013) states that "accurate description of uranium desorption from contaminated 300 Area sediments requires the use of kinetic models."

In general, surface complexation modeling is a more rigorous, multi-species modeling approach that is thought to be necessary for 300 Area applications because of the highly variable aqueous chemical conditions that result from cyclic incursion of river water of different chemical composition into the unconfined aquifer. Appropriately parameterized surface complexation models respond realistically to changes in aqueous chemical compositions, and also account for the finite sorption capacity of the sediments. In contrast, the standard K_d-based model is strictly applicable to the typically small range of variability of the single aqueous species [e.g., U(VI)] for which the K_d values were estimated, it does not account for kinetic behavior, and it does not consider the finite sorption capacity of the sediment. Although they can be highly inaccurate for conditions outside of the range of chemical compositions for which the K_d values were estimated, K_d-based flow and transport models are typically much faster than models using multi-species surface complexation reactions, and much easier to apply owing to reduced data/parameter requirements.

Attempts have been made to adapt and improve the application of K_d-based models to account for the effects of spatially variable chemical compositions by using equilibrium surface complexation reactions (Meyer et al. 2007a or empirical correlations (Nichols 2012) to define effective K_d values for different zones or regions, each of which may experience a smaller range of chemical conditions compared to the overall domain. Although this zoned-K_d approach may provide some improvement over a constant K_d, the current consensus among the subsurface flow and transport modeling communities at PNNL, other national laboratories, and the U.S. Geological Survey is that surface complexation models are needed to provide accurate descriptions of uranium sorption behavior in many natural systems, including the hyporheic zone along the Columbia River shoreline bounding the 300 Area. One particular surface complexation model for uranium that was developed with support from DOE-SC is described later in this section.

2.5.1 Uranium Aqueous Speciation

Reactive transport modeling requires consideration of aqueous speciation reactions. Key variables influencing U(VI) speciation in Hanford vadose zone and groundwater include pH, [U(VI)tot], CO_3^{2-}, Ca^{2+}, Mg^{2+}, and PO_4^{3-}. The reactions of interest for the current study and their equilibrium constants are summarized later in this report (Table 2.2). Figure 2.14 and Figure 2.15 are based on the reactions of interest and show the aqueous speciation of U(VI) for variations in some of these key variables, calculated using Geochemists Workbench (Bethke 2005). Portions of the following discussion about these figures are taken from an earlier summary by Peterson et al. (2008).

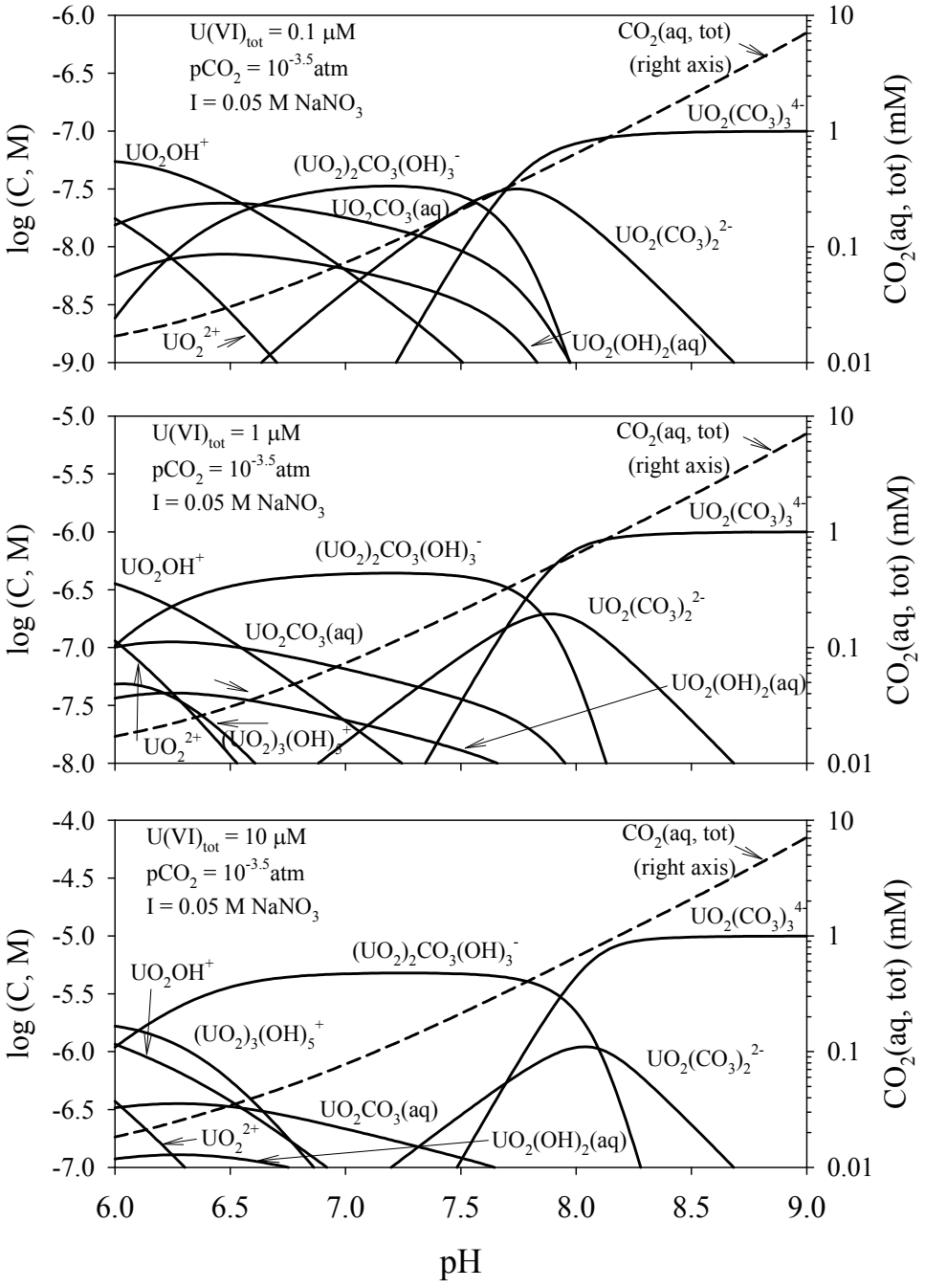

Figure 2.14. Aqueous U(VI) speciation as a function of pH, total aqueous U(VI), and carbonate concentrations in Hanford sediment pore water. The carbonate concentration is in equilibrium with a CO_2(g) pressure of $10^{-3.5}$ atmospheres (after Peterson et al. 2008).

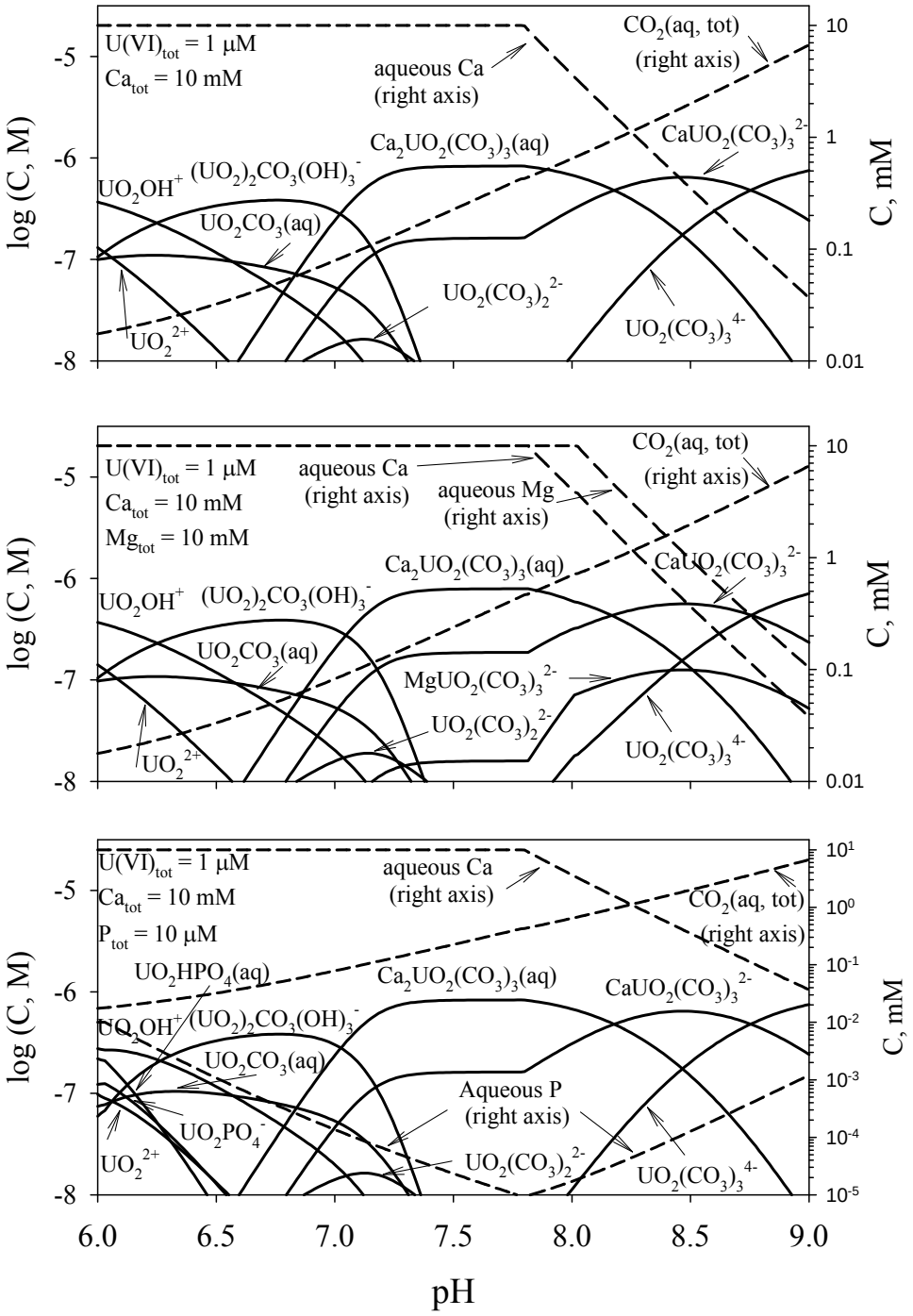

Figure 2.15. Aqueous U(VI) speciation in the presence of Ca (top panel), Ca and Mg (middle panel), and Ca and PO_4 (bottom panel) in Hanford sediment pore water. The total concentration of Ca was 10 mM, including both aqueous and solid phases in equilibrium. The solid calcium was represented by calcite. The total Mg concentration was 10 mM, including both aqueous and solid phase dolomite in equilibrium. The phosphate concentration was in equilibrium with the mineral hydroxyl apatite (after Peterson et al. 2008).

Figure 2.14 and Figure 2.15 assume carbonate concentrations to be in equilibrium with atmospheric $CO_{2(g),}$ such that total aqueous carbonate concentration increases with pH through carbonic acid dissociation. As noted by Peterson et al. (2008), the presence of calcium significantly changes uranyl speciation above pH 7, and has no effect below pH 6.5. Calcium is typically a very minor but common component in Hanford sediments. Between pH 7 and 8, U(VI) speciation is dominated by $Ca_2UO_2(CO_3)_{(aq)}$. Above pH 8, speciation is dominated by a combination of the species $CaUO_2(CO_3)_3^{2-}$ and $UO_2(CO_3)_3^{4-}$.

The effect of Mg^{2+} is relatively minor compared to Ca^{2+}. The effect of phosphate is also minor on U(VI) aqueous speciation (bottom panel in Figure 2.14) because its aqueous concentration is regulated to low levels by solubility equilibrium with various phosphate minerals. However, further discussion on phosphate is warranted owing to the planned use of polyphosphate for treatment of the U(VI) contamination in vadose zone sediments. The calculated aqueous phosphate concentration in these calculations was fixed by equilibrium with hydroxyapatite, $Ca_5(PO_4)_3(OH)$, which has a low solubility in the calculated pH range. Phosphate influences U(VI) aqueous speciation below pH 6.5 where species $UO_2HPO_4(aq)$ and $UO_2PO_4^-$ are contributing but not major aqueous species. The concentrations of uranyl phosphate aqueous complexes decrease dramatically with increasing pH as the solubility of hydroxyapatite decreases, and carbonate concentrations increase. Highly stable uranyl carbonate species tend to out-compete those with phosphate at increasing pH.

Most Hanford uncontaminated or slightly contaminated pore waters and groundwater exhibit a pH between 7.5 to 8.5, Ca^{2+} concentrations between 0.5 to 10 mmol/L, and equilibrium with $CO_{2(g)}$ that is slightly above atmospheric pressures (e.g., $>10^{-3.5}$ atm). Higher pH and calcium concentrations in these ranges generally occur in sediments containing greater than a few weight-percent calcite. The speciation diagrams show that U(VI) under average Hanford geochemical conditions will be distributed between multiple species with $(UO_2)_2CO_3(OH)_3^-$ and $UO_2(CO_3)_3^{4-}$ predominating at lower Ca^{2+} concentrations and $Ca_2UO_2(CO_3)_{3(aq)}$ and $CaUO_2(CO_3)_3^{2-}$ predominating at higher Ca^{2+} concentrations. These differences may be significant because calcium-uranium-carbonate complexes have been shown to be less susceptible to both adsorption and biologic reduction than those containing just uranium and carbonate (Brooks et al. 2003; Dong et al. 2005; Fox et al. 2006).

2.5.2 Multi-rate Surface Complexation

Liu and colleagues have performed a number of carefully controlled laboratory experiments using sediments from the 300 Area, and have tested a variety of models describing U(VI) surface complexation, mass transfer, and geochemical reactions (Liu et al. 2008; Ma et al. 2010; Greskowiak et al. 2011; Shang et al. 2011; Stoliker et al. 2013; Shang et al. 2014). They have found that kinetic (as opposed to equilibrium) and multi-rate surface complexation models are needed to provide accurate descriptions of laboratory experimental data. Given the highly dynamic nature of aqueous chemical compositions over a large portion of the uranium-contaminated aquifer in the 300 Area, it is assumed that a kinetic, multi-rate surface complexation modeling approach is also needed to accurately describe uranium fate and mass transfer in the field. Consequently, we utilized a multi-rate surface complexation modeling approach for the reactive transport modeling reported herein. The following surface complexation reactions were used

$$>SOH + UO_2^{2+} + H_2O = >SOUO_2OH + 2H^+ \qquad K_1 \qquad (2.2)$$

$$>SOH + UO_2^{2+} + H_2CO_3 = SOUO_2HCO_3 + 2H^+ \qquad K_2 \tag{2.3}$$

where >SOH represents a surface site for uranyl adsorption; $>SOUO_2OH$ and $>SOUO_2HCO_3$ are adsorbed uranyl species; and K_1 and K_2 are conditional equilibrium constants with values (logK1 = -5.2 and logK2 = -1.0) estimated from laboratory batch experiments (Bond et al. 2008). The multi-rate surface complexation model of Liu et al. (2008; 2009) was adopted, as described by the following equations

$$\frac{\partial C_i}{\partial t} + \frac{(1-\theta)\rho_s}{\theta}\sum_{j=1}^{N_s}\left(\alpha_{ij}\sum_{k=1}^{M_j}\frac{\partial q_j^k}{\partial t}\right) = \nabla\cdot\left(vC_i + D\nabla C_i\right), \quad i = 1,2,...,N, \tag{2.4}$$

$$\frac{\partial q_j^k}{\partial t} = \alpha_j^k(Q_j^k - q_j^k), \quad j = 1,2,...,N_s; \quad k = 1,2,...,M_j \tag{2.5}$$

where C_i is the total aqueous concentration of chemical component i; q_j^k is the concentration of adsorbed species j at adsorption site k; θ is the porosity or volumetric water content; ρ_s is the density of the solids; **D** is the dispersion tensor; α_{ij} is a stoichiometric coefficient of chemical component i in adsorbed species j; N is the total number of chemical components in the system; N_s is the total number of adsorbed species; M_j is the total number of adsorption sites for adsorbed species j; v is the pore water velocity; α_j^k is the rate constant of adsorbed species j at site k; Q_j^k is the adsorption extent of adsorbed species j at site k, which is defined as the theoretical concentration of adsorbed species j at site k in equilibrium with the aqueous solution; ∇ is a gradient operator; and **v** is the pore water velocity vector. Values for the equilibrium constants, K_1 and K_2 that have been used for modeling laboratory experiments are provided by Liu et al. (2008). Following Liu et al. (2008, 2009), in order to minimize the number of model parameters, the rate constants for the multi-rate model are assumed to follow a log-normal probability distribution

$$p(\alpha) = \frac{1}{\sqrt{2\pi}\alpha\sigma}\exp\left[-\frac{1}{2\sigma^2}(\ln(\alpha)-\mu)^2\right] \tag{2.6}$$

where p is the probability that a site has rate constant α; and μ and σ are parameters defining the log-normal distribution. With α and σ known, the rate constant α_k is calculated from

$$f_k = S_T\int_{\alpha_k-\Delta\alpha/2}^{\alpha_k+\Delta\alpha/2} p(\alpha)d\alpha \tag{2.7}$$

where f_k is the site density [mol/m^2] for site k that has an average rate constant α_j^k; and S_T is the total adsorption site concentration [mol/g] for the sediment. The site density for site k is usually taken as $f_k = S_T/M_T$ (Liu et al. 2008, 2009), where M_T is the total number of adsorption sites for all adsorbed species, N_s.

Several different approaches have been used to estimate the site density available for uranium surface complexation. The most straightforward approach is to assume a common, generic sorption site density, f_G = 3.84 x 10^{-6} mol/m^2 (Davis and Kent 1990), and to compute surface site concentration from surface area. For the example presented in Appendix A, Table A.3, the surface site concentration for the bulk sediment is calculated as

$$\text{Surface site concentration, } S_T \text{ [mol/g]} = \text{Surface area, } SA_T \text{ [m}^2\text{/g]} * \text{Site density, } f_G \text{ [mol/m}^2\text{]} \quad (2.8)$$

$$= (9.94 \text{ m}^2\text{/g}) * (3.84 \times 10^{-6} \text{ mol/m}^2)$$

$$= 3.82 \times 10^{-5} \text{ mol/g}$$

For field applications, if spatially distributed grain size distribution data are available, the grain size-SA correlation function from Appendix A, Figure A.7 (top plot) could potentially be used to compute spatially distributed surface areas based on the additivity concept. Spatially distributed surface site concentrations could then be calculated using Eq. (2.8). Otherwise, as a first approximation it may be reasonable to assume that the value of surface site concentration calculated for the IFRC core example shown above (3.82 × 10^{-5} mol/g) is representative of Hanford fm sediments in the 300 Area. We make this assumption for the field-scale modeling described later in this report.

The adsorbed or total U(VI) estimated for the bulk sediment from core samples collected in both the vadose zone and underlying aquifer must be partitioned over the total number of adsorption sites, M_T, that are used in the surface complexation model. To specify initial conditions we first calculate

$$q_j^k = \frac{\left[\frac{(\mu g\ U / g\ soil)(1\ g\ U / 10^6\ \mu g\ U)}{(238\ g\ U / mol)} \right]}{M_T} \quad (2.9)$$

where the first term in the numerator of Eq. (2.9) represents measured, sediment-associated uranium. Recall that $U_{<2mm}$ and $U_{grav\text{-}corr}$ are expected to overestimate and underestimate the true values, respectively. A choice must also be made between using measurements of total or labile uranium. Liu et al. (2008) treated the total measured U(VI) in the sediment as the initial adsorbed concentration. Shang et al. (2013, in review) partitioned the measured labile and non-labile (total–labile) U fractions over fast and slow sorption sites, respectively. Other studies have essentially ignored the non-labile fraction completely and have used only the measured labile fraction. Given the calculations shown in Appendix A, Table A.3, the recent results of Shang et al. (2014), and the frequent lack of concomitant grain size distribution data with the sediment U(VI) data, a reasonable compromise may be to simply use measured values of labile U on the <2 mm size fraction to estimate the adsorbed U for the bulk sediment. The calculations in Appendix A, Table A.3, show that the "true" values of adsorbed and total U for the bulk sediment in this example are 0.59 and 2.32 ug/g, respectively, while the adsorbed U for the <2 mm size fraction lies in between at a value of 1.07 ug/g.

Initial aqueous species concentrations for U(VI) and other constituents are estimated from the average concentrations of major ions and total aqueous U(VI) measured in groundwater. Equilibration of the complete chemical system then requires solution of the full reaction network. The adsorption extent Q_j^k

for >$SOUO_2OH$ and >$SOUO_2HCO_3$ can be calculated from the surface complexation reactions, Eq. (2.2) and Eq. (2.3), using Liu et al. (2009)

$$Q^k_{SOUO_2OH} = \frac{S_k K_1 \{UO_2^{2+}\} \{H^+\}^{-2}}{1 + K_1 \{UO_2^{2+}\} \{H^+\}^{-2} + K_2 \{UO_2^{2+}\} \{CO_3^{2-}\}} \tag{2.10}$$

$$Q^k_{SOUO_2HCO_3} = \frac{S_k K_2 \{UO_2^{2+}\} \{CO_3^{2-}\}}{1 + K_1 \{UO_2^{2+}\} \{H^+\}^{-2} + K_2 \{UO_2^{2+}\} \{CO_3^{2-}\}} \tag{2.11}$$

where S_k is the surface site concentration [mol/g] at site k, { } denotes activities for the aqueous species shown, and other parameters have been previously defined. These expressions, as well as the original surface complexation reactions in Eq. (2.2) and Eq. (2.3), indicate that uranium surface complexation is primarily dependent on pH and the activities of UO_2^{2+} and CO_3^{2-}, which are in turn dependent on the other aqueous species defined by the reaction network. Assuming $f_k = S_T/M_T$ (see Eq. (2.7)), is tantamount to assuming that $S_k = (SA_T/M_T)$ x f_G.

Finally, it should be noted that the concentrations of surface complexed species that are input to STOMP and eSTOMP must be normalized to aqueous volume

$$m^k_j = \frac{(1-\theta)}{\theta} \rho_s q^k_j \tag{2.12}$$

where m_j^k is the concentration of sorbed species j at site k, normalized to aqueous volume, and all other symbols have been previously defined.

2.5.2.1 Model Evaluation with Laboratory Experimental Data

The multi-rate surface complexation model described above was implemented in both STOMP and eSTOMP. Prior to field-scale modeling, a laboratory column experiment performed on an intact core sample from the IFRC site was simulated to test the implementation of the model. The aqueous speciation reactions used for this reactive transport modeling are shown in Table 2.2.

The experiment, known as Intact Core Experiment 1 (ICE-1), was performed on a core sample from the 35.8 - 36.8 ft depth in borehole C6203, which was completed as well 399-3-26 within the triangular array of wells that define the IFRC site. The field core had a length of 25 cm and an internal diameter of 8.9 cm, for a total volume of 1555 cm^3, with an estimated pore volume of 465 cm^3 (30% porosity). A flow rate of 3.24 mL/min, or ~10 pore volumes (PV) per day, was used. The experiment was performed in three phases as described below.

Phase A. U Desorption

The cores were saturated and then leached with synthetic 300 Area groundwater at 10 PV per day (~5 L/day) for 2 days (48 hours). After a stop-flow period of 3 days (72 hours), another 5 PV (12 hours) of the synthetic groundwater was injected.

Phase B. Br/PFBA Tracer Test

The second phase of the experiment, Phase B, started 132 hours (5.5 days) after Phase A was finished. Synthetic groundwater with 25 mg/L Br and 25 mg/L PFBA was pumped through the cores for 1 day (24 hours) at 10 PV/day. After 1 day, the tracer solution was switched back to synthetic groundwater without Br and PFBA. This solution was injected at a rate of 10 PV/day. After 5 PV of this second solution had passed through the column, there was another 48-hour stop-flow period, followed by another 5 PV of synthetic groundwater passing through the column. The tracer data from Phase B (results not shown) were used to estimate the dispersion coefficient and mobile-immobile water fractions used in a dual-domain mass transfer and multi-rate surface complexation model (Zachara et al. 2013, in press).

Phase C. U Tracer Experiment

Phase C of the experiment started 92 hours (3 days and 20 hours) after Phase B was completed. Synthetic groundwater spiked with 60 ug/L natural U was pumped through the column at a flow rate of 10 PV/day for a period of 2 days (48 hours). After the injection period, the electrolyte was switched back to synthetic groundwater without U, which was pumped through the column for 5 PV. This was followed by a 48-hour stop flow period, after which another 10 PV of synthetic groundwater was passed through the column.

Effluent samples from all three phases were analyzed for major cations and anions, U, and for phase B the tracers (Br and PFBA) were analyzed. Only the aqueous U(VI) effluent results are discussed in detail here. Complete experimental details and modeling results for this and two other intact cores from the IFRC site are described by Zachara et al. (2013, in press).

Although the log-normal rate distribution function of Eq. (2.6) is fully defined using only two parameters, μ and σ, in practice this function must be discretized and separate mass balance equations must be solved for each discrete rate. Liu et al. (2008, 2009) used $M_j = 50$ for modeling uranium mass transfer observed during multiple stop-flow events in one-dimensional laboratory flow-through column experiments. With two surface complexation reactions (Eq. (2.2) and Eq. (2.3)), and $M_j = 50$, 100 separate rate equations must be solved for each grid cell in the model domain. The computational effort needed to solve the mass balance equations is proportional to M_T. Ma et al. (2010) simulated a much larger spatial domain representing a two-dimensional vertical cross-section of the unconfined aquifer in the 300 Area and used $M_j = 10$. For two surface complexation reactions, $M_j = 10$ results in 20 separate mass balance equations.

It has been argued that for the typical time frames involved in many laboratory experimental studies on uranium sorption and mass transfer which are used to parameterize the multi-rate surface complexation model, such as ~600 hours (25 days) for ICE-1, the sites represented by the slower rates in the log-normal distribution function may not contribute significantly to the experimental observations. This fact and run-time considerations for field-scale modeling suggest that reducing the number of sites and rates to include only those expected to contribute significantly to experimental observations, may provide sufficiently accurate results with far less computational effort. To evaluate this possibility, simulations were performed of the ICE-1 experiment using different numbers of uranium surface complexation adsorption sites and rates (varying parameter M_j) and adjusted site densities.

Figure 2.16 shows observed and simulated effluent U(VI) results for three cases: $M_j = 5$, $M_j = 6$, and $M_j = 50$. The first case, with $M_j = 5$, used only the five fastest rates for each of the two surface complexation reactions, with adjusted site density. The second case, with $M_j = 6$, used six rates distributed over the log-normal distribution, with adjusted site density. The third case used $M_j = 50$, which represents the typical number of rates used for discretizing the log-normal rate distribution function in the multi-rate surface complexation model for simulation of laboratory column experiments (Liu et al. 2008, 2009). Case 1 with $M_j = 5$ arguably fits the data nearly as well as Case 3 with $M_j = 50$, but Case 3 took 40 times longer to run than Case 1 for this 20 node test problem. Based on these results, for 3D modeling at the 300 Area uranium plume scale, we used $M_j = 5$ (Case 2) for each of the two surface complexation reactions Eq. (2.2) and Eq. (2.3), for a total of 10 kinetic equations associated with surface complexation.

Table 2.2. Aqueous speciation reactions and equilibrium constants used for modeling.

Aqueous Speciation Reaction	log K(I=0)	Source
$UO_2^{2+} + H_2O = UO_2OH^+ + H^+$	-5.25	1
$UO_2^{2+} + 2H_2O = UO_2(OH)_2(aq) + 2H^+$	-12.15	1
$UO_2^{2+} + 3H_2O = UO_2(OH)_3^- + 3H^+$	-20.25	1
$UO_2^{2+} + 4H_2O = UO_2(OH)_4^{2-} + 4H^+$	-32.40	1
$2UO_2^{2+} + H_2O = (UO_2)_2OH^{3+} + H^+$	-2.70	1
$2UO_2^{2+} + 2H_2O = (UO_2)_2(OH)_2^{2+} + 2H^+$	-5.62	1
$3UO_2^{2+} + 4H_2O = (UO_2)_3(OH)_4^{2+} + 4H^+$	-11.90	1
$3UO_2^{2+} + 5H_2O = (UO_2)_3(OH)_5^+ + 5H^+$	-15.55	1
$3UO_2^{2+} + 7H_2O = (UO_2)_3(OH)_7^- + 7H^+$	-32.20	1
$4UO_2^{2+} + 7H_2O = (UO_2)_3(OH)_7^+ + 7H^+$	-21.90	1
$UO_2^{2+} + CO_3^{2-} = UO_2CO_3(aq)$	9.94	1
$UO_2^{2+} + 2CO_3^{2-} = UO_2(CO_3)_2^{2-}$	16.16	1
$UO_2^{2+} + 3CO_3^{2-} = UO_2(CO_3)_3^{4-}$	21.84	1
$3UO_2^{2+} + 6CO_3^{2-} = (UO_2)_3(CO_3)_6^{6-}$	54.0	1
$2UO_2^{2+} + CO_3^{2-} + 3H_2O = (UO_2)_2CO_3(OH)_3^- + 3H^+$	-0.855	1
$3UO_2^{2+} + CO_3^{2-} + 3H_2O = (UO_2)_3O(OH)_2HCO_3^+ + 3H^+$	0.655	1
$11UO_2^{2+} + 6CO_3^{2-} + 12H_2O = (UO_2)_{11}(CO_3)_6(OH)_{12}^{2-} + 12H^+$	36.43	1
$2Ca^{2+} + UO_2^{2+} + 3CO_3^{2-} = Ca_2UO_2(CO_3)_3$	30.70	2
$Ca^{2+} + UO_2^{2+} + 3CO_3^{2-} = CaUO_2(CO_3)_3^{2+}$	27.18	2
$Mg^{2+} + UO_2^{2+} = 3CO_3^{2-} = MgUO_2(CO_3)_3^{2+}$	26.11	2
$UO_2^{2+} + NO_3^- = UO_2NO_3^+$	0.30	1
$Ca^{2+} + CO_3^{2-} = CaCO_3(aq)$	3.22	3
$Ca^{2+} + H^+ + CO_3^{2-} = CaHCO_3^+$	11.43	3
$Ca^{2+} + NO_3^- = CaNO_3^+$	0.5	3
$Ca^{2+} + H_2O = CaOH^+ + H^+$	-12.70	3
$CO_3^{2-} + 2H^+ = H_2CO_3(aq)$	16.68	1
$CO_3^{2-} + H^+ = HCO_3^-$	10.33	1
$H_2O = OH^- + H^+$	-14.00	3

1. Guillaumont et al. (2003); 2. Dong and Brooks (2006); 3. NIST (2001).

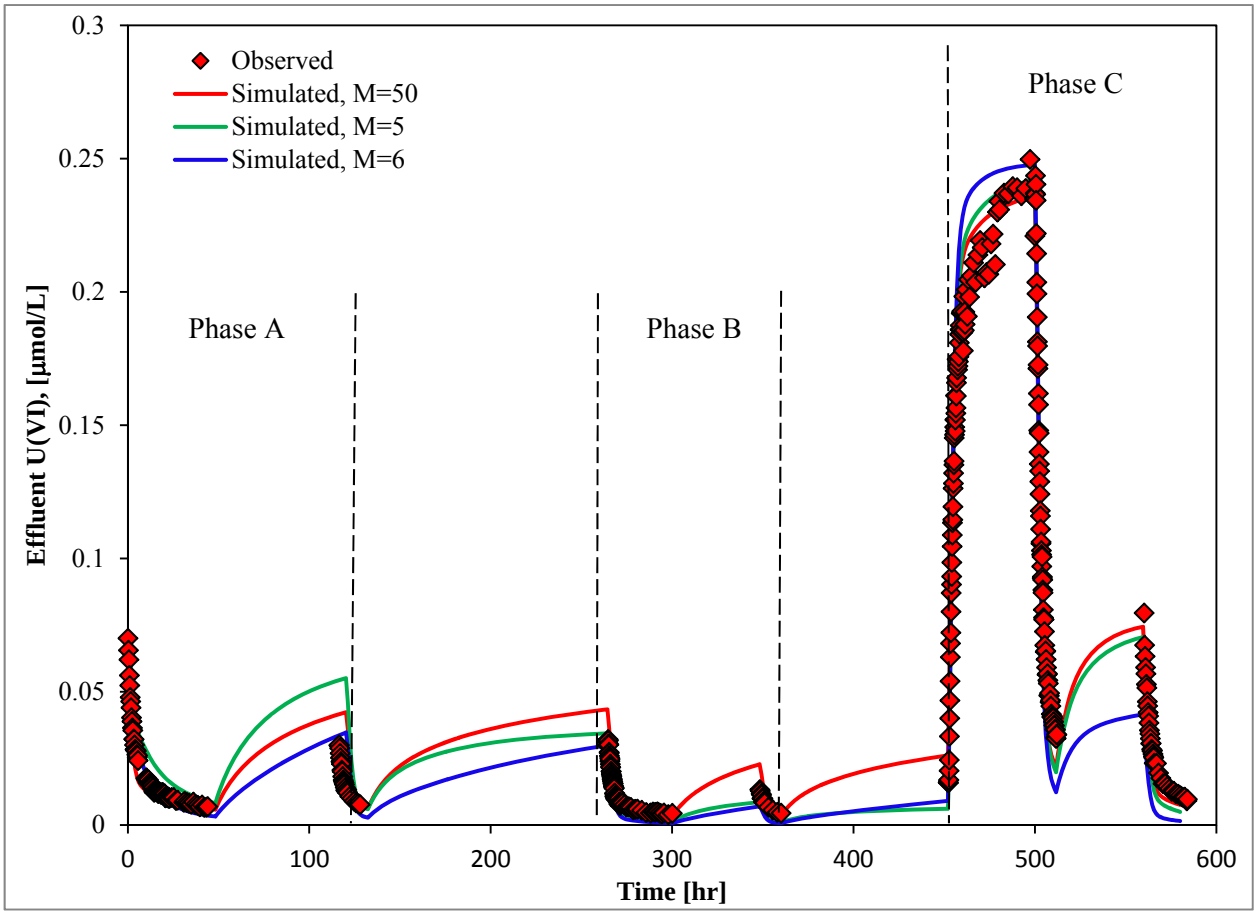

Figure 2.16. Observed aqueous U(VI) concentrations from a column experiment performed on an intact core from the IFRC site (35.8-36.8 ft depth interval in borehole C6203, completed as well 399-3-26), with simulation results from multi-rate surface complexation model using different numbers of sorption sites and rates.

2.5.3 Alternative Models with Polyphosphate Reactions

Aquifer injection and vadose zone infiltration of aqueous solutions of polyphosphate have been proposed as a means of stabilizing uranium in the subsurface (Vermeul et al. 2009; Wellman et al. 2007). Laboratory investigations related to this treatment technology are reported by Wellman et al. (2006) and Szecsody et al. (2012). Results of a field treatability test, described earlier, are reported by Vermeul et al. (2009).

Other recent evaluation of the effectiveness of polyphosphate treatment for stabilizing U(VI) includes the work of Fanizza et al. (2013), who performed pore-scale experiments and modeling of uranyl phosphate precipitation in a (micro-) model groundwater system. The only mineral that was found to precipitate in the experiments was chernikovite ($UO_2HPO_4 \cdot 4H_2O$). Precipitation occurred over a time scale of hours to days, with rates being 2.3 times slower in the presence of SO_4^{2-} and 1.4 times faster in the presence of Ca^{2+}. Interestingly, available thermodynamic data suggest that chernikovite is the least thermodynamically favored mineral to precipitate based on its saturation ratio, SR, ($0<SR<1$), compared to uranyl hydrogen phosphate and Na-autunite ($13<SR<40$), and uranyl orthophosphate and Ca-autunite

(when Ca++ is present; SR > 105). The experiments also showed that uranium-phosphate mineral precipitation as chernikovite can block pores, alter fluid flow paths, and potentially limit mixing and precipitation. This laboratory-based observation of permeability reduction following polyphosphate injection is consistent with field observations for the Hanford 300 Area (Vermeul et al. 2009).

The reaction network developed by Fanizza et al. (2013) was used as a starting point for modeling polyphosphate remediation of uranium. Eight primary species (HCO_3^-, Ca^{++}, H^+, HPO_4^{--}, Mg^{++}, NO_3^-, Na^+, UO_2^{++}) were included in the reaction network. In addition to the equilibrium reactions listed in Table 2.2, the equilibrium reactions listed in Table 2.3 were also considered.

Parameters for additional kinetic reactions needed to model polyphosphate remediation of uranium are developed in the following three subsections, by first calibrating to results of the ICE-1 column experiment, described previously, and then modeling results from column experiments by Oostrom and Wietsma (unpublished) and by Wellman et al. (2008).

2.5.3.1 Simulation of Uranium Release from ICE Column using Kinetic Langmuir Adsorption

In order to include additional kinetic reactions in the reaction network for phosphate remediation simulations, a simpler approach to modeling uranium release was needed. The multi-rate uranium surface complexation model requires a "reduced equilibrium" option in order to converge with reasonable run times. With this option, the equilibrium aqueous speciation reactions are decoupled from the kinetic reactions. However, this reduced equilibrium option proved to be incompatible with other types of kinetic equations available in STOMP, so alternative reactions networks were developed.

For the alternative reaction networks, uranium release from Hanford sediments was simulated using a kinetic version of the Langmuir adsorption isotherm. This model has the form (Fetter 1993)

$$\frac{\partial C^*}{\partial t} = k_f C(\beta - C^*) - k_b C^* \tag{2.13}$$

where C^*= sorbed concentration, C = aqueous concentration, k_f = forward rate constant, k_b = backward rate constant, and β = maximum amount of species that can be adsorbed. The sorbed species (C*) is assumed to be $>SOUO_2(HCO_3CO_3)^{2-}$, and the aqueous species (C) is assumed to be $UO_2(CO_3)_2^{2-}$, which is consistent with the single-site surface complexation model used in Liu et al. (2013).

The ICE-1, described in section 2.5.2.1, was modeled using the kinetic Langmuir adsorption isotherm for uranium release. The best match was obtained using $k_f = k_b$ = 1 mol/hr and $\beta = 3.82 \times 10^{-5}$ mol/g Figure 2.17).

Table 2.3. Additional aqueous equilibrium reactions used for phosphate remediation simulations

Equilibrium Reaction	Log Equilibrium Constant
$2Mg^{2+} + CO_3^{2-} = Mg_2CO_3^{2+}$	3.59[a]
$Mg^{2+} + CO_3^{2-} = MgCO_3(aq)$	2.92[b]
$H^+ + Mg^{2+} + CO_3^{2-} = MgHCO_3^+$	11.34[b]
$Mg^{2+} + H_2O = H^+ + MgOH^+$	-11.417[a]
$Na^+ + CO_3^{2-} = NaCO_3^-$	1.27[a]
$Na^+ + H^+ + CO_3^{2-} = NaHCO_3(aq)$	10.029[a]
$Na^+ + NO3- = NaNO_3(aq)$	-0.55[a]
$Na^+ + H_2O = H^+ + NaOH(aq)$	-13.897[a]
$3UO_2^{2+} + 6CO_3^{2-} = (UO_2)_3(CO_3)_6^{6-}$	54.000[a]
$CaHPO_4(aq) = Ca^{2+} + HPO_4^{2-}$	-2.740 [b]
$CaPO_4^- + H^+ = Ca^{2+} + HPO_4^{2-}$	5.8618 [b]
$NaPO4-- + H^+ = Na+ + HPO_4^{2-}$	10.8918 [a]
$NaHPO4- = HPO_4^{2-} + Na+$	-0.9200 [a]
$UO_2(HPO_4)_2^{2-} = UO_2^{2+} + 2HPO_4^{2-}$	-18.344[a]
$PO_4^{3-} + H^+ = HPO_4^{2-}$	12.3218 [b]

[a] Visual MINTEQ database (http://www2.lwr.kth.se/English/OurSoftware/vminteq/)
[b] Wolery and Jarek 2003

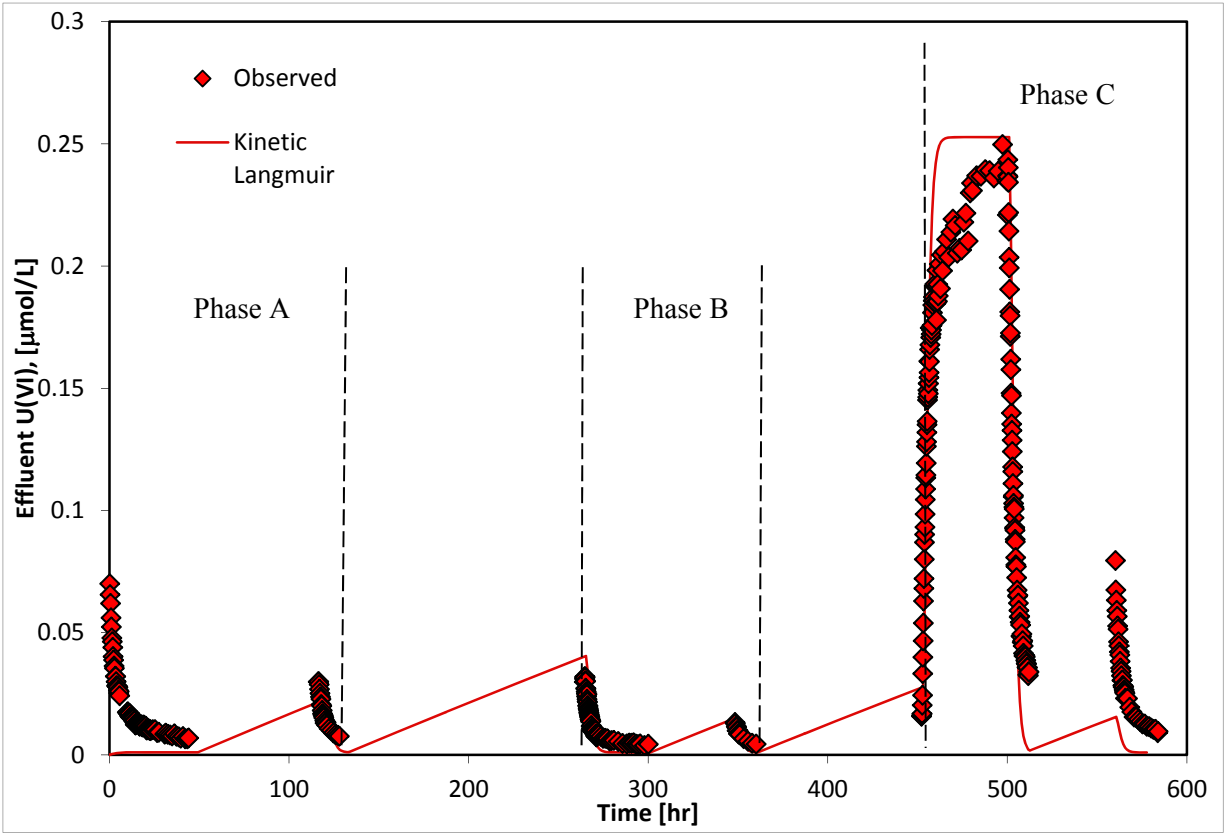

Figure 2.17. Uranium release from ICE-1 column modeled using kinetic Langmuir adsorption isotherm.

2.5.3.2 Simulation of Ortho-, Pyro- and Tripolyphosphate Transport and Sorption in Hanford Sediment

Simulations of unsaturated flow and phosphate transport through a 1-m column were performed with the STOMP simulator (White and Oostrom 2006) to quantify hydrolysis and sorption rates for tripoly-, pyro- and orthophosphate in Hanford sediment. These experiments were performed by Mart Oostrom and Tom Wietsma in 2009, and were designated experiments 60295-41 and 6295-46A. For these simulations, the STOMP-W operational mode was used with Courant-limited TVD solute transport. The column was one meter in length, with a cross-sectional area of 20.27 cm^2. The column is assumed to be fully packed with Hanford sediment. Hydraulic and solute transport properties used to model the experiments are shown in Table 2.4.

Water was injected at the top boundary of the vertical column, and allowed to drain out the bottom at atmospheric pressure. Boundary conditions for each experiment are shown in Table 2.5. The boundary conditions are very similar, except that the flow rate for experiment 60295-46A, 10 cm/hr, is twice that for experiment 60295-41, 5 cm/hr.

Retardation of phosphate species was simulated using kinetic Langmuir sorption isotherms (Eq. (2.13)). Parameters for this model were fitted to experimental results for ortho-, pyro- and tripolyphosphate.

Table 2.4. Hydraulic and solute transport properties used for Hanford sediment in column experiments 60295-41 and 60295-46A.

Parameter	Value
Porosity, ϕ, %	30.2
Bulk density, ρ_b	1.85
Hydraulic conductivity, cm/min	30.5
van Genuchten α, 1/cm	0.82
van Genuchten n	2.68
Irreducible water saturation, s_r	0.024
Solute diffusion coefficient, cm^2/s	$1x10^{-9}$

Table 2.5. Upper boundary conditions for two columns packed with Hanford Sediment

Parameter	Experiment 60295-41	Experiment 60295-46A
Flow Rate, cm/hr	5	10
Injection Time, hr	23.05	26.75
Average Inlet Br Concentration, mg/L	110.86	95.28
Average Inlet Orthophosphate Conc., mg/L	4889.6	4555.31
Average Inlet Pyrophosphate Conc., mg/L	38.96	38.46
Average Inlet Tripolyphosphate Conc., mg/L	476.74	421.56

The hydrolysis reactions for sodium tripolyphosphate and sodium pyrophosphate were assumed to have the forms

$$Na_5P_3O_{10} + H_2O \rightarrow Na_4P_2O_7 + NaPO_4^{2-} + 2H^+ \tag{2.14}$$

$$Na_4P_2O_7 + H_2O \rightarrow 2NaPO_4^{2-} + 2Na^+ + 2H^+ \tag{2.15}$$

Constant hydrolysis rates were assumed for each species.

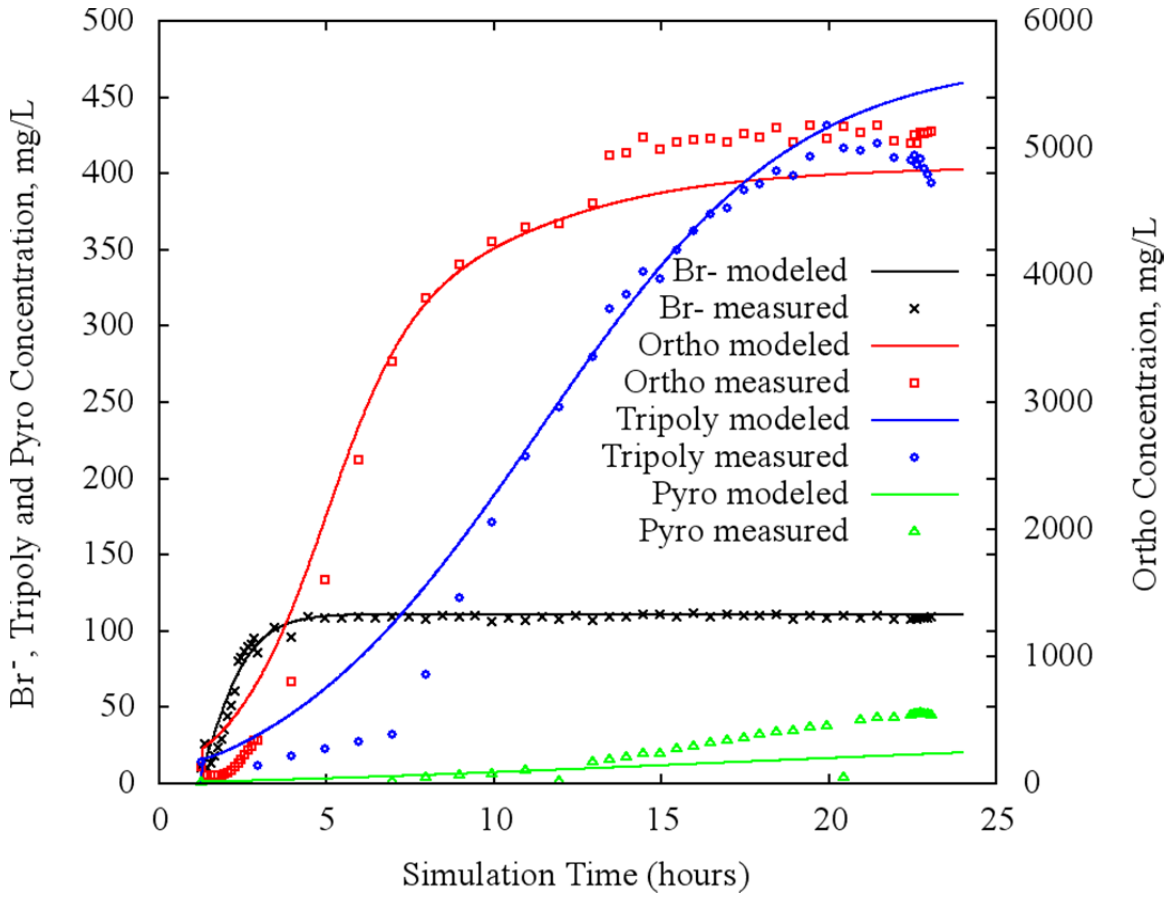

Figure 2.18. Comparison of measured and modeled results for experiment 60295-41 with 5 cm/hr flow rate.

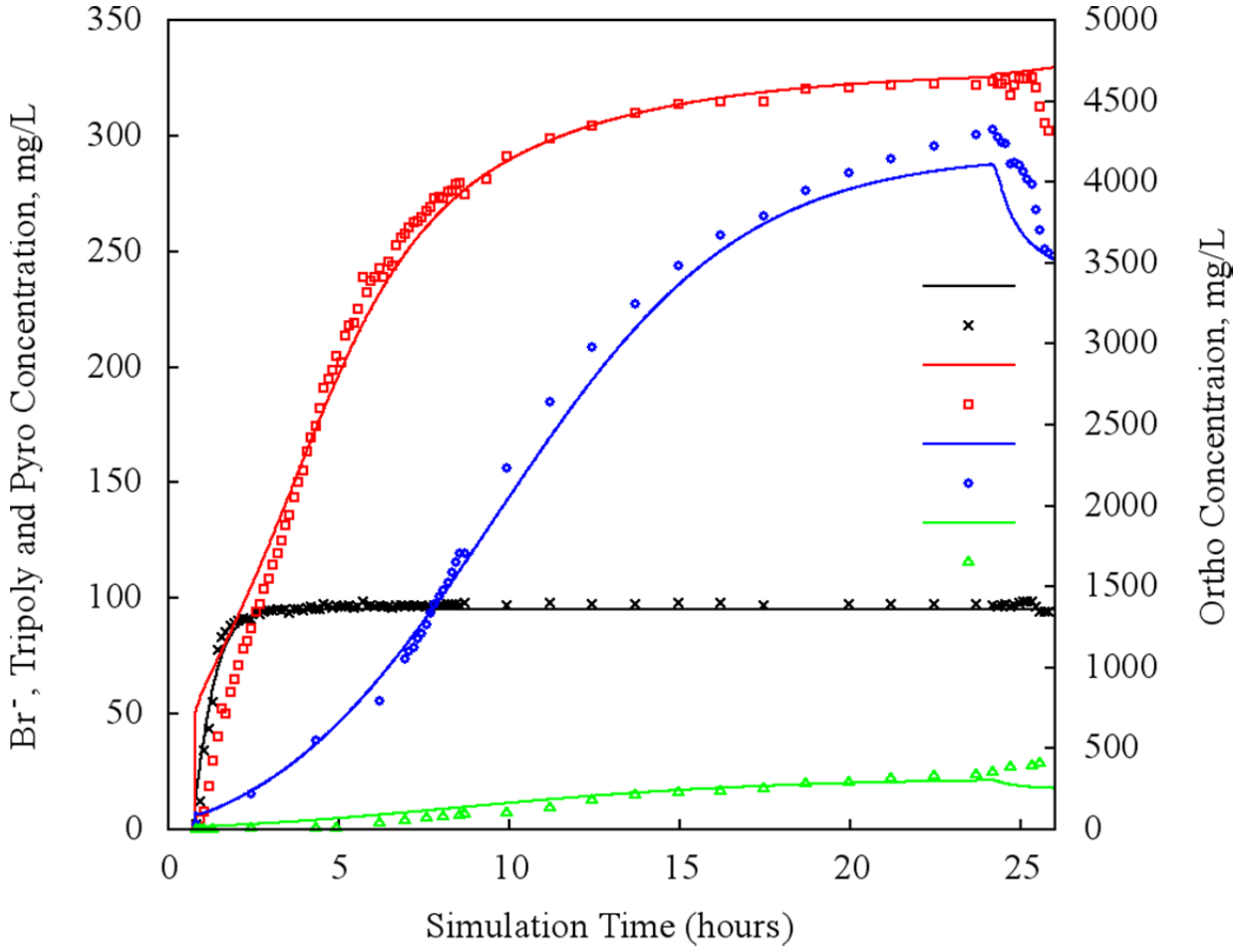

Figure 2.19. Comparison of measured and modeled results for experiment 60295-46A with 10 cm/hr flow rate

Parameters for Eq. (2.13), Eq. (2.14), and Eq. (2.15) were varied to best fit the observed Br and P species from experiments 60529-41 (Figure 2.18) and 60529-46A (Figure 2.19).

A longitudinal dispersion coefficient of 10 cm was obtained by calibrating to the Br- breakthrough curves for each experiment. Parameters for the kinetic Langmuir adsorption Eq. (2.13) for each phosphate species were fit to data for each of the two experiments (Table 2.6). Sorption rates and amounts are within the same order of magnitude for both experiments. The maximum amount of each of the phosphate species sorbed (β) ranges from 8×10^{-4} to 1.75×10^{-2} mol/kg, which is consistent with the total amount of phosphate adsorbed during the experiments, between 1×10^{-2} and 2×10^{-2} mol/kg.

Table 2.6. Parameters for kinetic Langmuir adsorption reactions calibrated to experimental data.

Species	Experiment	Forward Rate (k_f)	Backward Rate (k_b)	Max. Amount Sorbed (β), mol/kg
Orthophosphate	60295-41	20 mol/min	20 mol/min	$1x10^{-2}$
	60295-46A	10 mol/min	10 mol/min	$1.75x10^{-2}$
Pyrophosphate	60295-41	1.0 mol/s	1.0 mol/s	$8x10^{-4}$
	60295-46A	1.0 mol/s	1.0 mol/s	$8x10^{-4}$
Tripolyphosphate	60295-41	1.0 mol/s	1.0 mol/s	$8x10^{-4}$
	60295-46A	1.3 mol/s	1.3 mol/s	$1.3x10^{-3}$

The model assumes that tripolyphosphate is converted to pyrophosphate and orthophosphate via Eq. (2.14). A constant forward-rate equation was used in ECKEChem. For experiment 60295-46A, the best fit to the steady-state tripolyphosphate concentrations is obtained by assuming a hydrolysis rate of 6.5×10^{-2} mol/min for tripolyphosphate and 6.5×10^{-3} mol/min for pyrophosphate. For experiment 60295-41, no hydrolysis of tripolyphosphate or pyrophosphate to orthophosphate is required to fit the data.

2.5.3.3 Simulation of Polyphosphate Remediation of North Process Pond Sediment

The reaction network developed thus far was used to model the North Process Pond sediment columns reported in (Wellman et al. 2008). Sediment from the North Process Pond in the 300 Area was treated with 100% tripolyphosphate solution in Hanford groundwater, as well as untreated groundwater, to assess the potential for tripolyphosphate remediation (Wellman et al. 2008). A 5-gal container with a shovel was used to collect the sample from an excavated trench approximately 8 m beneath the current ground surface. These sediments were collected prior to the excavation activities being completed and overlaid a U(VI) groundwater plume containing U(VI) concentrations that range from ~0.042 to 1.05 μmol/L; fluctuations in the Columbia River stage can cause the groundwater elevation to vary significantly. The cobble size and material >0.635 cm were removed during field collection.

Dynamic tests were conducted under unsaturated conditions using the pressurized unsaturated flow (PUF) system (Pierce et al. 2006; Wierenga and van Genuchten 1989). Columns were packed with Hanford vadose zone sediment in approximately 5-g increments that were tamped and the surface was scored prior to adding subsequent layers. Flow was initiated through the columns with Hanford groundwater until steady-state water content was attained at the desired degree of saturation. After the attainment of hydraulic and chemical equilibrium, the influent solution was changed to Hanford groundwater containing the polyphosphate formulation. A control column with groundwater was also run for comparison.

Additional kinetic reactions involving minerals were considered (Table 2.7). Calcite was included as a primary mineral species. The other minerals are potential secondary precipitates.

For the control column (Figure 2.20), the observed trend in uranium concentrations for the control column could be matched by assuming the same kinetic Langmuir adsorption parameters (Table 2.8) as were used for the ICE-1 column in section 2.5.3.1. In order to match the observed decrease in uranium for the tripolyphosphate column (Figure 2.21), the log K for either Na-meta-autunite or chernikovite had to be lowered to a value of -33. Otherwise, simulated uranium concentrations remained high. This is

consistent with results of Fanizza et al. (2013), who observed chernikovite precipitation despite the unfavorable equilibrium constant.

The observed trend in Ca concentrations for both columns could be matched by assuming a small amount of calcite, 1% by volume, was initially present in the sediment, with a surface area of 0.1 m^2/kg. The observed trends in total phosphate for both columns could be matched using similar rate parameters (Table 2.8) to those used to model the experiments in section 2.5.3.1. The observed trends in total sodium are consistent with Hanford groundwater concentrations and the additional sodium added by the tripolyphosphate solution.

Table 2.7. Parameters for kinetic Langmuir adsorption reactions calibrated to North Process Pond column.

Species	Forward Rate (k_f)	Backward Rate (k_b)	Max. Amount Sorbed (β), mol/kg
$>SOUO_2(HCO_3CO_3)^{2-}$	1 mol/hr	1 mol/hr	$3.82x10^{-5}$ mol/g
Orthophosphate	1 mol/min	1 mol/min	$3x10^{-2}$
Pyrophosphate	1.0 mol/s	1.0 mol/s	$1x10^{-3}$
Tripolyphosphate	1.0 mol/s	1.0 mol/s	$4x10^{-3}$

Table 2.8. Kinetic mineral reactions for polyphosphate remediation simulations.

Kinetic mineral reaction	Log K	Rate, mol m^{-3} s^{-1}
$Ca\text{-Meta-Autunite} = Ca^{2+} + 2PO_4^{3-} + 2UO_2^{2+} + 3H_2O$	-48.36[a]	$3.15x10^{-9}$[d]
$Na\text{-Meta-Autunite} = PO_4^{3-} + Na^{+} + UO_2^{2+} + H_2O$	-23.64[a]	$1.48x10^{-9}$[d]
$Hydroxyapatite + 4H^{+} = 3HPO_4^{2-} + 5Ca^{2+}$	-7.3676[b]	$1.0x10^{-6}$[e]
$Chernikovite = UO_2^{2+} + HPO_4^{2-}$	-24.20[a]	$1x10^{-8}$[f]
$Uranyl\ Hydrogen\ Phosphate = UO_2^{2+} + HPO_4^{2-}$	-25.52[c]	$1x10^{-8}$[f]
$Uranyl\ Orthophosphate = 3UO_2^{2+} + 2PO_4^{3-}$	-49.36[a]	$1x10^{-8}$[f]
$Calcite + H+ = Ca^{2+} + HCO_3^{-}$	1.6995[b]	$1.55x10^{-6}$[e]

(a) Grenthe et al. 1992
(b) Wolery and Jarek 2003
(c) Gorman-Lewis et al. 2009
(d) Gudavalli et al. 2013
(e) Palandri and Kharaka 2004
(f) Estimate

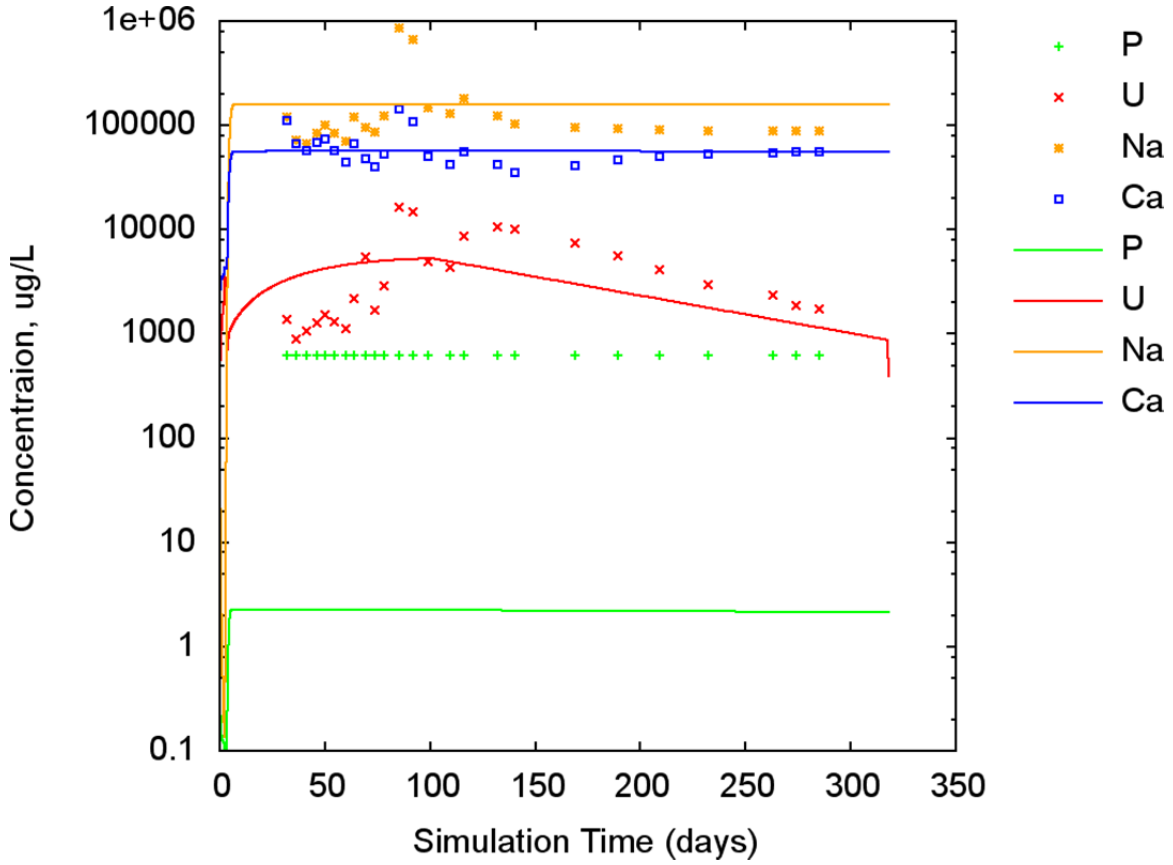

Figure 2.20. Comparison of measured and modeled results for the North Process Pond control PUF column. Reported phosphate concentrations are at the detection limit.

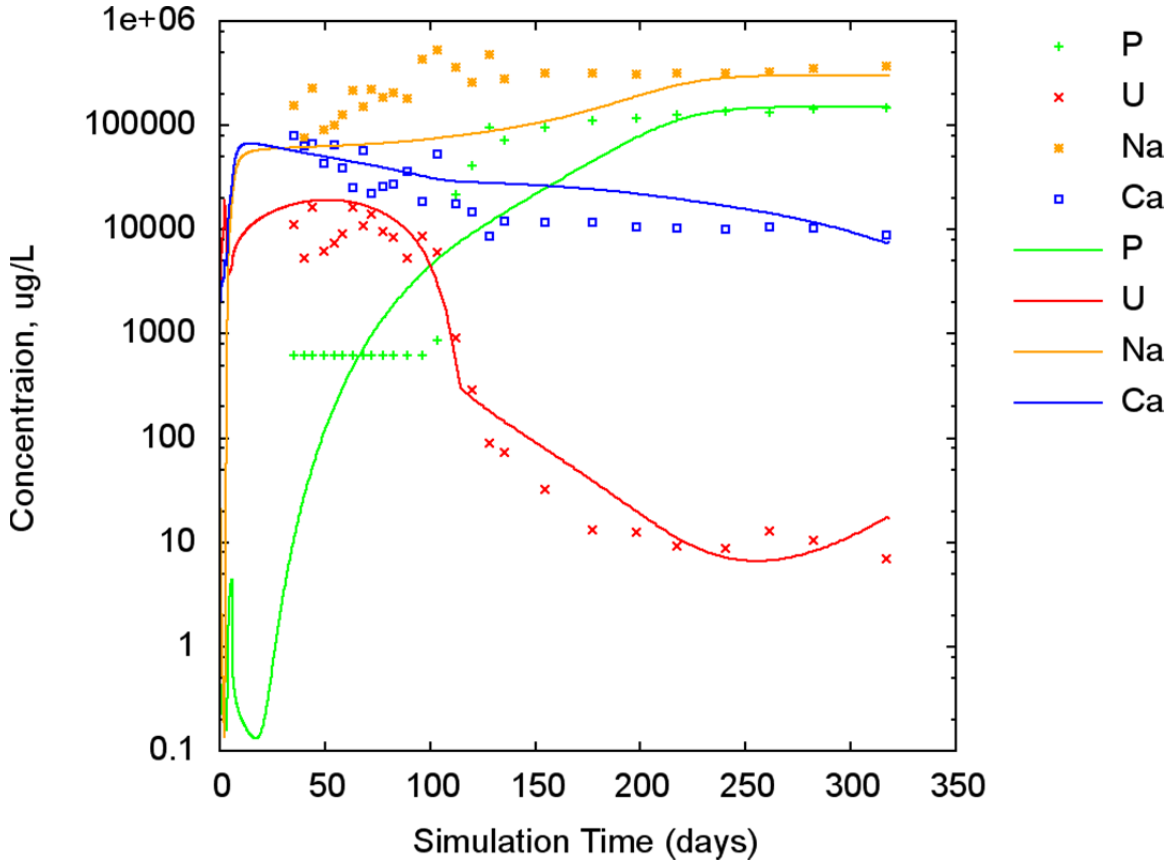

Figure 2.21. Comparison of measured and modeled results for the North Process Pond tripolyphosphate PUF column.

Although preliminary, these simulation results are encouraging in terms of the development of a reaction network that reproduces laboratory experimental results. The data shown in Figure 2.21 reveal a reduction in U(VI) concentrations by three orders of magnitude resulting from the addition of polyphosphate. The actual effectiveness of the polyphosphate treatment technology applied to vadose zone U(VI) contamination in the field still remains to be seen. The models developed herein may be useful for evaluating this impact. Some preliminary results are described in the next section.

3.0 Field-Scale Simulations

Field-scale simulations were performed of water flow, tracer transport, and reactive transport of uranium with polyphosphate reactions to illustrate model capabilities. All simulations were performed on PNNL's Olympus computing cluster. Olympus has 694 compute nodes (dual socket, 2.1 GHz, 16 core AMD Interlagos, with 64 GB, 1600 MHz memory), for a total of 22,208 processors, and is capable of ~185 Teraflops peak performance.

3.1 River Water Incursion and Tracer Transport at IFRC Site

Prior to reactive transport simulations, the flow and tracer transport model was calibrated. Figure 3.1 shows a simulated chloride concentration distribution at the 105 m elevation based on the calibrated model. The region in red, showing chloride concentrations >35 mg/L, is a tracer plume from the spring 2011 tracer test performed at the IFRC site. The time shown is 3000 hr since Jan. 1, 2011, 00:00.

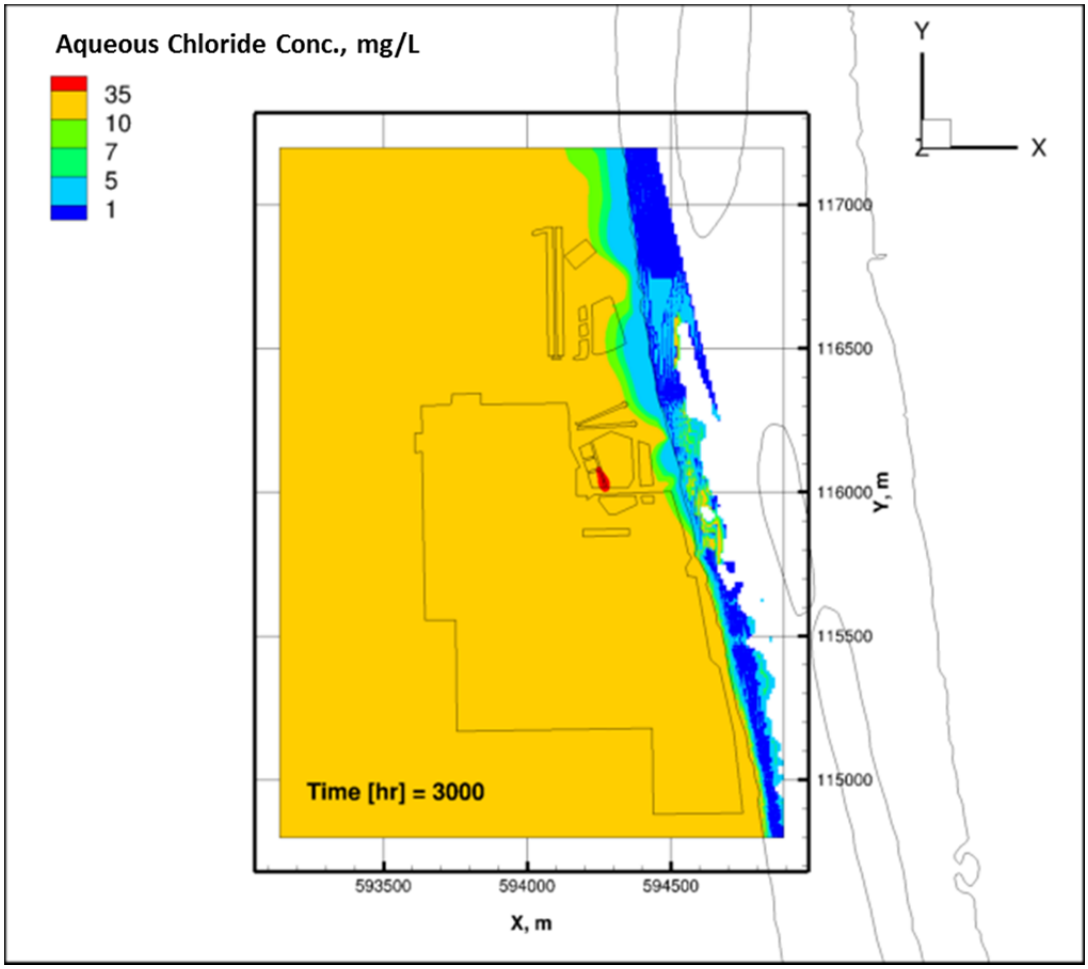

Figure 3.1. Simulated chloride concentration distribution over the 300 Area and tracer plume from the spring 2011 tracer test at IFRC site, for a time of 3000 hr since Jan 1, 2011.

Figure 3.2 shows a simulated chloride concentration distribution over the 300 Area for a time of 4100 hr since Jan. 1, 2011, 00:00. This time is near the maximum river stage for 2011. Note that the tracer plume from the IFRC site is no longer visible from this view. These results, and measured well concentration data, indicate that under current dam operations river water can easily move 300 meters or more inland. Thus, the areas underlying most or all of the former liquid effluent disposal areas can experience water compositions ranging from ambient groundwater to relatively dilute groundwater influenced by river water incursion. The highly dynamic nature of this groundwater system provided many challenges to the field experimental campaigns and modeling for the IFRC site.

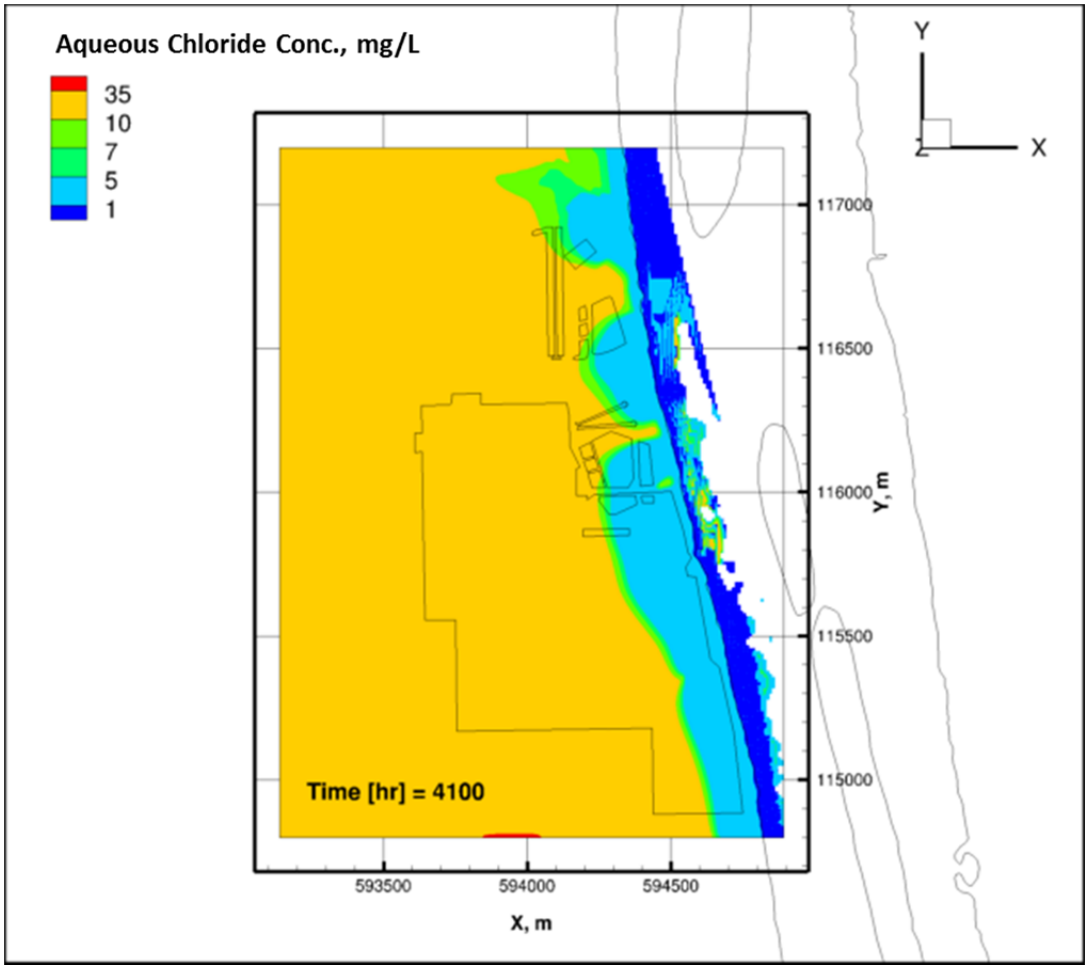

Figure 3.2. Simulated chloride concentration distribution over the 300 Area for a time of 4700 hr since Jan 1, 2011. Note that the higher concentrations shown by the very small red region at the lower central portion of the model domain are not from the IFRC tracer test, but are from specified boundary conditions developed from monitoring well data.

3.2 Response of Uranium-Contaminated Sediments to Polyphosphate Infiltration

The DOE proposed cleanup plan for the Hanford 300 Area calls for polyphosphate injection for treatment of the periodically rewetted zone during high river stage, followed by infiltration of a polyphosphate solution over a ~3 acre area to treat vadose zone sediments

(http://www.hanford.gov/files.cfm/CAL_300_Area_Fact_Sheet_Final_071513.pdf; last referenced Sept. 30, 2013). Preliminary simulations were performed of the second stage of this plan with polyphosphate infiltration over the uranium hot spot shown previously in Figure 2.3, using the polyphosphate reaction network described in section 2.5. Simulations were performed for a scenario with a constant infiltration rate of 10 cm/hr applied for four days during a period of low river stage, with 4.74e-2 mol/L PO_4^{---} and 1.75e-3 mol/L $Na_5P_3O_{10}$(aq) contained in the infiltrating water. Figure 3.3 shows simulated aqueous PO_4^{--} concentrations in the area of infiltration overlying the uranium hot spot.

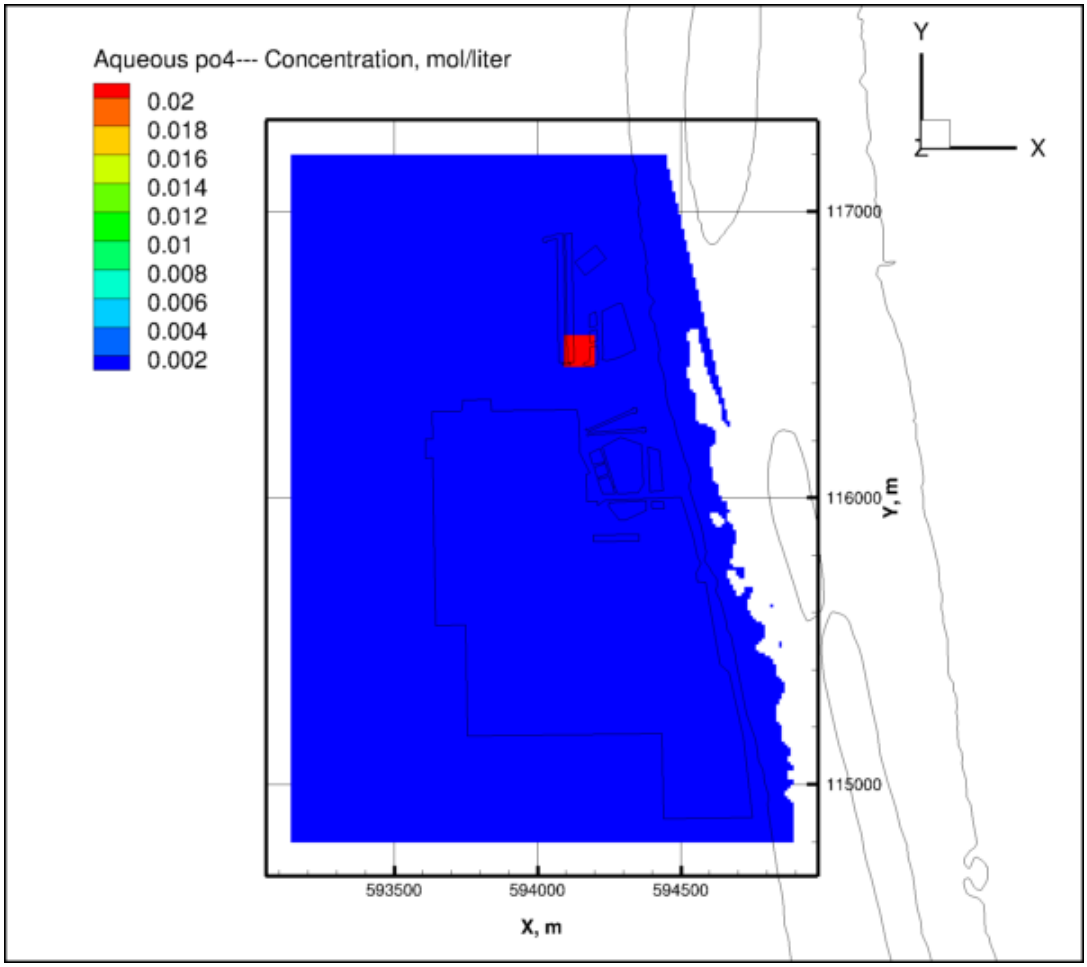

Figure 3.3. Simulated phosphate distribution at ground surface during polyphosphate infiltration over a uranium hot spot.

Figure 3.4 shows the total aqueous uranium concentrations at the 107.5 m elevation after 4 days of infiltration. The wetting front of the infiltrating polyphosphate solution appears to be displacing a fraction of the mobile uranium from the vadose zone and upper capillary fringe region in what essentially amounts to soil flushing, with calculated total aqueous uranium concentrations at the displayed elevation exceeding 400 µg/L. These results suggest that it may be prudent to provide treatment in the underlying groundwater. The extent to which mineralization may stabilize residual uranium after the initial emplacement of the polyphosphate and displacement of some of the uranium has not yet been evaluated. However, it would seem from these preliminary results that further investigation is warranted.

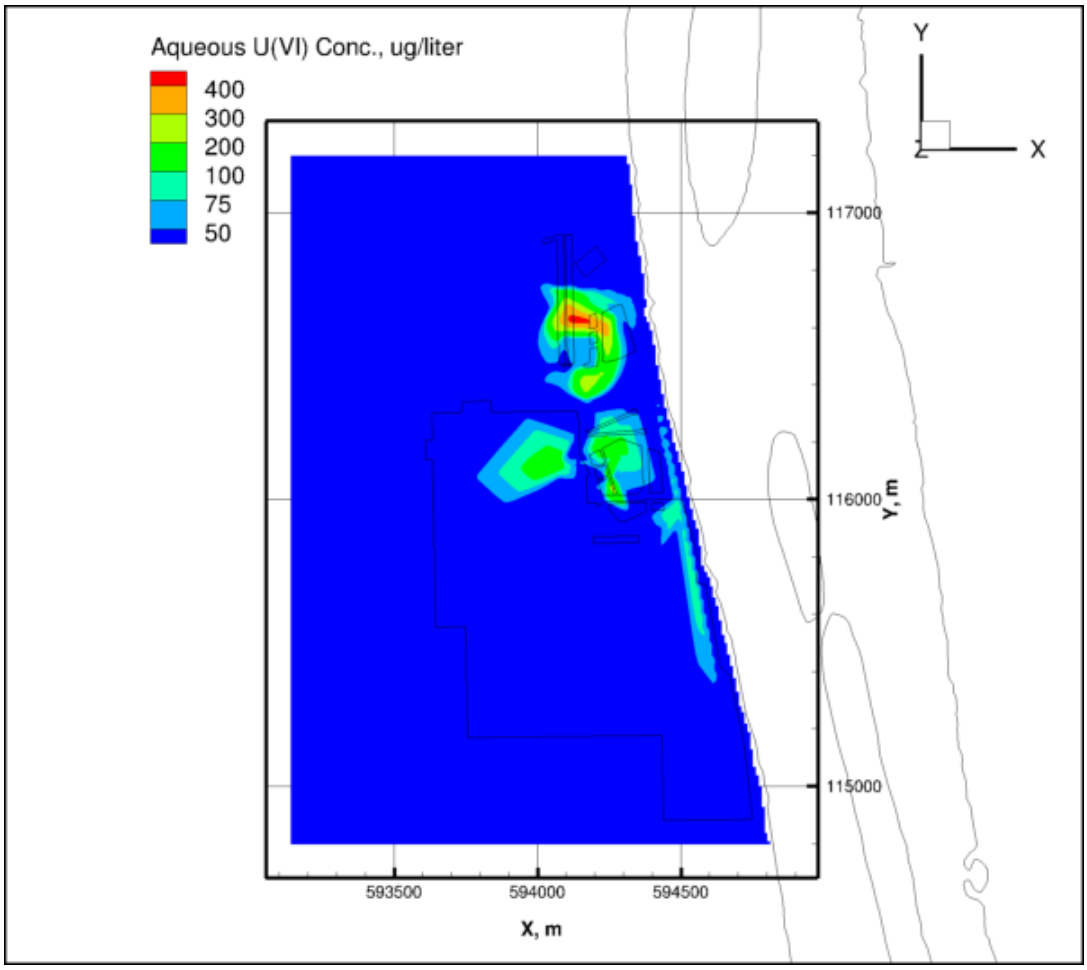

Figure 3.4. Simulated aqueous uranium concentrations at the 107.5 m elevation after four days of polyphosphate infiltration.

The system-scale model of the 300 Area can be readily used to evaluate different scenarios related to infiltration rates, polyphosphate species mixture composition and concentrations, and the resulting impact on uranium displacement and mineral formation.

One related issue that should be mentioned is the permeability of the near-surface sediments in this part of the 300 Area. PNNL performed a series of infiltration experiments (unpublished) in anticipation of a subsequent polyphosphate infiltration treatment test. The permeability of the near-surface sediments was found to be much lower than that of the underlying aquifer materials. Scraping and shallow excavation was required to remove low permeability silt and caliche material to obtain reasonable infiltration rates. Similar measures will likely be needed prior to the actual polyphosphate infiltration test.

4.0 Conclusions

A system-scale model of the 300 Area was developed to provide DOE with a decision support tool that integrates all relevant site characterization and monitoring data with process models for subsurface flow and uranium reactive transport with polyphosphate reactions. This decision support tool enables the effective evaluation of remediation endpoints and assists with design and implementation of specific remedial activities. To the best of our knowledge this work represents the first successful attempt to model the reactive transport of uranium in the 300 Area at the full plume scale, including reactions associated with an active remediation approach using polyphosphate, and with accurate accounting of remaining in-ground inventory of contaminant uranium.

The model synthesizes and integrates historical data and the latest characterization, monitoring, and experimental data, and process models from DOE Office of Science, Office of Environmental Management, and Richland Operations Office studies. The hydraulic properties of the model were calibrated using observed water levels and chloride data that included results from a field tracer test performed at the IFRC site. Very good correspondence was obtained between simulated water levels and chloride concentrations, and measured data from 24 observation wells. Reaction networks for the model were also developed using laboratory experimental data generated with support from multiple DOE offices. Good matches were obtained for simulated and observed uranium data and other aqueous species concentrations measured in the laboratory column experiments. The model was applied to evaluate the possible effects of polyphosphate infiltration over a uranium hot spot on uranium mobility. The results, which did not consider any pretreatment of the periodically rewetted zone, suggest that infiltration without such pretreatment may result in significant mobilization of uranium. The simulations also did not consider treatment of groundwater to capture mobilized uranium. The preferred alternative for additional remediation of the 300 Area calls for pretreatment of the periodically rewetted zone and groundwater, which may mitigate uranium mobilization and subsequent transport in groundwater.

Prior to application of the system-scale model of the 300 Area to evaluation of remediation endpoints or specific remediation scenarios, several additional activities should be considered. First, other field experimental data (uranium desorption/adsorption) are available from both the IFRC site and from the polyphosphate treatability test site that were not used in the current study. These data could be used for additional testing, calibration, and model refinement in specific areas of interest for site remediation. Second, continued monitoring of the 300 Area well network and river gauging station will be required to provide data for initial and boundary conditions for time periods beyond 2012. Third, additional characterization of the near surface sediments in the area of the proposed polyphosphate infiltration test may be warranted since field permeameter tests showed that this material has much lower permeability than the sediments in the underlying aquifer. Updating local hydraulic properties in the model to reflect polyphosphate infiltration site characteristics should improve its accuracy. The system-scale model described herein can be readily used to evaluate scenarios involving variable infiltration rates, different solution compositions, optimal well placement for monitoring or plume capture, and the potential long-term impacts of remedial activities. Finally, simulation results in this report were generated using eSTOMP, a parallel version of the STOMP simulator. This code is currently undergoing verification and benchmark testing for NQA-1 qualification. Testing is nearing completion, but documentation of the code and test results will not be finished until late FY14 or early FY15. The code or model cannot be used to provide formal support for license- or regulatory–related applications until NQA-1 qualifications are complete.

5.0 References

40 CFR 141.66, "Federal Safe Drinking Water Act," *Code of Federal Regulations*, Subpart G – National Primary Water Regulations: Maximum Contaminant Levels and Maximum Residual Disinfectant Levels; Maximum Contaminant Levels for Radionuclides, as amended.

Bethke CM. 2005. *Geochemist Workbench Release 6.0.* University of Illinois, Urbana-Champaign, Illinois.

Bethke CM and PV Brady. 2000. "How the Kd approach undermines ground water cleanup." *Ground Water* 38(3):435-443, doi: 10.11 11/j.1745-6584.2000.tb00230.x.

Bond DL, JA Davis, and JM Zachara. 2008. "Uranium (VI) release from contaminated vadose zone sediments: Estimation of potential contributions from dissolution and desorption," in *Adsorption of Metals by Geomedia II: Variables, Mechanisms, and Model Applications*, MO Barnett and DB Kent (eds.), chap 14, pp. 375-416, Elsevier, Amsterdam, Netherlands.

BHI. 1998. 300 Area Process Trenches Verification Package. BHI-01164, Bechtel Hanford, Inc. Richland, Washington.

BHI. 2002. *Protection of 300 Area Groundwater from Uranium-Contaminated Soils at Remediation Sites*. BHI-01667, Rev. 0, Bechtel Hanford, Inc. Richland, Washington.

BHI. 2003. Cleanup Verification Package for the South Process Pond (WIDS Site 316-1), the Retired Filter Backwash Pond (WIDS Site 300 RFBP), 300-262 Contaminated Soil, and Unplanned Release Sites UPF-300-32, UPR-300-33, UPR-300-34, UPR-300-35, UPR-300-36, UPR-300-37, and UPR-300-FF-1. CVP-2003-00002, Rev. 0, Bechtel Hanford Inc., Richland, Washington.

Bjornstad BN, JA Horner, VR Vermeul, DC Lanigan, and PD Thorne. 2009. *Borehole Completion and Conceptual Hydrogeologic Model for the IFRC Well Field, 300 Area, Hanford Site. Integrated Field Research Challenge Project*. PNNL-18340, Pacific Northwest National Laboratory, Richland, Washington.

Brooks SC, JK Fredrickson, SL Carroll, DW Kennedy, JM Zachara, AE Plymale, SD Kelly, KM Kemner, and S Fendorf. 2003. "Inhibition of bacterial U(VI) reduction by calcium." *Environmental Science and Technology* 37:1850-1858.

Chen X, H Murakami, MS Hahn, GE Hammond, ML Rockhold, JM Zachara, and Y Rubin. 2012. "Three-dimensional Bayesian geostatistical aquifer characterization at the Hanford 300 Area using tracer data." *Water Resour. Res.* 48:W06501, doi:10.1029/2011WR010675.

Coleman AM, DL Ward, KB Larson, and JW Lettrick. 2010. *Development of a high-resolution bathymetry dataset for the Columbia River through the Hanford Reach*. PNNL-19878, Pacific Northwest National Laboratory, Richland, Washington.

Davis JA and DB Kent. 1990. "Surface complexation modeling aqueous geochemistry," in *Mineral-Water Interface Geochemistry, Reviews in Mineralogy*, MF Hochella and AF White (eds.), pp. 177-260, Mineralogical Society of America, Washington, D.C.

DOE-RL. 1992. Expedited Response Action Assessment for the 316-5 Process Trenches. DOE/RL-91-11, U.S. Department of Energy, Richland Operations Office, Richland, Washington.

DOE-RL. 1994a. *Phase 1 Remedial Investigation Report for the 300-FF-5 Operable Unit*. DOE/RL-93-21, Rev. 0, Vols. 1 (information) and 2 (data listings), U.S. Department of Energy, Richland, Operations Office, Richland, Washington.

DOE-RL. 1994b. *Remedial Investigation/Feasibility Study Report for the 300-FF-5 Operable Unit*. DOE/RL-94-85, U.S. Department of Energy, Richland, Operations Office, Richland, Washington.

DOE-RL. 2013a. *Remedial Investigation/Feasibility Study for the 300-FF-1, 300-FF-2, and 300-FF-5 Operable Units*. DOE/RL-2010-99, Rev. 0, CH2MHILL Plateau Remediation Company, Richland, Washington.

DOE-RL. 2013b. Hanford Site Groundwater Monitoring Report for 2012. DOE/RL-2013-22, Rev. 0, Prepared form U.S. Department of Energy by CH2M Hill Plateau Remediation Company, Richland, Washington.

DOE-RL. 2005. *300-FF-1 Operable Unit Remedial Action Report*. DOE/RL-2004-74, Rev. 0, U.S. Department of Energy, Richland, Washington.

Doherty JE and RJ Hunt. 2010. *Approaches to highly parameterized inversion – A guide to using PEST for groundwater-model calibration*. U.S. Geological Survey Scientific Investigations Report 2010-5169.

Dong W, WP Ball, C Liu, Z Wang, AT Stone, J. Bai, and JM Zachara. 2005. "Influence of calcite and dissolved calcium on uranium(VI) sorption to a Hanford subsurface sediment." *Environmental Science and Technology* 39:7949-7955.

Dong W and SC Brooks. 2006. "Determination of the formation constants of ternary complexes of uranyl and carbonate with alkaline earth metal (Mg2+, Ca2+, Sr2+, and Ba2+) using anion exchange method." *Environ. Sci. Technol*. 40:4689-4695.

Fanizza MF, H Yoon, C Zhang, M Oostrom, TW Wietsma, NJ Hess, ME Bowden, TJ Strathmann, KT Finneran, and CJ Werth. 2013. "Pore-scale evaluation of uranyl phosphate precipitation in a model groundwater system." *Water Resour. Res.* 49(2):874-890.

Fetter CW. 1993. Contaminant Hydrogeology. Macmillan Publishing Company, New York.

Fox PA, JA Davis, and JM Zachara. 2006. "The effect of calcium on aqueous uranium(VI) speciation and adsorption to ferrihydrite and quartz." *Geochim. Cosmochim. Acta* 70(6):1379-1387.

Gorman-Lewis D, T Shvareva, K-A Kubatko, DMW Peter C. Burnsa, B McNamara, JES Szymanowski, A Navrotsky, and JB Fein. 2009. "Thermodynamic properties of autunite, uranyl hydrogen phosphate, and uranyl orthophosphate from solubility and calorimetric measurements." *Environmental Science and Technology* 43:7416-7422.

Grenthe I, J Fuger, RJM Konings, RJ Lemire, AB Muller, C Nguyen-Trung, and H Wanner. 1992. *Chemical Thermodynamics, Volume 1: Chemical Thermodynamics of Uranium*. North-Holland, Amsterdam.

Greskowiak J, MB Hay, H Prommer, C Liu, VEA Post, R Ma, JA Davis, C Zheng, and JM Zachara. 2011. "Simulating adsorption of U(VI) under transient groundwater flow and hydrochemistry: Physical versus chemical nonequilibrium models." *Water Resour. Res.* 47:W08501, doi:10.1029/2009WR008819.

Gudavalli RKP, YP Katsenovich, DM Wellman, M Idarraga, LE Lagos, and B Tansel. 2013. "Comparison of the kinetic rate law parameters for the dissolution of natural and synthetic autunite in the presence of aqueous bicarbonate ions." *Chemical Geology* 351:299-309.

Hammond GE and PC Lichtner. 2010. "Field-scale model for the natural attenuation of uranium at the Hanford 300 Area using high performance computing." *Water Resour. Res.* 46, W09527, doi:10.1029/2009WR008819, 1-31.

Hammond GE, PC Lichtner, and ML Rockhold. 2011. "Stochastic simulation of uranium migration at the Hanford 300 Area." *J. Contam. Hydrol.* 120-121:115-128.

Hill MC. 1998. Methods and Guidelines for Effective Model Calibration. Water-Resources Investigations Report 98-4005, U.S. Geological Survey, Denver, Colorado.

Lagos LE, J Varona, A Zidan, and R Gudavalli. 2007. *Fixative analysis for soil stabilization activities at Hanford*. Applied Research Center, Florida International University, Miami, Florida.

Lerch JA. 1999. 300-FF-1 Operable Unit, North Process Pond/Scraping Disposal Area Verification Package. BHI-01298, Rev. 0, Bechtel Hanford, Inc. Richland, Washington.

Lindberg JW and FW Bond. 1979. *Geohydrology and Groundwater Quality Beneath the 300 Area, Hanford Site, Washington.* PNL-2949, Pacific Northwest National Laboratory, Richland, Washington.

Liu C, J Shang, S Kerisit, JM Zachara, and W Zhu. 2013. "Scale-dependent rates of uranyl surface complexation reaction in sediments." *Geochimica et Cosmochimica Acta* 105:326-341.

Liu C, S Shi, and JM Zachara. 2009. "Kinetics of uranium(VI) desorption from contaminated sediments: Effect of geochemical conditions and model evaluation." *Environ. Sci. Tech.* 43(17):6560-6566.

Liu C, JM Zachara, NP Qafoku, and Z Wang. 2008. "Scale-dependent desorption of uranium from contaminated subsurface sediments. *Water Resour. Res.* 44, W08413, doi.1029/2007WR006478.

Ma R, C Zheng, H Prommer, J Greskowiak, C Liu, J Zachara, and M Rockhold. 2010. "A field-scale reactive transport model for U(VI) migration influenced by coupled multirate mass transfer and surface complexation reactions." *Water Resour. Res.* 46, W05509, doi:10.1029/2009WR008168.

Meyer PD, M Ye, SP Neuman, and ML Rockhold. 2007a. "Application of Maximum Likelihood Bayesian Model Averaging to Groundwater Flow and Transport at the Hanford Site 300 Area." In *ModelCARE 2007, Proceedings of the International Conference on Calibration and Reliability in Groundwater Modeling*, Sept. 9-13. Copenhagen, Denmark.

Meyer PD, M Ye, ML Rockhold, SP Neuman, KJ Cantrell. 2007b. *Combined estimation of hydrogeologic conceptual model, parameter, and scenario uncertainty with application to uranium transport at the Hanford Site 300 Area*. NURGE/CR-6940/PNNL-16396, Pacific Northwest National Laboratory, Richland, Washington.

Murakami H, X Chen, MS Hahn, ML Rockhold, VR Vermeul, JM Zachara, and Y Rubin. 2010. "Bayesian approach for three-dimensional aquifer characterization at the Hanford 300 Area." *Hydrology and Earth System Sciences* 14:1989-2001, doi:10.5194/h3ss-14-1989-2012

Murray CJ, JM Zachara, JP McKinley, A Ward, Y-J Bott, K Draper, and D Moore. 2012. "Establishing a geochemical heterogeneity model for a contaminated vadose zone - aquifer system." *J. Contam. Hydrol.* doi: 10.1016/j.jconhyd.2012.02.003.

Nichols WE. 2012. *Groundwater Flow and Uranium Transport Modeling in Support of the 300 Area FF-5 RI/FS Document*. ECF-300FF5-11-0151, Rev. 3, CH2MHill, Richland, Washington.

Palandri JL and YK Kharaka. 2004. *A Compilation of Rate Parameters of Water-Mineral Interaction Kinetics for Application to Geochemical Modeling*. U.S. Geological Survey, Menlo Park, California.

Peterson RE (editor). 2005. *Contaminants of Potential Concern in the 300-FF-5 Operable Unit: Expanded Annual Groundwater Report for FY2004*. PNNL-15127, Pacific Northwest National Laboratory, Richland, Washington. (Contributors: EJ Freeman, CJ Murray, RE Peterson, PD Thorne, MJ Truex, VR Vermeul, MD Williams, SB Yabuskai, JM Zachara, JL Lindberg, and JP McDonald).

Peterson RE (editor). 2008. *Uranium Contamination in the Subsurface Beneath the 300 Area, Hanford Site, Washington*. PNNL-17034. Pacific Northwest National Laboratory, Richland, Washington. (Contributors: RE Peterson, ML Rockhold, RJ Serne, PD Thorne, and MD Williams)

Pierce EM, BP McGrail, MM Valenta, and DM Strachan. 2006. "The Accelerated Weathering of a Radioactive Low-Activity Waste Glass Under Hydraulically Unsaturated Conditions: Experimental Results from a Pressurized Unsaturated Flow Test." *Nuclear Technology* 155(2):149-165.

Richmond MC and WA Perkins. 2009. "Efficient Calculation of Dewatered and Entrapped Areas Using Hydrodynamic Modeling and GIS." *Environmental Modeling & Software* 24(12):1447-1456. doi:10.1016/j.envsoft.2009.06.001

Rockhold ML, DL Saunders, CE Strickland, SR Waichler, and RE Clayton. 2009. *Soil Water Balance and Recharge Monitoring at the Hanford Site – FY09 Status Report*. PNNL-18807, Pacific Northwest National Laboratory, Richland, Washington.

Rockhold ML, DH Bacon, VL Freedman, MJ Lindberg, and RE Clayton. 2012. *Numerical Modeling of ^{90}Sr and ^{137}Cs Transport from a Spill in the B-Cell of the 324 Building, Hanford Site 300 Area*. PNNL-21214, Pacific Northwest National Laboratory, Richland, Washington.

Shang J, C Liu, Z Wang, and JM Zachara. 2011. "Effect of grain size on uranium (VI) surface complexation kinetics and adsorption additivity." *Environ. Sci. Technol.* 45(14):6025-6031.

Shang J, C Liu, Z Wang, and JM Zachara. 2014. "Long-term kinetics of uranyl desorption from sediments under advective conditions." *Water Resour. Res.*50, 855-870, doi:10.1002/2013WR013949.

Simpson BC, RA Corbin, MJ Anderson, CT Kincaid, and JM Zachara. 2006. *Identification and Classification of the Major Uranium Discharges and Unplanned Releases at the Hanford Site using the Soil Inventory Model (SIM) Rev. 1 Results*. NUV-06-21106-ES-001-DOC, Rev.1, Nuvotec USA, Richland, Washington.

Stoliker DL, DB Kent, and JM Zachara. 2011. "Quantifying differences in the impact of variable chemistry on equilibrium uranium(VI) adsorption properties of aquifer sediments." *Environmental Science & Technology* 45:8733-8740.

Stoliker DL, C Liu, DB Kent, and JM Zachara. 2013. "Characterizing particle-scale equilibrium and kinetics of U(VI) desorption from U-contaminated sediments." *Water Resour. Res.* 49:1163 - 1177, doi:10.1002/wrcr.20104.

Szecsody JE, L Zhong, M Oostrom, VR Vermeul, JS Fruchter, and MD Williams. 2012. *Use of Polyphosphate to Decrease Uranium Leaching in Hanford 300 Area Smear Zone Sediments*. PNNL-21733; RPT-DVZ-AFRI-003, Pacific Northwest National Laboratory, Richland, Washington.

Vermeul VR, BN Bjornstad, BG Fritz, JS Fruchter, RD Mackley, DP Mendoza, DR Newcomer, ML Rockhold, DM Wellman, and MD Williams. 2009. *300 Area Uranium Stabilization through Polyphosphate Injection: Final Report*. PNNL-18529, Pacific Northwest National Laboratory, Richland, Washington.

Vermeul VR, JP McKinley, DR Newcomer, RD Mackley, and JM Zachara. 2011. "River-induced flow dynamics in long-screen wells and impact on aqueous samples." *Groundwater* 49:515-524.

Wang G, RJ Serne, MJ Lindberg, W Um, BN Bjornstad, BD Williams, IV Kutnyakov, Z Wang, and N Qafoku. 2012. *Uranium in Hanford Site 300 Area: Extraction Data on Borehole Sediments*. PNNL-22032/RPT-DVZ-AFRI-009. Pacific Northwest National Laboratory, Richland, Washington.

Wellman DM, JS Fruchter, VR Vermeul, and MD Williams. 2008. *Challenges Associated with Apatite Remediation of Uranium in the 300 Area Aquifer*. PNNL-17480, Pacific Northwest National Laboratory, Richland, Washington.

Wellman DM, JP Icenhower, and AT Owen. 2006. "Comparative Analysis of Soluble Phosphate Amendments for the Remediation of Heavy Metal Contaminants: Effect on Sediment Hydraulic Conductivity." *Environmental Chemistry* 3:219-224.

Wellman DM, JI Icenhower, EM Pierce, BK McNamara, SD Burton, KN Geiszler, SR Baum, and BC Butler. 2005. "Polyphosphate Amendments for In Situ Immobilization of Uranium Plumes." In *Third International Conference on Remediation of Contaminated Sediments*, RF Olfenbuttel and PJ White (eds.), Battelle Press, New Orleans, Louisiana.

Wellman DM, EM Pierce, DH Bacon, M Oostrom, KM Gunderson, SM Webb, CC Bovaird, EA Cordova, ET Clayton, KE Parker, RM Ermi, SR Baum, VR Vermeul, and JS Fruchter. 2008. 3*00 Area Treatability Test: Laboratory Development of Polyphosphate Remediation Technology for In Situ Treatment of Uranium Contamination in the Vadose Zone and Capillary Fringe*. PNNL-17818, Pacific Northwest National Laboratory, Richland, Washington.

Wellman DM, EM Pierce, EL Richards, BC Butler, KE Parker, JN Glovack, SSD Burton, R Baum, ET Clayton, and EA Rodriguez. 2007. *300 area uranium plume treatability demonstration project*. PNNL-16683, Pacific Northwest National Laboratory, Richland, Washington.

White MD and M Oostrom. 2006. *STOMP: Subsurface Transport Over Multiple Phases, Version 4.0, User's Guide*. Pacific Northwest National Laboratory, Richland, Washington.

Wierenga PJ and MT van Genuchten. 1989. "Solute transport through small and large unsaturated soil columns." *Ground Water* 27(1):35-42.

Williams BA, CF Brown, W Um, MJ Nimmons, RE Peterson, BN Bjornstad, DC Lanigan, RJ Serne, FA Spane, and ML Rockhold. 2007. *Limited Field Investigation Report for Uranium Contamination in the 300-FF-5 Operable Unit at the 300 Area, Hanford Site, Washington*. PNNL-16435, Pacific Northwest National Laboratory, Richland, Washington.

Williams MD, ML Rockhold, PD Thorne, and Y Chen. 2008. *Three-dimensional groundwater models of the 300 Area at the Hanford Site, Washington State*. PNNL-17708, Pacific Northwest National Laboratory, Richland, Washington.

Wolery TW and RL Jarek. 2003. *Software User's Manual, EQ3/6, Version 8.0*. Sandia National Laboratories, Albuquerque, New Mexico.

Yabusaki SB, Y Fang, and SR Waichler. 2008. "Building conceptual models for field-scale reactive transport in a dynamic vadose zone-aquifer-river system." *Water Resour. Res.* 44:W12403, doi:10.1029/2007WR006617.

Young JS and JS Fruchter. 1991. *Addendum to Data Compilation Task Report for the Source Investigation of the 300-FF-1 Operable Unit Phase I Remedial Investigation*. EMO-1026. Prepared by Environmental Management Operations for the U.S. Department of Energy, Richland, Washington.

Zachara JM (editor). 2005. *Uranium Geochemistry in Vadose Zone and Aquifer Sediments from the 300 Area Uranium Plume.* PNNL-15121, Pacific Northwest National Laboratory, Richland, Washington. (Contributors: JA Davis, C Liu, JP McKinley, N Qafoku, DM Wellman, and SB Yabusaki)

Zachara JM, CF Brown, J Christensen, PE Dresel, S Kelly, JP McKinley, RJ Serne, and W Um. 2007. *A Site-Wide Perspective on Uranium Geochemistry at the Hanford Site*. PNNL-17031, Pacific Northwest National Laboratory, Richland, Washington.

Zachara JM, MD Freshley, GV Last, RE Peterson, BN Bjornstad. 2012. *Updated Conceptual Model for the 300Area Uranium Groundwater Plume*. PNNL-22048, RPT-DVZ-AFRI-007, Pacific Northwest National Laboratory, Richland, WA.

Zachara J, C Liu, M Oostrom, JP McKinley, T Wietsma, and CT Resch. 2013 (in press). "Mass transfer limited adsorption and desorption of U in intact sediment cores retrieved from a contaminated aquifer." *Environ. Sci. Technol.*

Appendix A

Hydrogeology and Geochemistry

Appendix A

Hydrogeology and Geochemistry

A.1 Geologic Framework

The general characteristics of the hydrogeology of the 300 Area have been described in detail elsewhere (Williams et al. 2008). Briefly, the unconfined aquifer consists of Ringold Fm and Hanford fm sediments, with the underlying Ringold Fm often being separated into several different subunits (Figure A.1). The hydraulic conductivity of the Hanford fm is generally two to three orders-of-magnitude greater than that of the underlying Ringold Fm. Recent detailed characterization studies at the 300 Area Integrated Field Research Challenge (IFRC) site (Zachara et al. 2012; Bjornstad et al. 2009), and drilling of new characterization and monitoring wells over the greater 300 Area, have provided additional details that have been used to refine the geologic framework model of the site.

EarthVision was used to develop the geologic framework model of the 300 Area depicted in Figure A.1 and described in detail by Williams et al. (2008). This geologic framework model was updated recently to account for all well drilling and geophysical logging data available through January 2012. The updated model was used as the basis for development of the system-scale flow and reactive transport model described for the current study.

A.2 Sediment properties

Williams et al. (2008) provide a relatively comprehensive summary of measured physical and hydraulic properties for 300 Area sediments that were available from investigations performed prior to the IFRC project. Additional physical, hydraulic, and geochemical property characterization data were generated for the IFRC and for other recent projects. Some of these new data were used for the current study and are described here.

A.2.1 Physical Properties

Grain size distribution data were collected for more than 100 sediment grab samples collected during drilling at the IFRC site. The geochemical properties of those sediment samples were also measured (Murray et al. 2012). In addition, physical and hydraulic properties were measured on 12 intact core samples from the site. The physical properties of these core samples are summarized in Table A.1.

All of the samples shown in Table A.1 were from the Hanford fm. The average porosity of these samples was 0.23 and the average gravel content was ~71%. These values are similar to those reported previously by Williams et al. (2008) for the Hanford fm sediments. Grain size analyses were performed using dry sieve and hydrometer or laser adsorption methods. The 12 samples fall into three textural classes—gravel, sandy gravel, and muddy sandy gravel—based on the Folk-Wentworth classification system.

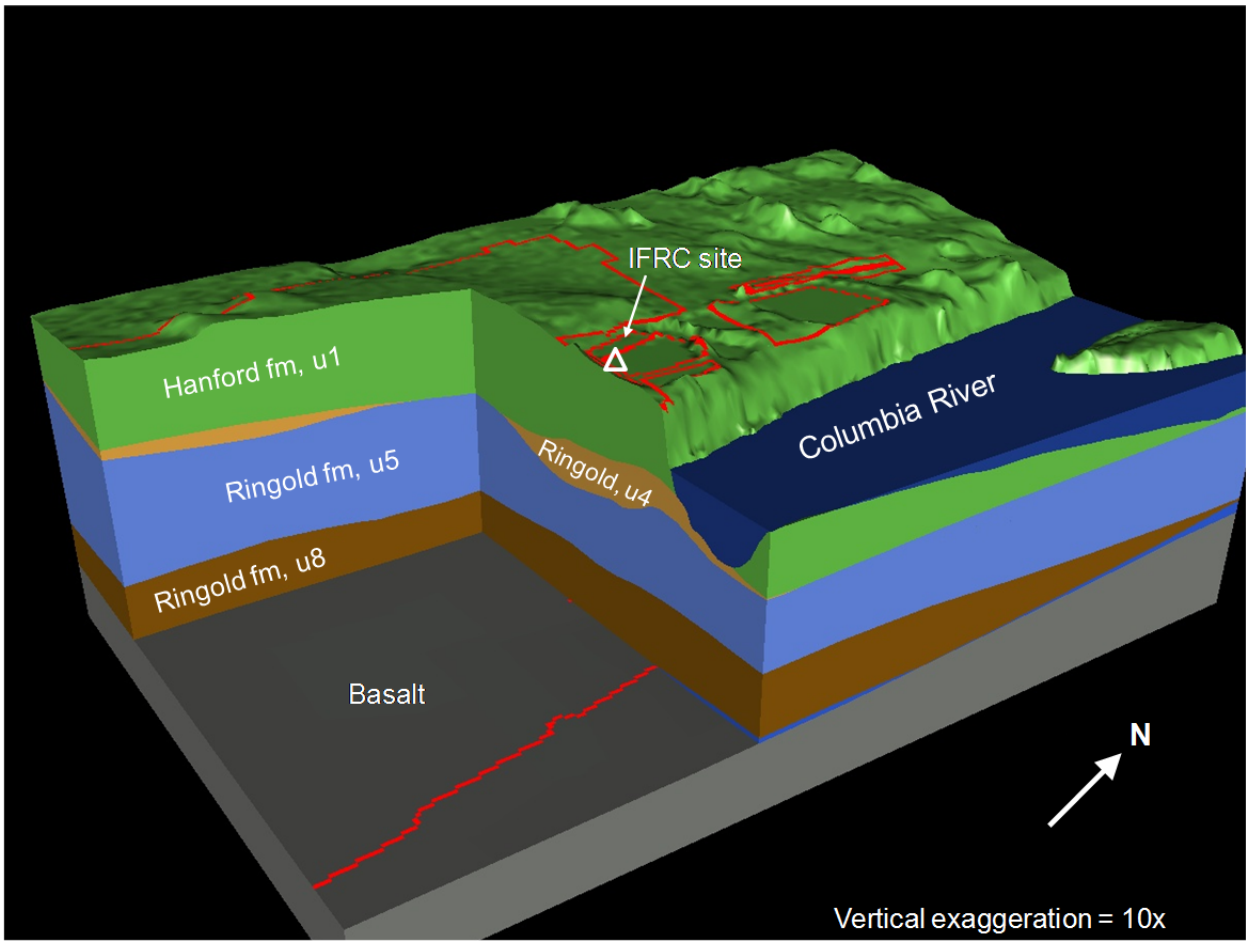

Figure A.1. Cutaway view of the major hydrogeologic units in the Hanford 300 Area based on an EarthVision model of the site. Note the location of the IFRC site in the southwest corner of the former south process pond.

Other grain size metrics shown in Table A.1, specifically d_g and σ_g, have been shown to be useful in estimating other properties of interest such as surface area, hydraulic conductivity, and water retention parameters (Ward et al. 2006; Williams et al. 2008). Hydraulic properties for these intact core samples were also measured and are reported on in the following section.

A.2.2 Hydraulic Properties

Williams et al. (2008) provide a summary of 300 Area aquifer test results that were generated prior to the establishment of the IFRC site. In general, most prior estimates of hydraulic conductivity for the Hanford fm sediments were somewhat inconclusive, usually establishing only lower bounds on the hydraulic conductivity (e.g., >5000 m/d) owing to the limitations of the aquifer (slug) test method that was used, which is not well-suited for very high permeability sediments. Slug test results were more definitive and reliable for the lower permeability Ringold Fm sediments that typically have hydraulic conductivity values that are 2 to 3 orders-of- magnitude or more lower than the Hanford fm (Williams et al. 2008).

A.2.2.1 Aquifer Testing

After the IFRC well field was installed in the summer of 2008, a series of short-duration, constant-rate aquifer injection tests were performed in 14 IFRC wells. Figure A.2 shows the layout of the well field and the calculated values of depth-average hydraulic conductivity based on these constant rate injection tests. The average value of the depth-averaged hydraulic conductivity is ~7000 m/d, with a range of ~4600 to ~11,000 m/d. Additional constant rate injection tests (results not shown) were performed at the IFRC site in February 2011, before and after the lower half of most of the wells were filled with bentonite to mitigate observed wellbore flow effects that were complicating the interpretation of aqueous sampling data from tracer tests.

Electromagnetic borehole flow-meter (EBF) testing was also performed in the IFRC wells to allow for partitioning of the bulk depth-averaged hydraulic conductivity (K) over discrete depth intervals to quantify the stratification of the sediment profile (Vermeul et al. 2011). Figure A.3 shows relative K profiles calculated from EBF measurements made in wells 399-2-9 and 399-3-28 in 2008 and again in 2011, prior to filling the lower half of most of the IFRC wells with bentonite to mitigate the wellbore flow effects. Differences between the 2008 and 2011 profiles are a result of different ambient flow conditions that were experienced during the two sets of tests. Calculations of relative K from the EBF data attempt to correct for ambient flow conditions, which are measured in each well immediately before and immediately after each test, by interpolating between the two measured ambient flow profiles. Owing to the high permeability of the sediments and the frequent fluctuations in Columbia River stage, the ambient flow conditions tended to be highly variable during these tests, which impacted the interpreted results.

In general the data for these and other IFRC wells show the profiles to be somewhat stratified, typically with lower values of hydraulic conductivity in the central portions of the profiles, and higher values of hydraulic conductivity at the tops and bottoms of the profiles. This stratification or layering structure is also evident from electromagnetic resistivity tomography (ERT) data (Johnson et al. 2012). However, this structure is not apparent from grain size distribution data or in spectral gamma log data measured in the temporary casings prior to well completion. The extent to which stratification observed at the IFRC site may or may not be continuous over the larger 300 Area is currently unknown.

Table A.1. Physical properties and textural classifications of selected Hanford fm sediment samples from the 300 Area IFRC site.

Borehole ID, Depth (ft)	Porosity	Dry bulk density (g/cm^3)	% gravel	% sand	% mud	d_g[†] (mm)	σ_g[‡]	d_g/σ_g	Class[§]
C6186, 18.4 - 19.4	0.152	2.30	82	15	3	6.27	6.03	1.040	G
C6186, 42 – 43	0.224	2.11	61	35	4	2.96	7.91	0.374	sG
C6197, 27 - 28	0.176	2.24	68	21	11	2.63	12.92	0.204	msG
C6197, 35 – 36	0.262	1.99	71	18	11	5.80	22.24	0.261	msG
C6197, 42 - 43	0.178	2.22	67	29	4	2.64	5.10	0.518	msG
C6197, 51 - 52	0.214	2.13	56	38	5	1.81	5.61	0.323	msG
C6200, 21 – 22	0.219	2.12	89	10	1	13.23	4.06	3.259	G
C6203, 16 – 17	0.213	2.14	81	13	6	7.52	10.7	0.703	G
C6203, 20 – 21	0.285	1.94	79	17	4	5.47	9.04	0.605	msG
C6203, 35.8 - 36.8	0.302	1.89	72	26	2	3.56	3.99	0.892	sG
C6203, 40-41	0.266	1.99	45	52	3	1.60	4.73	0.338	sG
C6208, 23 – 24	0.246	2.05	77	19	4	5.51	8.43	0.654	msG
Min.	0.152	1.89	45	10	1	1.60	3.99	0.204	
Max.	0.302	2.30	89	52	11	13.23	22.24	3.259	
Mean	0.228	2.09	70.7	24.4	4.83	4.92	8.40	0.764	
Stdev	0.046	0.13	12.32	12.23	3.16	3.25	5.17	0.826	
CV (%)	20.1	5.99	17.4	50.1	65.3	66.0	61.2	108.2	
Number of samples	12	12	12	12	12	12	12	12	

[†] Geometric mean grain diameter
[‡] Geometric standard deviation
[§] Folk-Wentworth classification (G = gravel, sG = sandy gravel, msG = muddy sandy gravel)

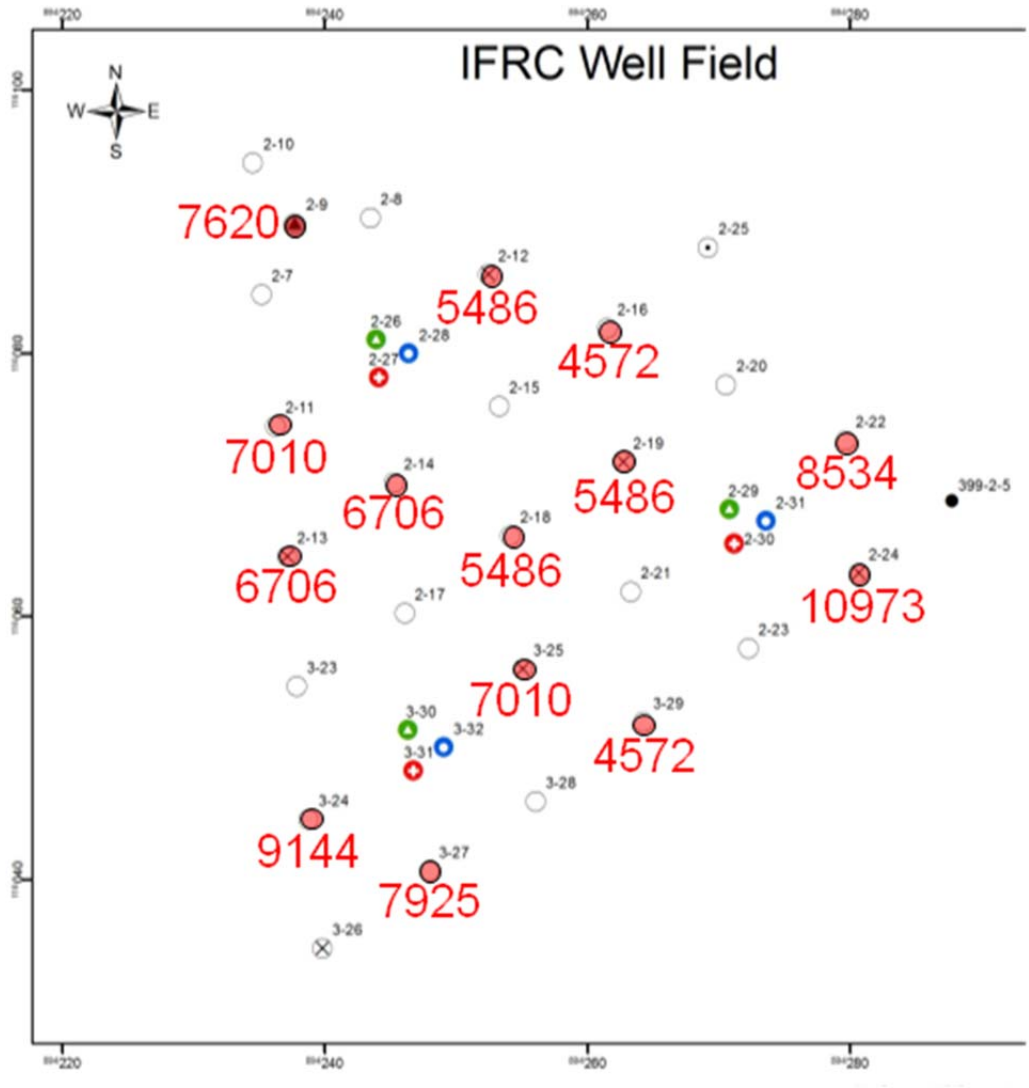

Figure A.2. Saturated hydraulic conductivity values (m/d) determined from short-duration constant rate injection tests that were performed in the fully screened wells at the IFRC site in 2008. The average value is ~7000 m/d.

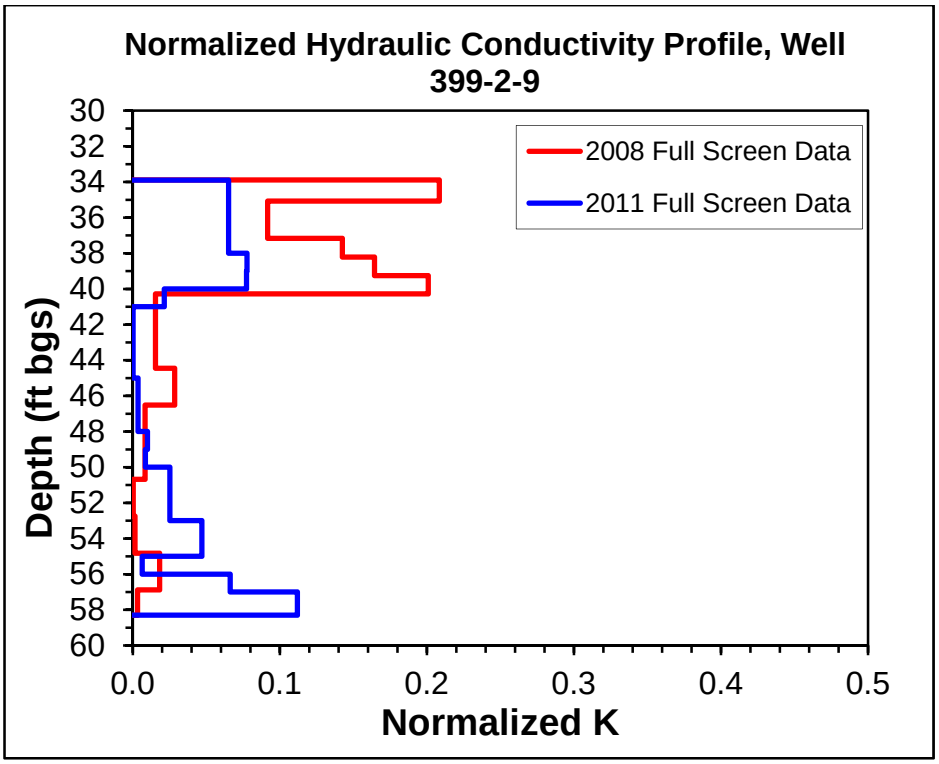

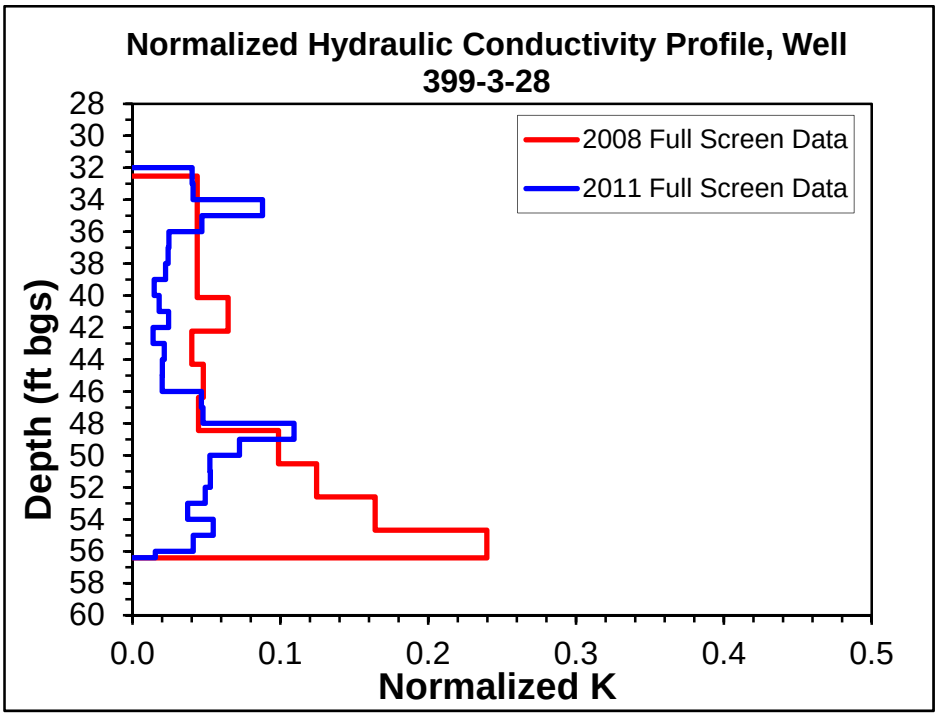

Figure A.3. Normalized K profiles for two IFRC wells generated by EBF testing.

A.2.2.2 Multistep Outflow Experiments on Sediment Cores

Multistep outflow experiments were performed on 11 of the intact core samples whose physical properties are listed in Table A.1. Figure A.4 shows one of the instrumented core samples used in a multistep outflow experiment. The primary purpose of these experiments was to generate data for estimating permeability-saturation-capillary pressure (k-S-p) relations that are needed for vadose zone flow and transport modeling.

Intact cores were hand-picked from a stockpile of cores collected from the IFRC site that were housed in a refrigerated storage unit located outside of PNNL's Research Technology Laboratory building. Cores were visually inspected prior to their selection by removing their end caps to ensure that they were well packed and did not contain any obvious large cobbles that could significantly obstruct flow. The end caps were replaced following inspection and the selected cores were then transferred to the Subsurface Flow and Transport Experimental Laboratory (SFTEL), housed in PNNL's Environmental Molecular Sciences Laboratory (EMSL). Multistep outflow experiments were then performed on the cores in the SFTEL.

Experimental preparation included trimming the ends of the 8.9-cm-diameter Lexan core sleeves and their contents to ensure that the packing was as uniform as possible over the areas in contact with end plates. The original and trimmed cores were 30 cm long and 25 cm long, respectively. Custom-made acrylic collars were attached to the end of each core by epoxy, for retaining a porous stainless-steel plate and outflow line at the bottom, and a gas inflow line fitting at the top. Acrylic transducer mounting plates were also attached to each core liner, 5 cm from both the top and bottom of each core. A hole was drilled through each transducer mounting plate into the column for placement of water-filled, stainless steel tensiometers. Pressure transducers (Figure A.4) were mounted to the tensiometers for measurement of aqueous pressure. After the cores were assembled and instrumented, they were saturated using synthetic 300 Area groundwater. The cores were typically held in a water-saturated state for approximately 1 week prior to initiation of the multistep outflow experiments.

Outflow of water was induced by increasing the gas pressure applied to the top of the columns in steps while maintaining a constant water pressure at the bottom of the columns. Outflow mass/volume was measured by an electronic balance. Aqueous pressure was monitored continuously using stainless steel tensiometers attached to pressure transducers. When pressures and outflow had stabilized for a given applied gas pressure, the gas pressure was increased to the next step, up to a maximum equivalent water pressure of ~200 cm, which is close to the bubbling pressure of the bottom porous stainless steel end plates. After termination of each multistep outflow experiment, subsamples from each core were used for 1-bar pressure plate measurements. The grain size distributions of the bulk sediments in each core were also measured after the multistep outflow experiments using dry sieve and hydrometer methods. The original data are contained in PNNL laboratory record books BNW-60209 and BNW-60210, maintained by Tom Wietsma, EMSL/1387.

Measured pressure data from two locations in each core and measured cumulative outflow data were used to calculate average capillary pressures and water contents. These data pairs were then fit using the van Genuchten (1980) and Brooks-Corey (1964) models to estimate water retention parameters. The measured pressures and cumulative outflow data were also used for inverse modeling using the STOMP and parallel PEST codes to simultaneously estimate parameters for both the water retention and unsaturated hydraulic conductivity functions (with fitting of the pore-interaction term in a generalized

relative permeability model). Results from this inverse modeling (not shown) yielded water retention parameters that are very similar to those shown in Table A.2.

Figure A.4. Photograph of intact sediment core from the IFRC site instrumented for a multistep outflow experiment.

The fitted water retention parameters for 10 cores from the Hanford fm sediments and associated statistics are shown in Table A.2. Figure A.5 shows the water retention curve for the average Brooks-Corey model parameters listed in Figure A.2, with $\theta_s = 0.23$, $\theta_r = 0$, $h_b = 5.6$ cm, and $\lambda = 0.267$. These average water retention parameters are assumed to be representative of the Hanford fm sediments in the 300 Area and were used for all field-scale modeling reported herein.

Table A.2. Hydraulic properties for selected intact core samples of Hanford fm sediments from the 300 Area IFRC site.

				van Genuchten model			Brooks-Corey model		
Borehole ID, Depth (ft)	K_s (cm/s)	θ_s	θ_r	α (1/cm)	n	SSE[†]	h_b (cm)	λ	SSE
C6186, 18.4 - 19.4	2.83E-04	0.152	0	0.0388	1.3776	0.0030	11.36	0.2455	0.0216
C6186, 42 – 43	6.78E-02	0.224	-	-	-	-	-	-	-
C6197, 27 - 28	4.33E-04	0.176	0	0.1150	1.3237	0.0113	6.07	0.2824	0.0107
C6197, 35 – 36	5.36E-02	0.262	-	-	-	-	-	-	-
C6197, 42 - 43	2.61E-02	0.178	0	0.0929	1.3655	0.0043	6.68	0.3028	0.0112
C6197, 51 - 52	5.43E-05	0.214	0	0.0435	1.2716	0.0066	9.41	0.1751	0.0342
C6200, 21 – 22	2.85E-01	0.219	0	0.0626	1.3829	0.0063	9.67	0.3115	0.0023
C6203, 16 – 17	1.06E-01	0.213	0	0.3580	1.1946	0.0076	1.65	0.1659	0.0125
C6203, 20 – 21	3.72E-03	0.285	0	0.2286	1.2691	0.0097	2.82	0.2322	0.0168
C6203, 35.8 - 36.8	3.26E-02	0.302	0	2.4189	1.2991	0.0366	0.38	0.2929	0.0363
C6203, 40-41	1.30E-02	0.266	0	0.2733	1.5094	0.0089	3.08	0.4778	0.0058
C6208, 23 – 24	2.13E-02	0.246	0	0.1479	1.2005	0.0155	4.87	0.1816	0.0123
Min.	5.43E-05	0.152		0.0388	1.1946		0.38	0.1659	
Max.	2.85E-01	0.302		2.4189	1.5094		11.36	0.4778	
Mean	5.08E-02	0.228		0.3780	1.3194	0.0110	5.60	0.2668	0.0164
Stdev	0.080518	0.046		0.7249	0.0946		3.70	0.0920	
CV [‡](%)	158.4	20.1		191.8	7.2		66.1	34.5	
Number of samples	12	12		10	10		10	10	

[†] SSE is sum of squared errors, describing goodness of fit.
[‡] CV(%) is coefficient of variation × 100 = Stdev/Mean × 100

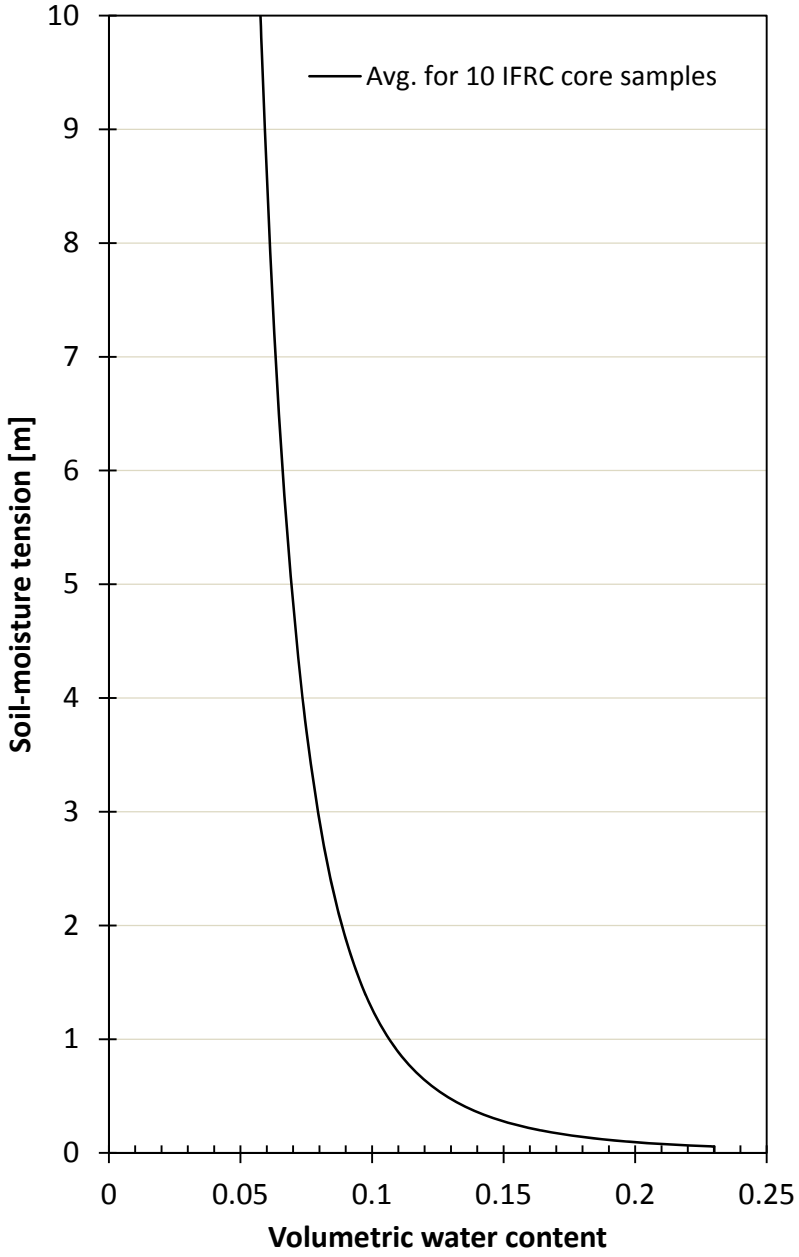

Figure A.5. Representative water retention curve for Hanford fm sediments in the 300 Area generated from the average of 10 sets of parameters determined from multistep outflow experiments on intact cores from the IFRC site (θ_s = 0.23, θ_r = 0, h_b = 5.6 cm, λ = 0.267).

A.2.3 Geochemical Properties

The bulk mineralogy of sediment samples collected from the IFRC site is reported by Murray et al. (2012).

A.2.4 Sediment-Associated Uranium

The determination of sediment-associated uranium does not follow an exact standard. Sediment-associated uranium has been measured using a variety of methods ranging from a bicarbonate extraction method, which determines the so-called *labile* or readily desorbable fraction (Murray et al. 2012), to nitric and hydrochloric acid-based extraction and microwave digestion methods, which determine *total* uranium (http://www.epa.gov/osw/hazard/testmethods/sw846/pdfs/3050b.pdf). Gamma spectrometry has also been used for measuring total uranium for Hanford sediments (Stoliker et al. 2013). Different periods of time have also been used by different research groups and commercial laboratories for extraction or leaching of uranium from the sediments with some of these different methods. The *labile* fraction is sometimes also referred to simply as *adsorbed* uranium. *Non-labile* uranium, which may exist in mineral phases and/or intra-grain pore spaces or micro-fractures that are not readily accessible to the bulk aqueous solution, is determined from the difference between *total* and *labile* uranium.

In addition to using different methods, researchers have also measured labile and total uranium on different size fractions of the sediments (Stoliker et al. 2013; Shang et al. 2011). Therefore, it is important to distinguish between both the method used and what it represents (i.e., labile – determined using bicarbonate extraction method; total – determined using acid extraction, microwave digestion, or gamma spectroscopy; and non-labile – determined as the difference between total and labile uranium), and the grain size fraction that was used in the measurements. If measurements are made only on a finer grain size fraction, say less than 2 mm, and if there is a significant mass fraction of coarser material, then corrections may be needed to scale the measured values so that they are representative of the bulk field sediments (including gravel and larger sizes). However, this requires that the mass fraction of sediments less than or greater than 2 mm be known, which is often not the case. Earlier assumptions that the gravel fraction is inert have also been shown recently to be incorrect (Stoliker et al. 2013; Shang et al.,2014), so the method used for up-scaling sediment-associated uranium data measured on finer size fractions to the bulk sample should also be specified. Methods to estimate total uranium from adsorbed uranium or vice versa, implications for reactive transport modeling, and mapping of the spatial distribution of sediment-associated contaminant uranium in the 300 Area are described in the following sections.

A.2.4.1 Relationships between Surface Area and Adsorbed and Total Uranium

Stoliker et al. (2013) recently reported on results from careful experimental studies with uranium-contaminated sediments from the lower vadose zone and capillary fringe region of the IFRC site. Characterization data were collected on individual size fractions and composite sediments. Figure A.6 shows data extracted from their paper (see Stoliker et al. 2013, Table 2) along with regression relationships for the apparent effective grain diameter, surface area (SA, measured by BET method), adsorbed U (determined using a bicarbonate extraction method for up to 5000 hr), and total U (measured by gamma spectrometry). The effective grain diameter shown in Figure A.6, d_{eff}, is defined here as

$$d_{eff} = \frac{d_{large} - d_{small}}{\ln(d_{large} / d_{small})} \quad \text{(A.1)}$$

where d_{large} and d_{small} are the diameters (mm) of two adjacent sieve sizes, or the sizes that otherwise define each particle size class (e.g., from hydrometer or laser diffraction methods used for the finer size fractions).

The relationship used to represent the apparent effective grain diameter versus SA shown in Figure A.6 (top plot) is a weighted average of fitted exponential and log functions shown in the figure

$$SA[m^2/g] = 0.56*log\_function = (1 - 0.56)*exp\_function \quad \text{(A.2)}$$

Having an analytic expression that relates the effective grain diameter to SA allows for the prediction of SA from more easily measured grain size distribution data, rather than having to measure it directly for each sample of interest.

The additivity concept has been shown to be applicable to particle surface area (Shang et al. 2011), so the surface area of the total or bulk sample, SA_T can be estimated as the mass-weighted average of the surface areas for each size fraction using

$$SA_T = \sum_{i=1}^{n} SA_i m_i \quad \text{(A.3)}$$

where SA_i and m_i *are* the surface area and mass fraction, respectively, for grain size class i. As shown by the data reported in Stoliker et al. (2013) and Shang et al. (2011), grain size distributions determined by dry sieving may not accurately represent the true grain size distribution of the sediments due to finer particles adhering to coarser particles, such that the apparent relative proportions of coarser to finer particles are typically greater for dry sieve data than for wet sieve data. Nevertheless, dry sieve data are more easily measured than wet sieve data and the bulk of the data available for Hanford sediments are dry sieve data. Dry sieve data are also more conducive to subsequent measurement of adsorbed U concentrations in size separates, since uranium is not removed in the process of washing the samples.

Interestingly, Figure A.6 (top plot) shows that the SA measurements for the wet-sieved sediments, measured independently by Stoliker et al. (2013) and Shang et al. (2011), are relatively constant for particles within the 0.1 to 2 mm size range, and actually show a slight increase in SA with increasing grain size over this range, which is counterintuitive. These results are apparently caused by increased intra-granular porosity (and/or surface roughness) as particle size increases. The wet sieve SA data shown in Figure A.6 for the smallest size class (from Shang et al. 2011) and for the largest size class (from Stoliker et al. 2013) follow the trend that would be expected based on simple calculations of the geometric surface areas of smooth spherical or ellipsoidal particles, with smaller particles having relatively larger surface areas on an equivalent mass basis.

Turning now to the bottom plot shown in Figure A.6, it should be noted that total soil U concentrations <3 ug/g are considered to be background (indicative of non-contaminated sediments) for the 300 Area (DOE-RL 2013). Therefore, the ranges of concentrations encountered in the sediments

analyzed by Stoliker et al. (2013) are actually quite low relative to some other sites in the 300 Area (Wang et al. 2012; Williams et al. 2007). Since the data shown in Figure A.6 represent a limited range of grain sizes and uranium concentrations for a single waste site (former South Process Pond), use of the regression relationships shown in Figure A.6 for extrapolation outside the ranges of these data should obviously be done with some caution. Pooling of data from other 300 Area characterization studies yields a somewhat different but consistent relationship between adsorbed and total uranium.

Figure A.7 shows adsorbed (a.k.a. labile) versus total U data from several sources (Wang et al. 2012, Williams et al. 2007), plotted with the data from Stoliker et al. (2013). The adsorbed data from the PNNL sources were generated using the bicarbonate extraction method, but typically with shorter extraction periods (504 - 672 hr) relative to the data reported by Stoliker et al. (2013), which represent extraction periods of up to 5000 hr, or the labile U data reported by Murray et al. (2012) which represent 1000-hr extraction periods. The total U data from PNNL sources was also determined using an acid-extraction method instead of the gamma spectroscopy method used by Stoliker et al. (2013). The red line in Figure A.7 represents the fit to the data of Stoliker et al. (2013), shown previously in Figure A.6, and the black line is a fit to the data from PNNL sources. Considering the differences in the methods that were used, the agreement between these data sets is considered good.

Stoliker et al. 2013 also performed flow-through column experiments, and Shang et al. (2011) performed stirred-flow reactor experiments on grain size separates and composited sediments from the 300A IFRC site. Their results show that the additivity concept is also applicable to estimation of uranium concentrations on 300 Area sediments, such that the adsorbed and total uranium for a bulk sample can be calculated as the mass-weighted average concentration of the uranium concentrations of all the grain size separates combined

$$U_{bulk} = \sum_{i=1}^{n} U_i m_i \tag{A.4}$$

where U_i and m_i are the uranium concentration [ug/g] and mass fraction, respectively, for sediment size class i.

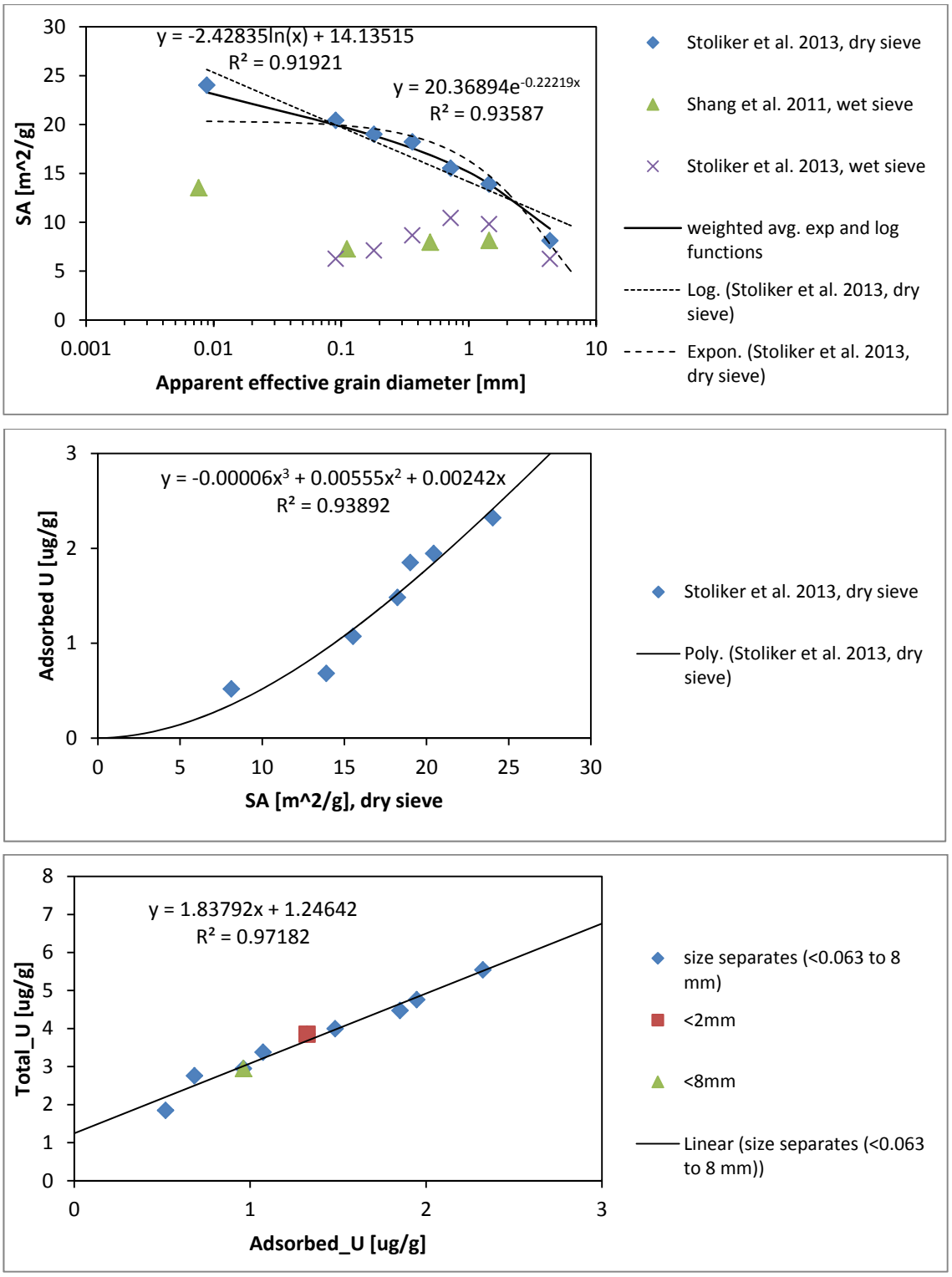

Figure A.6. Data from Stoliker et al. (2013) and correlations between effective grain diameter, surface area (SA), adsorbed uranium and total uranium for sediments from the Hanford 300 Area IFRC site.

A.2.4.2 Implications for Reactive Transport Modeling

Zachara et al. (2012) provide a high-level summary of findings from the IFRC project and an update to the conceptual model of uranium mass transfer in the 300 Area. They briefly describe a recent study by Shang et al. (2014), who performed relatively long-term uranium desorption experiments (141 to 175 days) in flow-through columns packed with grain size separates and composited sediments from the same batch of IFRC site sediments that were used by Stoliker et al. 2013. Two key findings of their study are (private communication with Chongxuan Liu, PNNL, July 2013):

- Contrary to an assumption that has been used in many earlier Hanford studies, the gravel fraction (>2 mm) is not inert and was actually found to make a significant contribution to U sorption, owing to the higher than expected SAs for the coarser size fractions resulting from intra-granular pores (and/or surface roughness).
- Uranium continued to be released from the sediments long after the "labile" pool of uranium had been depleted.

These findings may call into question the application of results based on some of the earlier laboratory experimental and modeling studies to modeling long-term uranium desorption and transport at the field scale. If the parameters used for field-scale modeling are based on earlier laboratory-based modeling studies that employed a gravel correction to the labile uranium concentrations measured on the <2 mm size fraction, then the total leachable sediment-associated uranium and its long-term impact to groundwater concentrations could both be significantly underestimated (Zachara et al. 2012; Shang et al. 2014). Successful modeling of the long-term U desorption data for the bulk sediments used in the study of Shang et al. (2014) required the use of a dual-domain (mobile-immobile region), multi-rate surface complexation model in which both labile and non-labile U were used and partitioned over the fast and slow sorption sites, respectively. In addition, in order to capture the evolution of major ions observed during the long-term experiments, the reaction network included the processes of calcite dissolution and re-precipitation, ion exchange, and denitrification. A similar reaction network was applied by Stoliker et al. (2013) to model their experiments. These studies (Stoliker et al. 2013; Shang et al. 2014) represent the most comprehensive analyses of uranium mass transfer performed for 300 Area sediments to date.

An open question is whether this level of complexity is really required for accurate field-scale modeling. For the reactive transport modeling reported here, we adopt a single domain, multi-rate surface complexation modeling approach, and an alternative reaction network that includes polyphosphate reactions. Both are evaluated and parameterized using laboratory experimental data, described in the main body of this report.

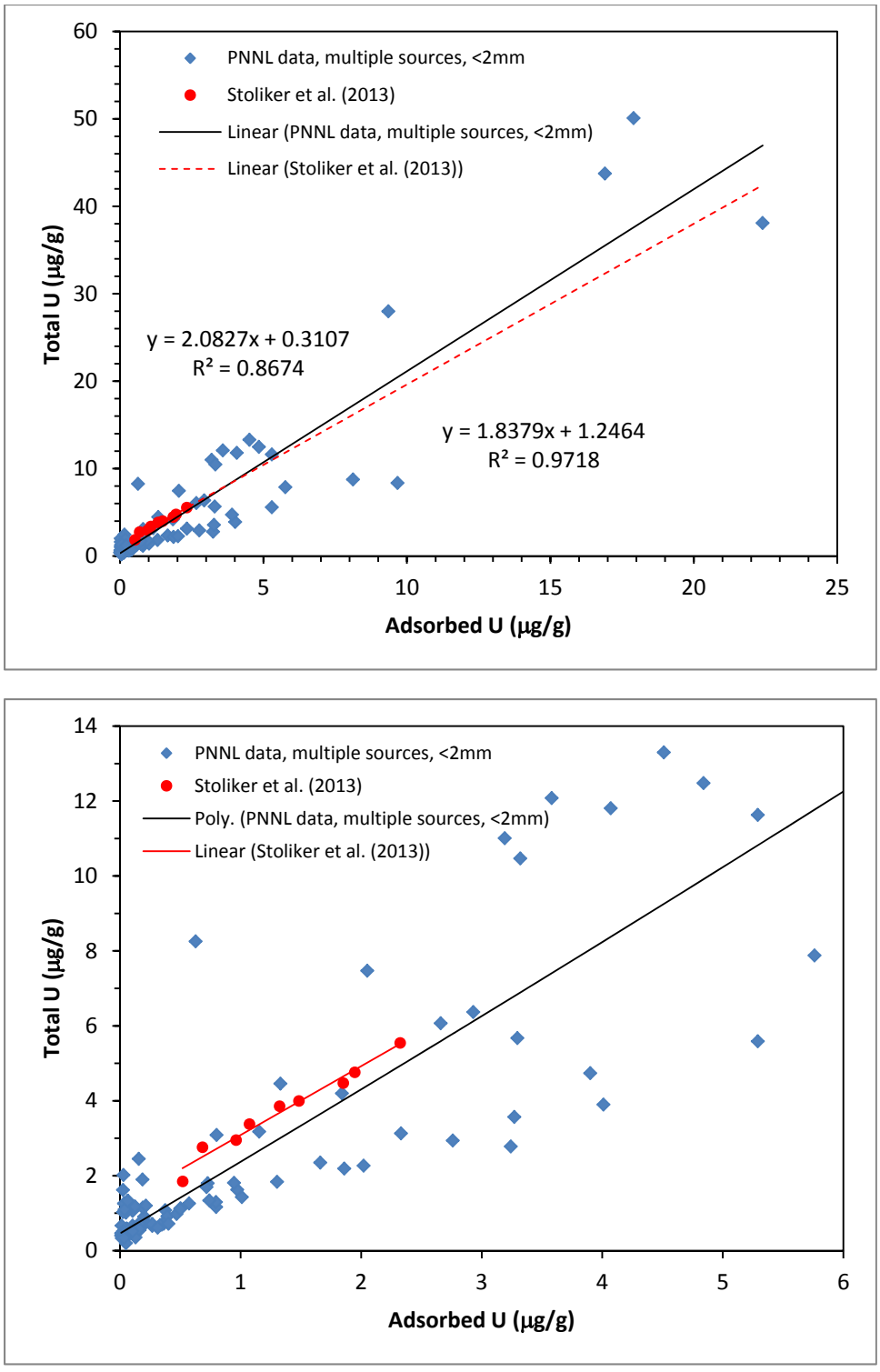

Figure A.7. Adsorbed and total uranium data from various PNNL source with data from Stoliker et al. (2013). See text for discussion on differences in the methods that were used.

To illustrate the potential for under- or over-estimation of soil uranium concentrations (depending on assumptions about the gravel fraction) the regression relationships shown in Figure A.6 for the data of Stoliker et al. (2013) were applied to the grain size distribution of a core sample from the IFRC site

(Figure A.8), which is considered to be representative of the coarse-grained Hanford fm sediments in the 300 Area. Values of SA, adsorbed U, and total U were calculated for each size fraction. The mass-weighted average SAs and concentrations for all size fractions combined were taken to be the true values for the bulk sediment. The mass-weighted SAs and U concentrations for just the <2 mm size fraction were also calculated. The calculated values of adsorbed and total uranium for the <2 mm size fraction were multiplied by the mass fraction of the <2 mm size fraction to estimate "gravel-corrected" values for the bulk sediment, $U_{grav\text{-}corr}$.

$$U_{grav-corr} = U_{<2mm} \cdot m_{<2mm} \tag{A.5}$$

This latter calculation is based on a common assumption that has been used in many previous Hanford studies that the gravel fraction is inert, and only serves to dilute the properties of the finer size fractions (Murray et al. 2012; Kaplan et al. 2000). However, the data from Stoliker et al. (2013) and Shang et al. (2011) clearly show that the gravel fraction is not inert with respect to U adsorption.

Table A.3 shows values of adsorbed (a.k.a. labile) and total uranium concentrations calculated by the three methods described above, namely 1) additivity calculations for bulk sample; 2) additivity calculations for the <2 mm size fraction, and; 3) gravel correction for results from the <2 mm size fraction. Using the gravel correction results in estimates of adsorbed and total uranium for the bulk sediment that are only 65% and 49%, respectively, of the "true" values. These calculations suggest that the standard practice of using gravel-corrected values for adsorbed and total U may significantly underestimate the true concentrations of uranium in the coarse-textured 300 Area sediments found in the field. If measurements of U for the <2 mm size fraction are assumed to be representative of the bulk sediment, without any gravel correction, the calculated adsorbed and total U concentrations are 182% and 138% of the true values, respectively.

Therefore, assuming that measurements for the <2 mm size fraction are representative of the bulk sediments would overestimate the true field concentrations if there is a significant gravel fraction. However, these calculations also suggest that these two approximations would likely bracket the true values, which may be useful for bounding calculations or sensitivity analyses. As shown in Table A.3, calculated values of SA may be similarly biased by the assumptions that are made about the influence of the gravel fraction. Matters are further complicated by the fact that the mass fractions of gravel, or of the <2 mm size fraction on which the soil U concentration measurements are typically made, may not even be reported. For conservatism, and to minimize assumptions when detailed grain size information is not available, it would appear that measurements of adsorbed (a.k.a. labile) uranium on the <2 mm size fraction should be used to represent sediment-associated uranium for inventory calculations and reactive transport modeling.

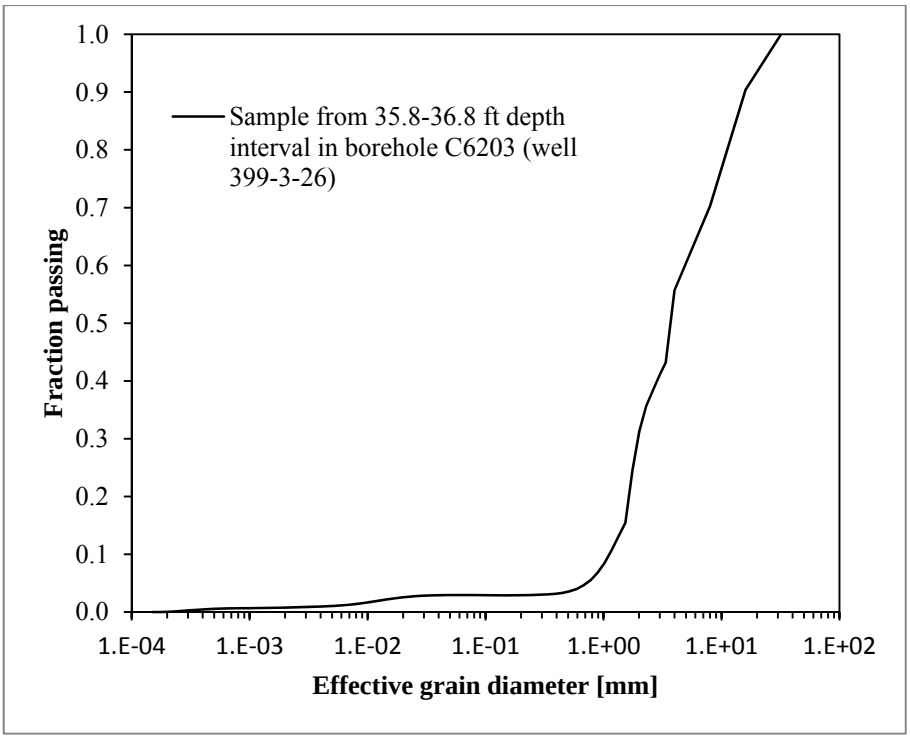

Figure A.8. Grain size distribution for sediment from a core sample collected at the IFRC site.

Table A.3. Calculated values of adsorbed and total uranium and surface area based on grain size distribution data from a representative core sample of the Hanford fm in the 300 Area (sample collected over the 35.8 - 36.8 ft depth interval in borehole C6203—completed as IFRC site well 399-3-26).

		Computed Values Based on		
	Variable	All sizes combined†	<2 mm†	Gravel Correction
Adsorbed U	Concentration (ug/g)	0.586	1.066	0.380
	% of "true" value	100	182	65
Total U	Concentration (ug/g)	2.323	3.205	1.142
	% of "true" value	100	138	49
Surface Area	SA (m^2/g)	9.942	14.683	5.234
	% of "true" value	100	148	53

† Calculations based on additivity concept using mass-weighted average values for all size classes within size range of interest and regression relationships based on data from Stoliker et al. (2013).

A.3 Groundwater and River Monitoring Data

The system-scale model of flow and reactive transport for the 300 Area requires water level and aqueous chemistry data to define initial and boundary conditions. Most of these data are available from measurements made in the 300 Area well monitoring network, and at the Columbia River gauging station located just off of the 300 Area. In addition to these data, which are described in more detail below, hourly and daily data have been generated from special studies performed at the IFRC site, using instrumented wells that are not part of the regular 300 Area well monitoring network.

The 300 Area water level monitoring network is not supported directly by DOE as a line item in the budget to PNNL or any subcontractor, but rather on an ad-hoc and piecemeal basis by whatever PNNL projects happen to be doing work in the 300 Area that need these data. Consequently, the wells that are instrumented have varied over time. Although a lot of monitoring data have been generated over the years, sensor failures and disruptions in funding for downloading data and maintaining the monitoring network have resulted in many data gaps. Consequently, whenever data are needed for a detailed modeling study such as this one, significant effort may be needed to review past data and to establish data quality and consistency (see Appendix B). To try to mitigate some of these problems in the future, statistical models were developed to predict water levels at selected monitoring wells from moving averages of river stage data (measured or produced by a computational fluid dynamics model, MASS1[1]), or from a combination of river stage and well water level data (see Appendix C). The statistical models do not replace the need for the actual data, but simply provide a means for filling gaps in the monitoring data when necessary. Additional details on some of these data types are now discussed.

A.3.1 Water Levels

The primary 300 Area water level monitoring network currently includes pressure transducers in ~43 wells for automated, hourly measurement of water pressure (see Appendix C). The pressure transducers, which are initially calibrated by the manufacturer, are connected to data loggers that automatically record and store the data, which are then uploaded periodically (typically every 4-6 weeks) for analysis. When the data are uploaded, manual measurements of water level are also taken using an e-tape, which is estimated to be accurate to ~0.02 ft or ~0.6 cm (private communication with Rob Mackley, PNNL, Sept. 2013). Figure A.9 shows hourly water level data from well 399-2-5 for 2011, together with the manual e-tape measurements. These manual measurements provide a means for checking data quality and consistency and for identifying when transducers fail or have been inadvertently moved. For example, when wells are sampled for water quality measurements, it is not uncommon for the samplers to bump or move the pressure transducers temporarily to facilitate sampling. Pressure transducers are periodically recalibrated or replaced when needed. Several additional wells were also recently instrumented for special studies on a DOE Office of Science project—John Zachara, Principal Investigator—in a smaller area adjacent to the Columbia River between the former north and south process ponds. The data from these special studies are not publicly available at this time.

Williams et al. (2008) provide a detailed analysis of the variability in groundwater flow directions inferred from water level data for the entire 300 Area based on measurements from 1991-1993. Figure A.10 shows measured water levels and calculated flow directions and head gradients during a tracer experiment that was performed at the IFRC site in November 2008 (Zachara et al. 2012). The IFRC site is located ~200 m from the Columbia River shoreline. Even at this distance, the changes in flow directions and gradients can be dramatic. During this 1-month period, during which water levels were relatively constant and stable compared to other times of the year, the azimuth of the flow vector ranged from ~130 to almost 270 degrees, and the gradient ranged from ~1.5e-4 to 8.5e-4. Assuming hydraulic conductivity and porosity values of 7000 m/d and 0.23, respectively, these gradients yield pore-water velocities ranging from ~4.6 to ~25.9 m/d, with an average of ~10 m/d. These calculated velocities are consistent with observed tracer plume migration rates at the polyphosphate treatment test site (Vermeul et al. 2009)

[1] Modular Aquatic Simulation System 1D

The extreme variability in flow directions shown in Figure A.10, even during a period of relative stability, argues against the use of idealized 2D cross-sections for representing subsurface flow and transport in the 300 Area. Zachara et al. (2012; Figure 2.11) show the computed trajectory of a particle injected at the IFRC site in April 2010, responding to the types of gradients and flow directions depicted in Figure A.10. The computed travel distance over a 5-month period (April 3, 2010 to August 31, 2010) was 3 - 4 times greater than the straight line distance between starting and ending points. This provides additional evidence that the use of idealized 2D vertical cross-sections is not appropriate, except perhaps for demonstration purposes. A 3D modeling approach is needed to accurately represent the highly dynamic nature of the flow and transport processes in the 300 Area.

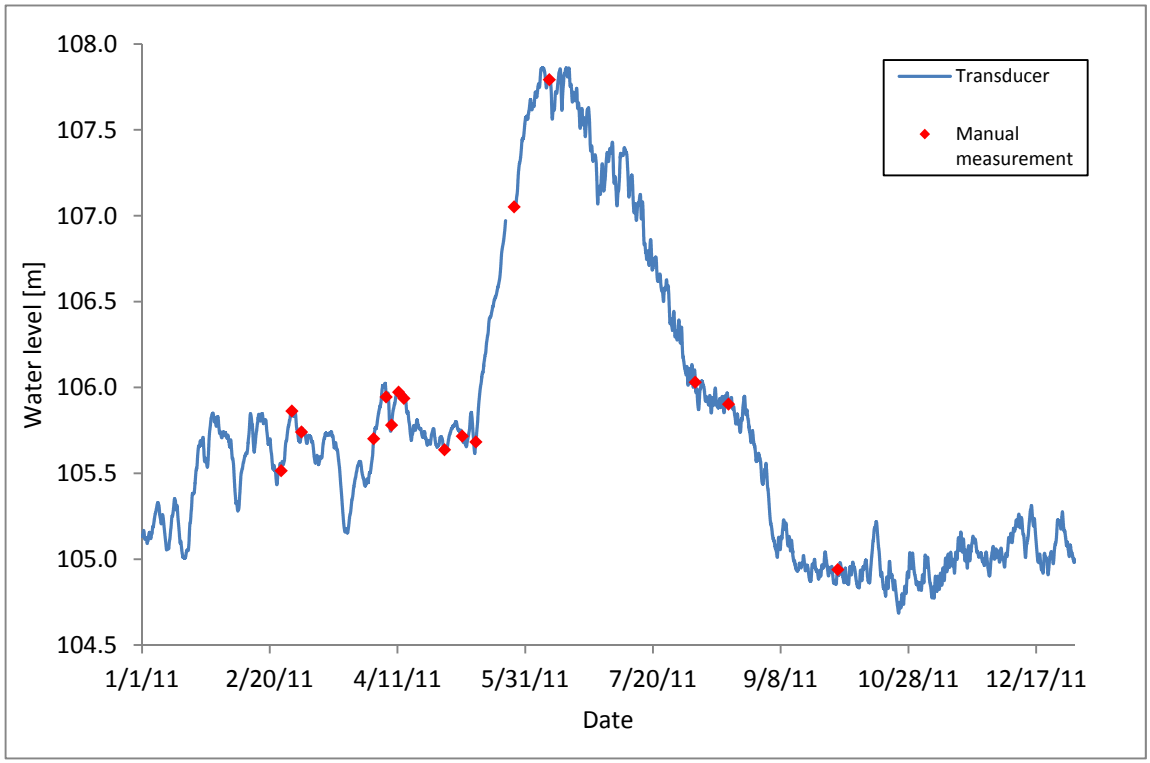

Figure A.9. Hourly measurements of water level in well 399-2-5, recorded using a dedicated transducer and data logger, and manual e-tape measurements used for data quality checks.

A single gauging station off of the 300 Area also collects hourly measurements of water level, water temperature, and specific conductance (SpC) for the Columbia River. However, it is well known that there is a gradient in river stage along the 300 Area, as it lies within the Hanford Reach, the longest free-flowing stretch of Columbia River, situated between the upstream Priest Rapids Dam and the downstream McNary Dam. Therefore, simulation results from a computational fluid dynamics model, MASS1, of the Columbia River for the Hanford Reach were also utilized for generating boundary conditions along the river shoreline (see Appendix C).

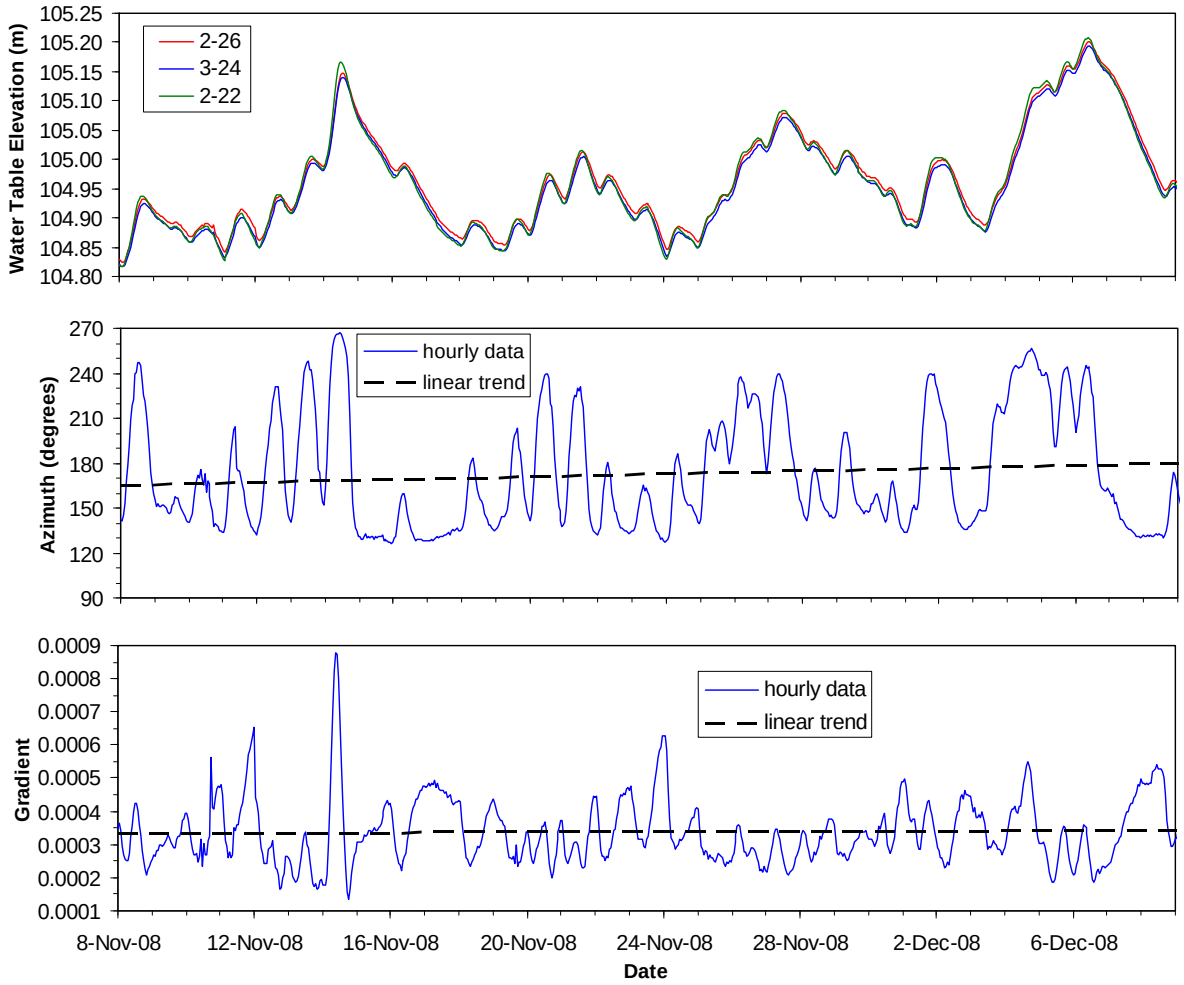

Figure A.10. Measured water levels for three IFRC wells, and computed azimuths of the flow vector and hydraulic head gradients for November through December 2008.

A.3.2 Specific Conductance

The specific conductance of water is a measure of its ability to conduct an electric current. This measurement is routinely made in many groundwater monitoring wells, but it has become of more interest lately owing to the increased use of ERT for imaging river water incursion into the unconfined aquifer and for mapping saline contaminant plumes in the vadose zone at Hanford (Johnson et al. 2012; Johnson and Wellman 2013). Electrical current in water is transported by ions in solution, so electrical conductivity increases as the concentration of ionic species increases. Owing to the differences between the average SpC of the Columbia River water (~142 µS/cm) and of groundwater in most of the 300 Area (>300 µS/cm), SpC can potentially be used as a surrogate tracer for river water incursion into the aquifer. However, some caution is warranted.

Use of SpC as a surrogate tracer is complicated by the fact that as river water enters the aquifer, the water table also rises, accessing the lower vadose zone. The vadose zone typically contains higher concentrations of dissolved ions relative to the underlying aquifer, since it has not been subjected to as much flushing with water and as a result of the concentrating effects of capillary rise and evaporation

from the shallow water table. Therefore, the initial rise of the water table into the lower vadose zone tends to result initially in higher values of SpC measured in wells due to solubilization and desorption of concentrated ionic species, followed by decreased values over time as more river water flows past a well, resulting in dilution (Figure A.11). Fluctuations in river stage and water table elevations can result in very complicated hysteretic patterns of SpC in the near-shore wells due to these superimposed solubilization/desorption and dilution effects. Interpretation of SpC data across multiple wells in the 300 Area is further complicated by differences in well screen intervals, spatial variability in aquifer and vadose zone properties, and contaminant distributions.

Variations in SpC across the 300 Area also reflect differences in the water sources entering the aquifer from the region surrounding the 300 Area. During low river stage, the shallow unconfined aquifer in the 300 Area is a convergent flow zone with groundwater entering the area from the southwest, west, and northwest. In general, wells farther from the river tend to have higher and more stable values of SpC. However, there is also a north-south trend in average SpC values across the 300 Area. At the southern end of the 300 Area, the SpC values measured in wells can exceed 1000 µS/cm, while at the northern end SpC values typically vary between 300 - 500 µS/cm. This difference results from higher dissolved ion concentrations at the southern end of the site presumably coming from the Horn Rapids landfill and irrigated agricultural fields located to the southwest of the 300 Area.

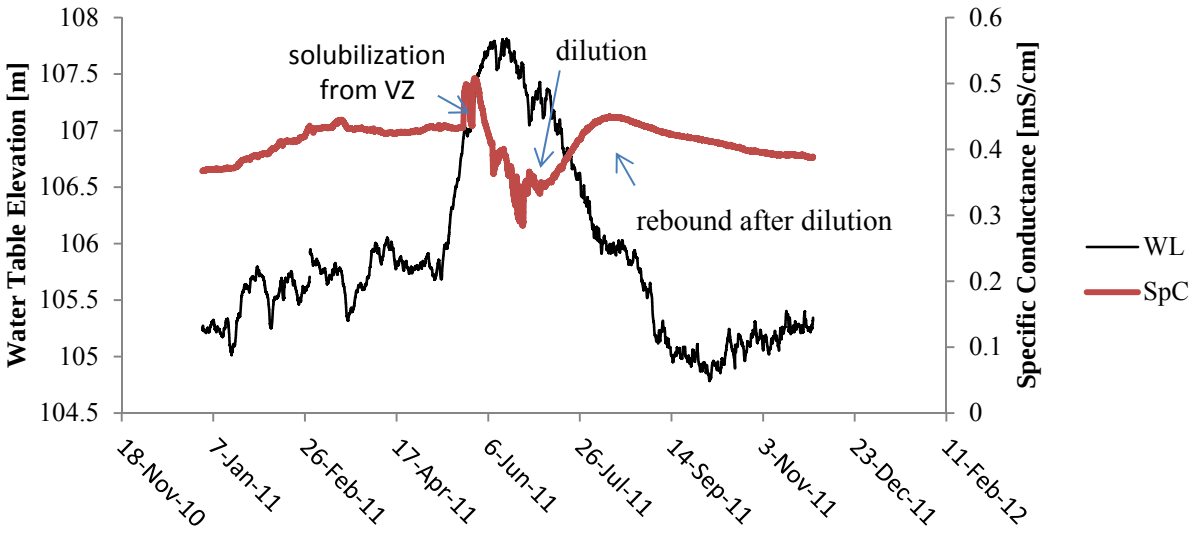

Figure A.11. Time series of hourly water level and specific conductance data for well 399-1-21A.

The specific conductance of a water sample can be estimated from the aqueous concentrations of the major ionic species in solution using the following equation (Tchobanoglous and Schroeder 1987)

$$SpC \cong \sum_i \left(C_i f_i \right) \tag{A.6}$$

where C_i is the concentration (mg/L) of ionic species i, and f_i is the conductivity factor for ionic species i (Table A.4). Figure A.12 shows measured values of specific conductance for Columbia River water samples from Richland, WA, collected from May 2008 through December 2010 (http://nwis.waterdata.

usgs.gov/nwis/qwdata?site_no=12473520&agency_cd=USGS&format=inventory_retrieval), and calculated values of SpC determined using Eq. (A.6).

Table A.4. Conductivity factors for major ionic species (from APHA 1980)

Ion	Conductivity factor, f_i (µS/cm) per meq/L	per mg/L
Cations		
Calcium (Ca++)	52.0	2.60
Magnesium (Mg++)	46.6	3.82
Potassium (K+)	72.0	1.84
Sodium (Na+)	48.9	2.13
Anions		
Bicarbonate (HCO3-)	43.6	0.715
Carbonate (CO3--)	84.6	2.82
Chloride (Cl-)	75.9	2.14
Nitrate (NO3-)	71.0	1.15
Sulfate (SO4--)	73.9	1.54

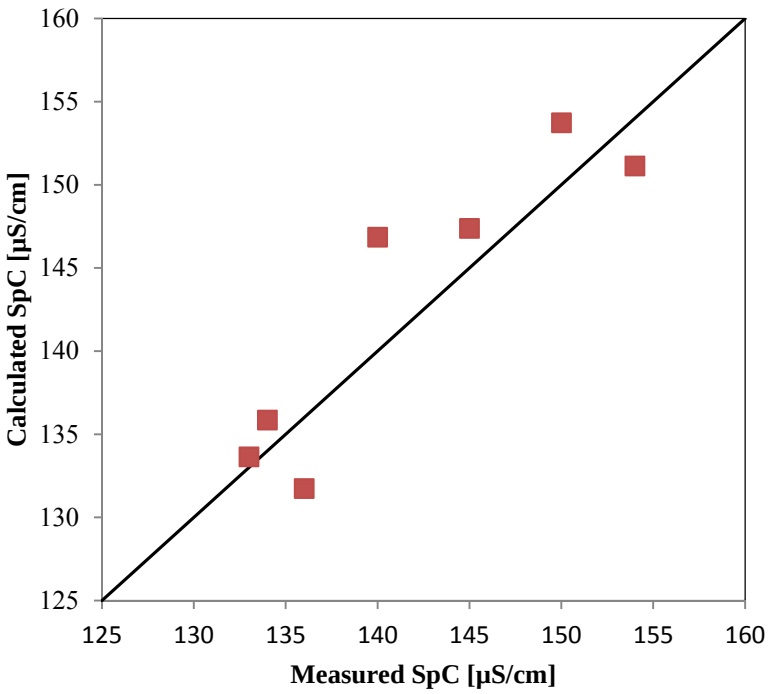

Figure A.12. Measured and calculated, from Eq. (A.6), values of specific conductance for samples of Columbia River water at Richland, WA.

A.3.3 Temperature

Hourly temperature data are collected from many of the wells in the automated 300 Area well monitoring network that are monitored for water levels, and also from a temperature sensor in the river at the 300 Area Columbia River gauging station, known as SWS-1 (see Appendix C). Like specific conductance, temperature has also been used as a surrogate tracer, although it is not strictly conservative owing to heat transfer through sediment grains.

Figure A.13 shows temperature and specific conductance data measured in well 399-2-5 during 2011. The decrease in the values of both variables shown in this figure is a result of river water incursion and rising water table. Note that the water levels for the same period in this well were shown previously in Figure A.9. The temperature and specific conductance tend to track each other fairly well, with differences arising from both solubilization effects (discussed earlier) and heat transfer effects that lead to non-conservative behavior. The average groundwater temperature is about 16 °C, but it can vary significantly, especially for wells close to the river. Fluid properties and biogeochemical reaction rates are temperature-dependent so temperature data are potentially very important. However, time-varying temperature data were not used directly in the current study.

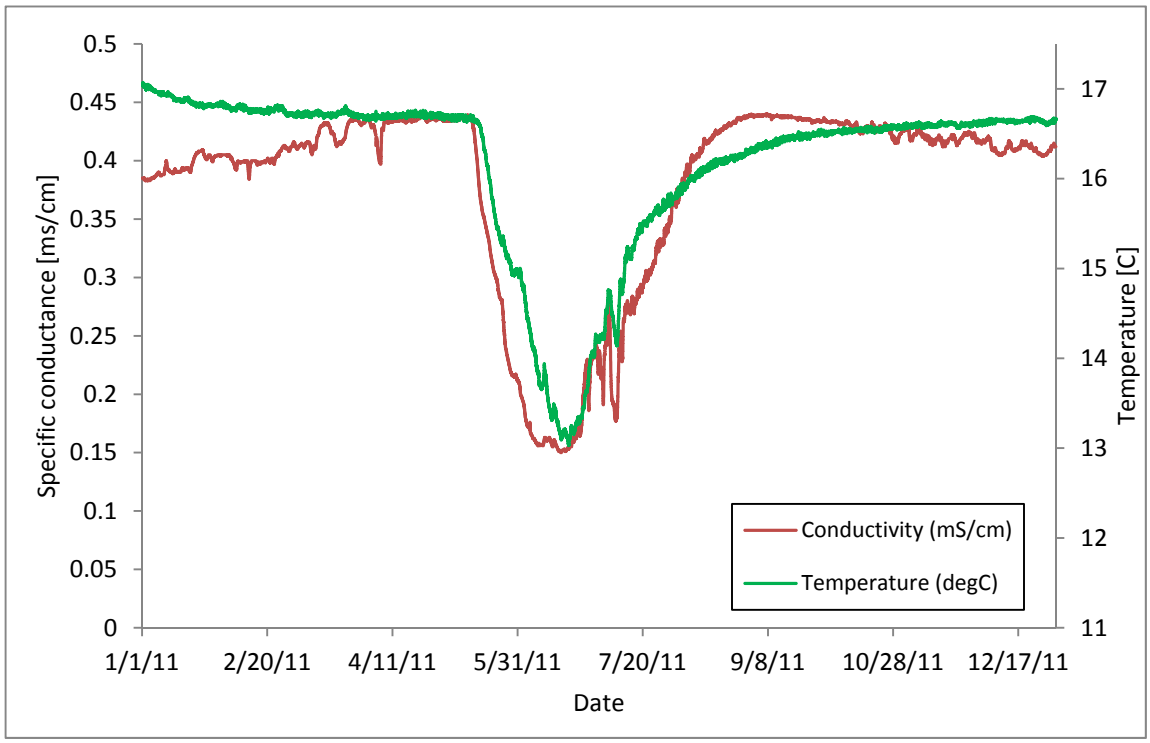

Figure A.13. Hourly measurements of temperature and specific conductance in well 399-2-5 in the Hanford 300 Area.

A.3.4 Aqueous Chemistry Data

Selected wells in the 300 Area are used by CHPRC for periodic sampling (typically semi-annually or quarterly) and measurement of major ions and contaminants of concern. Aqueous concentrations of major ions and uranium in 300 Area wells that are routinely monitored as part of DOE's groundwater

monitoring program (DOE-RL 2013b) were obtained from the Hanford Environmental Information System (HEIS) database.

Figure A.14 shows HEIS data for chloride and uranium measured over a 5-year period, from 2008 through 2012, for wells 399-1-10A, 399-1-16A, and 399-3-18. Chloride and uranium tend to respond in-phase with one another, with the magnitude of the uranium concentrations reflecting proximity to source areas. Deviations of this in-phase behavior occur where more local sources of uranium are accessed during periods of high water.

Aqueous chemistry data for river water are available from the U.S. Geological Survey (USGS) for several locations along the Columbia River, including one at Richland, located immediately downstream of the 300 Area. Figure A.15 shows chloride and temperature data for the Columbia River at Richland for 2008-2010.

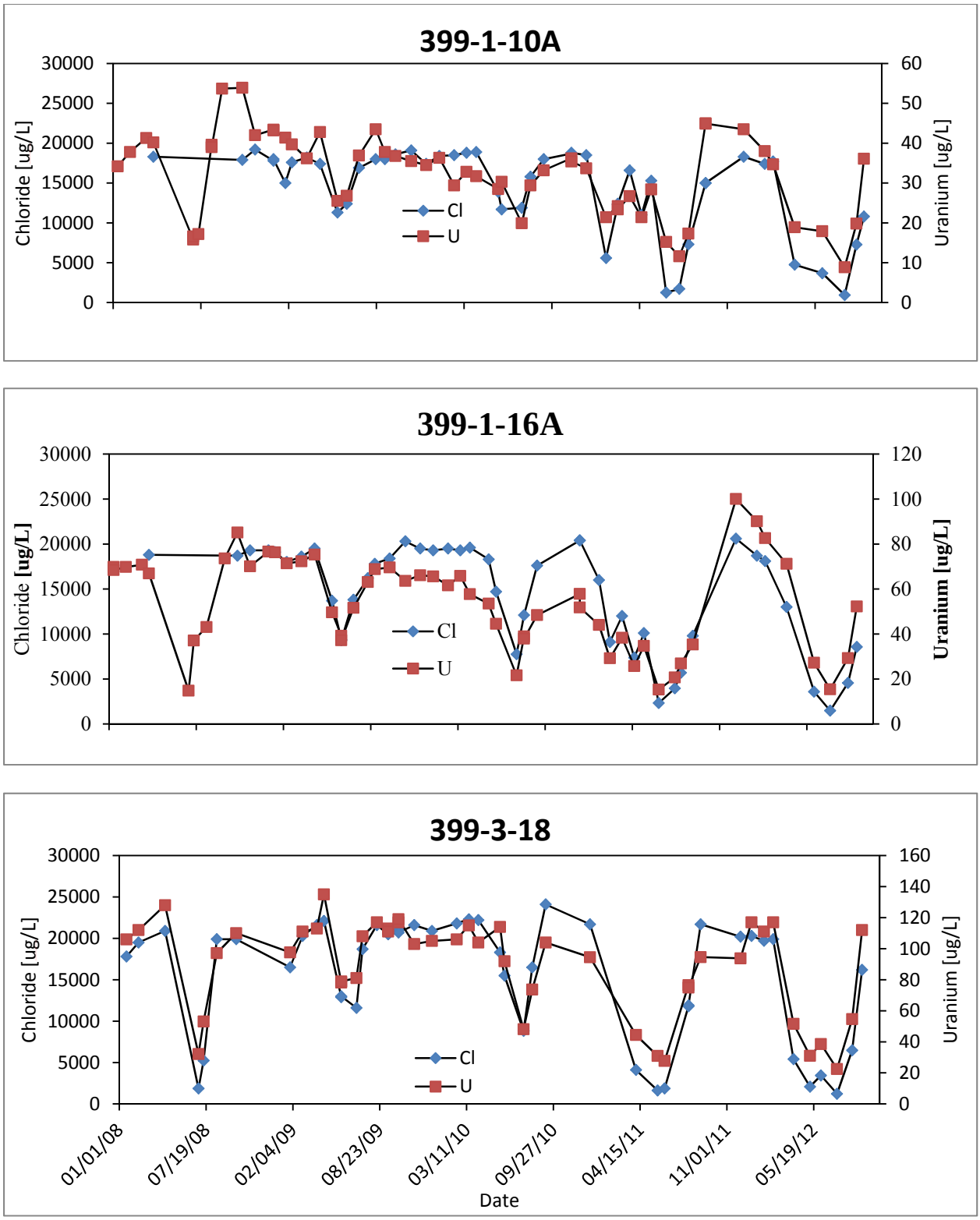

Figure A.14. Chloride and uranium data measured for three 300 Area wells in 2008-2012.

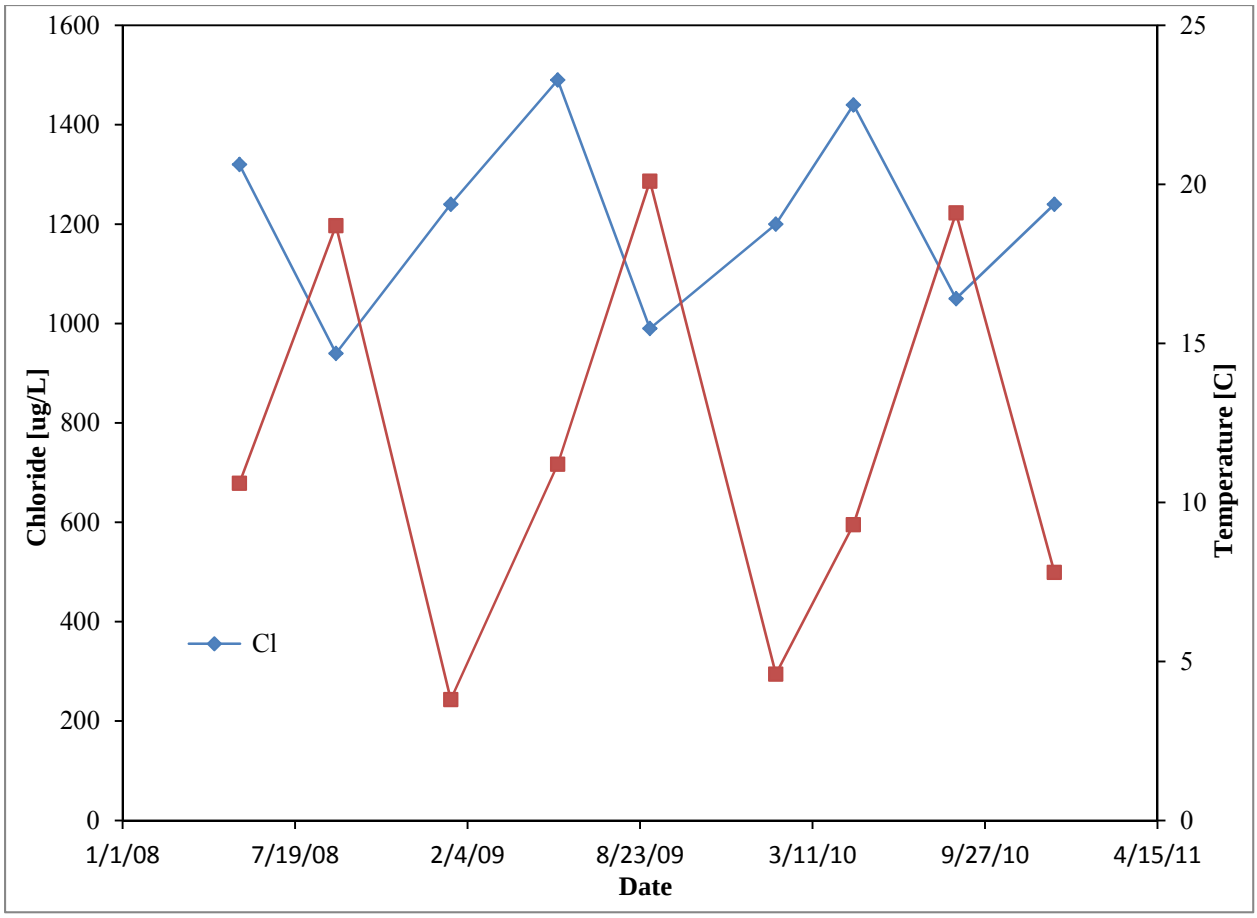

Figure A.15. Chloride and temperature data for the Columbia River at Richland, WA.

Based on these data, the average chloride concentration for the river is 1212 ug/L, ranging from ~900 - 1500 ug/L. The concentrations of chloride and other major ions are inversely correlated with river temperature, as shown in Figure A.15.

Reactive transport modeling typically requires data for all major ions, and for select species associated with the measurement of alkalinity. Molar concentrations (mol/L or M) of the anions hydroxide, [OH^-], carbonate, [CO_3^{2-}], and bicarbonate, [HCO_3^-] were calculated from reported values of sample pH and alkalinity using the USGS advanced speciation method (http://or.water.usgs.gov/alk/methods.html; last referenced June 17, 2013)

$$[OH^-] = K_w^{'} \cdot 10^{pH} \tag{A.7}$$

$$[CO_3^{2-}] = \frac{Alk_0 - K_w^{'} \cdot 10^{pH} + \frac{10^{-pH}}{\gamma}}{1 + \frac{10^{-pH}}{K_2^{'}}} \tag{A.8}$$

$$[HCO_3^-] = \frac{Alk_0 - K_w^{'} \cdot 10^{pH} + \frac{10^{-pH}}{\gamma}}{1 + 2K_2^{'} \cdot 10^{pH}} \quad \text{(A.9)}$$

where K_w' and K_2' are the temperature-dependent acid-dissociation constants for water and carbonic acid, respectively, Alk_0 is the alkalinity (eq/L), and γ is the ion activity coefficient for H^+. The activity coefficient for H^+ was calculated using the extended Debye-Hückel approximation (Stumm and Morgan 1996).

$$\log \gamma = -Az^2 \left(\frac{\sqrt{I}}{1 + Ba\sqrt{I}} \right) \quad \text{(A.10)}$$

where I is the ionic strength (M), z is the charge of the ion, and a is the size of the ion (Å). The parameters A and B in Eq. (A.8) are defined as

$$A = 1.82 \times 10^6 (\varepsilon T)^{-3/2} \quad B = 50.3(\varepsilon T)^{-1/2} \quad \text{(A.11)}$$

$$B = 50.3(\varepsilon T)^{-1/2} \quad \text{(A.12)}$$

where ε is the dielectric constant (a.k.a. dielectric permittivity) of water. Coefficients reported by the USGS were used for describing the temperature dependence of the acid-dissociation constants. Tabular data for the temperature dependence of the dielectric constant of water (Lide 1996) were also used, and an average groundwater temperature of 16 °C was assumed. For the pH range and other chemical conditions of groundwater in the 300 Area, carbonate equilibrium is dominated by bicarbonate, $[HCO_3^-]$.
The major ion chemistry data available from HEIS and the concentrations of bicarbonate calculated from the USGS advanced speciation method were used to define the primary species for the reaction network, and the boundary conditions used for modeling. Initial conditions were established using interpolated aqueous concentrations, and adsorbed uranium concentration data available from core and grab sampling, described previously.

A.4 References

APHA. 1980. *Standard Methods for the Examination of Water and Wastewater*, 15th Ed. American Public Health Administration, New York.

Bjornstad BN, JA Horner, VR Vermeul, DC Lanigan, and PD Thorne. 2009. *Borehole Completion and Conceptual Hydrogeologic Model for the IFRC Well Field, 300 Area, Hanford Site. Integrated Field Research Challenge Project*. PNNL-18340, Pacific Northwest National Laboratory, Richland, Washington.

Brooks RH and AT Corey. 1964. *Hydraulic Properties of Porous Media*. Colorado State University, Hydrology Paper No. 3, 27 pp.

DOE-RL. 2013a. *Remedial Investigation/Feasibility Study for the 300-FF-1, 300-FF-2, and 300-FF-5 Operable Units*. DOE/RL-2010-99, Rev. 0, CH2MHILL Plateau Remediation Company, Richland, Washington.

DOE-RL. 2013b. Hanford Site Groundwater Monitoring Report for 2012. DOE/RL-2013-22, Rev. 0, Prepared form U.S. Department of Energy by CH2M Hill Plateau Remediation Company, Richland, Washington.

Johnson TC, RJ Versteeg, ML Rockhold, LD Slater, D Ntarlagiannis, WJ Greenwood, and JM Zachara 2012. "Characterization of a contaminated wellfield using 3D electrical resistivity tomography implemented with geostatistical, discontinuous boundary, and known conductivity constraints." *Geophysics* 77(6), Article No. EN85. Doi:10.1190/geo2012-0121.1.

Johnson TC and DM Wellman. 2013. *Re-inversion of Surface Electrical Resistivity Tomography Data for the Hanford Site B-Complex*. PNNL-22520; RPT-DVZ-AFRI-014, Pacific Northwest National Laboratory, Richland, Washington.

Kaplan DI, IV Kutnyakov, AP Gamerdinger, RJ Serne, and KE Parker. 2000. "Gravel-Corrected Kd Values." *Ground Water* 38(6):851-857.

Lide DR (editor). 1996. CRC Handbook of Chemistry and Physics, 77th ed., CRC Press, New York.

Murray CJ, JM Zachara, JP McKinley, A Ward, Y-J Bott, K Draper, and D Moore. 2012. "Establishing a geochemical heterogeneity model for a contaminated vadose zone - aquifer system." *J. Contam. Hydrol.* doi: 10.1016/j.jconhyd.2012.02.003.

Shang J, C Liu, Z Wang, and JM Zachara. 2011. "Effect of grain size on uranium (VI) surface complexation kinetics and adsorption additivity." *Environ. Sci. Technol.* 45(14):6025-6031.

Shang J, C Liu, Z Wang, and JM Zachara. 2014. "Long-term kinetics of uranyl desorption from sediments under advective conditions." *Water Resour. Res.* 50:855-870, doi:10.1002/2013WRR013949.

Stoliker DL, C Liu, DB Kent, and JM Zachara. 2013. "Characterizing particle-scale equilibrium and kinetics of U(VI) desorption from U-contaminated sediments." *Water Resour. Res.* 49:1163 - 1177, doi:10.1002/wrcr.20104.

Stumm W and JJ Morgan. 1996. *Aquatic Chemistry – Chemical Equilibria and Rates in Natural Waters.* John Wiley and Sons, Inc., New York

Tchobanoglous G and ED Schroeder. 1987. *Water Quality*. Addison-Wesley, Reading, Massachusetts.

Van Genuchten MTh. 1980. "A closed-form equation for predicting the hydraulic conductivity of unsaturated soils." *Soil Sci. Soc. Am. J.* 44: 892-898.

Vermeul VR, BN Bjornstad, BG Fritz, JS Fruchter, RD Mackley, DR Newcomer, DP Mendoza, ML Rockhold, DM Wellman, and MD Williams. 2009. *300 Area Uranium Stabilization Through Polyphosphate Injection: Final Report*. PNNL-18529, Pacific Northwest National Laboratory, Richland, Washington.

Vermeul VR, JP McKinley, DR Newcomer, RD Mackley, and JM Zachara. 2011. "River-induced flow dynamics in long-screen wells and impact on aqueous samples." *Groundwater* 49:515-524.

Wang G, RJ Serne, MJ Lindberg, W Um, BN Bjornstad, BD Williams, IV Kutnyakov, Z Wang, and N Qafoku. 2012. *Uranium in Hanford Site 300 Area: Extraction Data on Borehole Sediments*. PNNL-22032/RPT-DVZ-AFRI-009. Pacific Northwest National Laboratory, Richland, Washington.

Ward AL, ME Conrad, WD Daily, JB Fink, VL Freedman, GW Gee, GM Hoverston, MJ Keller, EL Majer, CJ Murray, MD White, SB Yabusaki, ZF Zhang. 2006. V*adose Zone Transport Field Study Summary report*. PNNL-15443, Pacific Northwest National Laboratory, Richland, Washington.

Williams BA, CF Brown, W Um, MJ Nimmons, RE Peterson, BN Bjornstad, DC Lanigan, RJ Serne, FA Spane, and ML Rockhold. 2007. *Limited Field Investigation Report for Uranium Contamination in the 300-FF-5 Operable Unit at the 300 Area, Hanford Site, Washington*. PNNL-16435, Pacific Northwest National Laboratory, Richland, Washington.

Williams MD, ML Rockhold, PD Thorne, and Y Chen. 2008. *Three-dimensional groundwater models of the 300 Area at the Hanford Site, Washington State*. PNNL-17708, Pacific Northwest National Laboratory, Richland, Washington.

Zachara JM, MD Freshley, GV Last, RE Peterson, BN Bjornstad. 2012. *Updated Conceptual Model for the 300Area Uranium Groundwater Plume*. PNNL-22048, RPT-DVZ-AFRI-007, Pacific Northwest National Laboratory, Richland, WA.

Appendix B

Documentation of Data Quality and Consistency for Well Water Level, Temperature, and Specific Conductance Data

Appendix B

Documentation of Data Quality and Consistency for Well Water Level, Temperature, and Specific Conductance Data

B.1 Background

Groundwater flow in the 300 Area is highly dynamic due to the very larger hydraulic conductivity of the aquifer and proximity to the Columbia River. The Columbia River has large daily, weekly, and season river stage fluctuations that are rapidly transmitted inland in the 300 Area water table aquifer. Additionally, the large hydraulic conductivity of the aquifer results in small hydraulic gradients between wells at any period of time. Therefore, high frequency, synchronized, and accurate measurements of water levels from the wells in the 300 Area are required to adequately capture the flow and transport of groundwater in the 300 Area water table aquifer. This has been accomplished through establishing water level monitoring networks in the 300 Area as described below.

Earlier automated well monitoring networks for the 300 Area used downhole pressure transducers and data loggers at each well with periodic manual water level checks. Monitoring was ramped up in early 1990s and ended by the mid-1990s (Campbell and Newcomer 1992; Campbell 1994). Further details are provided by Williams et al. 2008. The Pacific Northwest National Laboratory (PNNL) Science and Technology Program started a new network in 2004 (Fritz et al. 2007) that was focused around the south end of the North Process Trench. This network was expanded and maintained by a number of different projects in the intervening years as listed below:

- 300-FF-5 Operable Unit Phase III Feasibility Study (DOE-RL 2005), specifically (Williams et al. 2008)
- Integrated Field Research Challenge project (2008-2012)
- This current project

Another project is continuing to operate some portions of the 300 Area Water Level Monitoring Network (PNNL-Science Focus Area project—Principal Investigator John Zachara)

B.2 Description of Current Network

The 300 Area Water Level, Temperature, and SpC network used in this study is shown in Figure B.1. Not all of the probes were operational during the period selected for the study and some probes were replaced. Note that in Figure B.1 not all wells have all three parameters collected (see legend).

Figure B.1. Water Level, Temperature, and SpC Monitoring Network used in this study. Note that some probes were not fully operational during the study period. Additionally, some wells had probes replaced during this time.

B.3 Data Evaluation

A formal test plan was not prepared prior to the collection of the data used in this study from the 300 Area Water Level, Temperature, and SpC network since they were legacy data (i.e., mostly collected before this study was initiated). However, a calculation package was prepared following the guidance of the Deep Vadose Zone Project quality requirements with an independent technical reviewer. The ID number is CALC-DVZ-AFRI-005 (in progress) titled "Water Level, Temperature, and Specific Conductance data from the 300 Area monitoring network." The probe descriptions, data files (along with file dates and sizes), methods used for evaluating the data, and results of the review are included in the calculation package.

The pressure transducers were either factory calibrated (if no drift was apparent from manual water level checks), calibrated in a PNNL laboratory, or calibrated using a linear regression using the manual water level checks. These are documented for each probe in the calculation package. Only manufacturer calibrations were used for temperature and specific conductance measurements. However, these data were checked by the reviewer to make sure the ranges and responses of these measurements were reasonable.

The independent technical review included hand-checking equations and calculations used in the Microsoft Excel spreadsheets, units and labels used in the spreadsheets, reasonableness of the calculated water levels from the pressure transducer measurements compared to manual water level measurements, and identification of spikes (mostly due to probe disturbance during other well operations) and data gaps. Data prior to 2011 was not checked since it was not used in the study. A number of iterations of revisions of the source files between the data provider and the independent technical reviewer along with other researchers on the project occurred during the review based on preliminary evaluations. The iterations and final results of the review are documented in the calculation package, CALC-DVZ-AFRI-005.

ASCII comma-separated value (CSV) files were also provided for use in the project simulations and analyses. These files were exported from the Microsoft Excel spreadsheets. These files were checked by comparing the trend plots independently generated from the CSV files with the trend plots in the Microsoft Excel spreadsheets for each well.

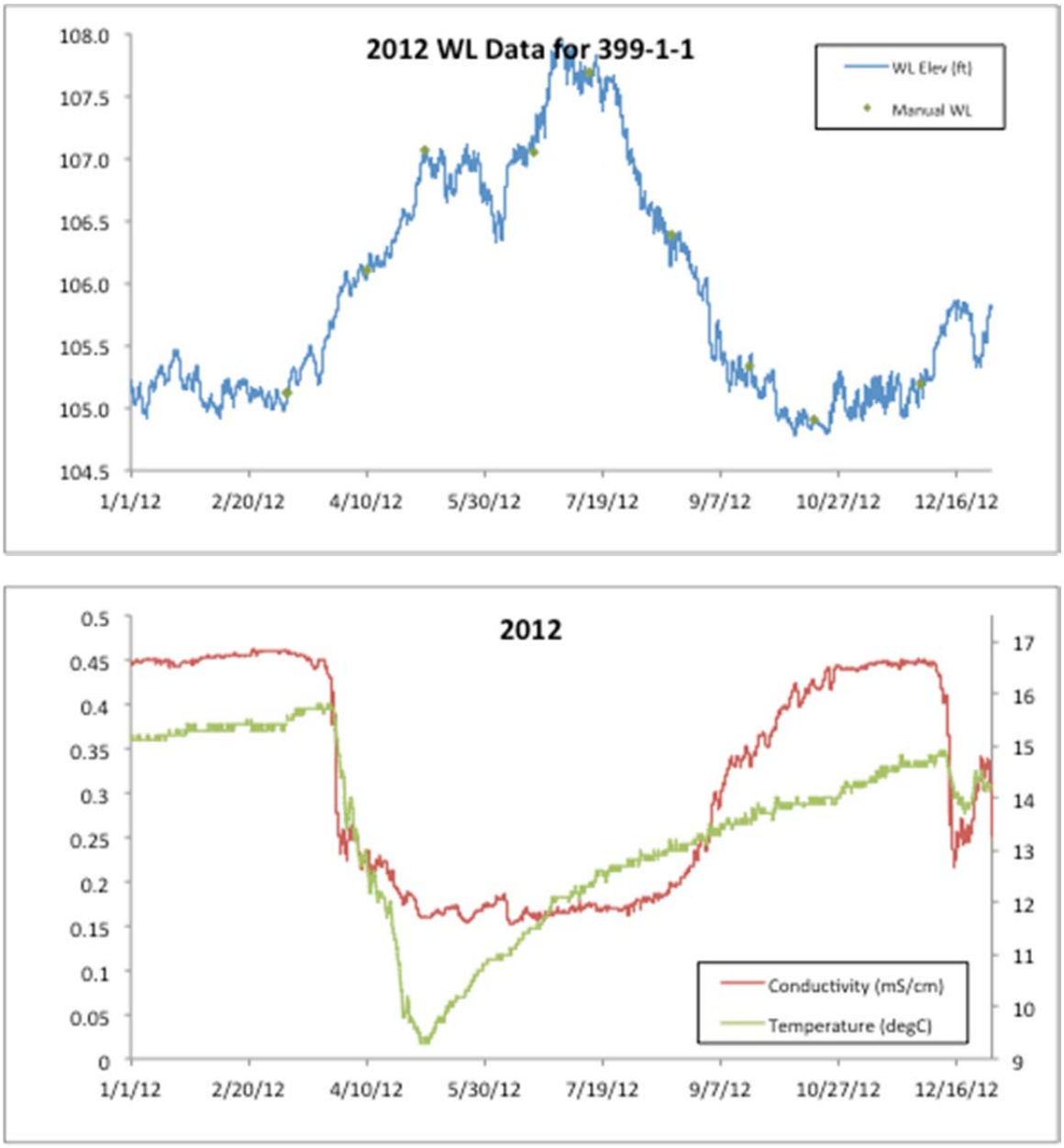

Figure B.2. 2012 Data for Well 399-1-1. (a) Example of Water Levels from Pressure Transducers Compared to Manual Water Level Measurements. (b) Temperature and SpC measurements.

B.4 References

Campbell MD and DR Newcomer. 1992. *Automatic Measurement of Water Levels Within the 300-FF-5 Boundary*. PNL-7874, Pacific Northwest Laboratory, Richland, Washington.

Campbell MD. 1994. *Monitoring Groundwater and River Interaction Along the Hanford Reach of the Columbia River*. PNL-9437, Pacific Northwest Laboratory, Richland, Washington.

DOE-RL 2005. *Work Plan for Phase III Feasibility Study 300-FF-5 Operable Unit*. DOE/RL-2005-41, Rev. 0, U.S. Department of Energy, Richland Operations Office, Richland, Washington.

Fritz BG, RD Mackley, NP Kohn, GW Patton, TJ Gilmore, DP Mendoza, D McFarland, AL Bunn, and EV Arntzen. 2007. *Investigation of the Hyporheic Zone at the 300 Area, Hanford Site*. PNNL-16805, Pacific Northwest National Laboratory, Richland, Washington.

Williams MD, ML Rockhold, PD Thorne, and Y Chen. 2008. *Three-Dimensional Groundwater Models of the 300 Area at the Hanford Site, Washington State*. PNNL-17708, Pacific Northwest National Laboratory, Richland, Washington.

Appendix C

Statistical Modeling of River and Groundwater Elevations

Appendix C

Statistical Modeling of River and Groundwater Elevations

Investigations of groundwater contamination problems in the 300 Area require knowledge of hydraulic head at points of interest and over time. Flow and transport simulation models require data or at least informed estimates of head at the model boundaries for purposes of forcing the model, and also for verification that the models are useful for predicting values inside the domain. Because head data are relatively limited, even in a relatively well-studied field area such as the 300 Area, methods are needed to estimate head for desired locations and time periods for which no data are available. This appendix describes the methods and results for creating complete time series of 300 Area river and well water levels for 2010-2012. In what follows, the term *data* refers exclusively to the observed, measured values collected in the field, while estimates from statistical model output are referred to as *values*, *output*, or *estimates*.

C.1 River Water Levels

It has long been recognized that the groundwater table in the 300 Area is strongly influenced by water levels in the Columbia River. Therefore, the first task was to create a complete water level record of the river for the period of interest. River level has been measured at station SWS-1 since the early 1990s, but many gaps exist in the data, typically for periods of high flow when recording instruments are out of their range. Hourly "raw" transducer data of water level head in millivolts (mV) were compared to actual manual measurements of water elevations in meters (NAVD88 datum) obtained at SWS-1 by Bob Edrington (formerly of CH2M HILL Plateau Remediation Company) during 2010. A simple linear regression of water elevations on millivolts was used to derive constants for the conversion:

$$L = a * mV + b, \tag{C.1}$$

where L = water level in meters, a = 0.3211115, and b = 104.1936 (Figure C.1).

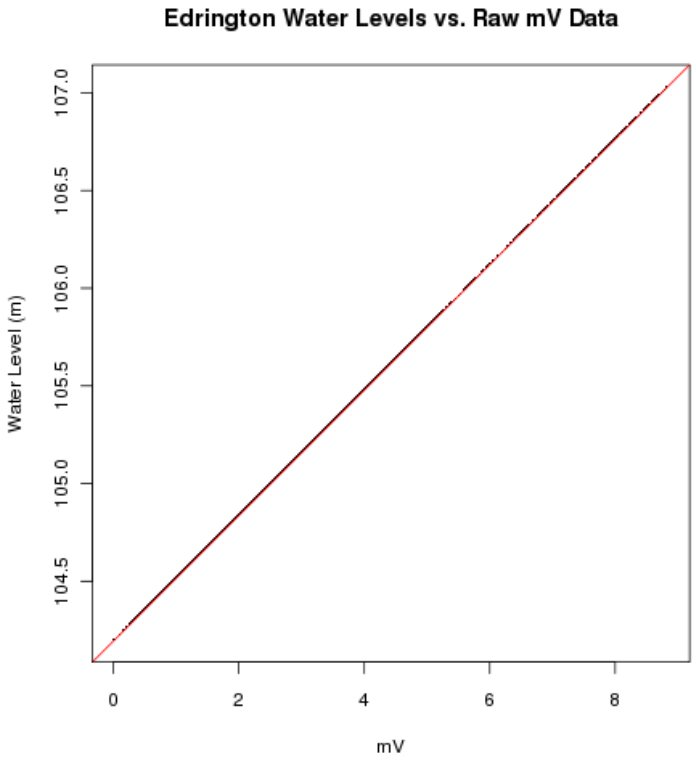

Figure C.1. Conversion of water level data measured in millivolts to elevation in meters. /pic/projects/hanford_300a/QA/scripts/C012/original/output/river_2010.png

Eq. (C.1) was then used to calculate water levels at SWS-1 for 2010-2012. These were in turn compared to river level data obtained from the Hanford Virtual Library (Figure C.2). These two datasets were nearly perfectly correlated (Intercept = 0.03282261, Slope = 0.9999853, R-squared = 1.0); the mean difference was 0.0313 m, or about 3 cm.

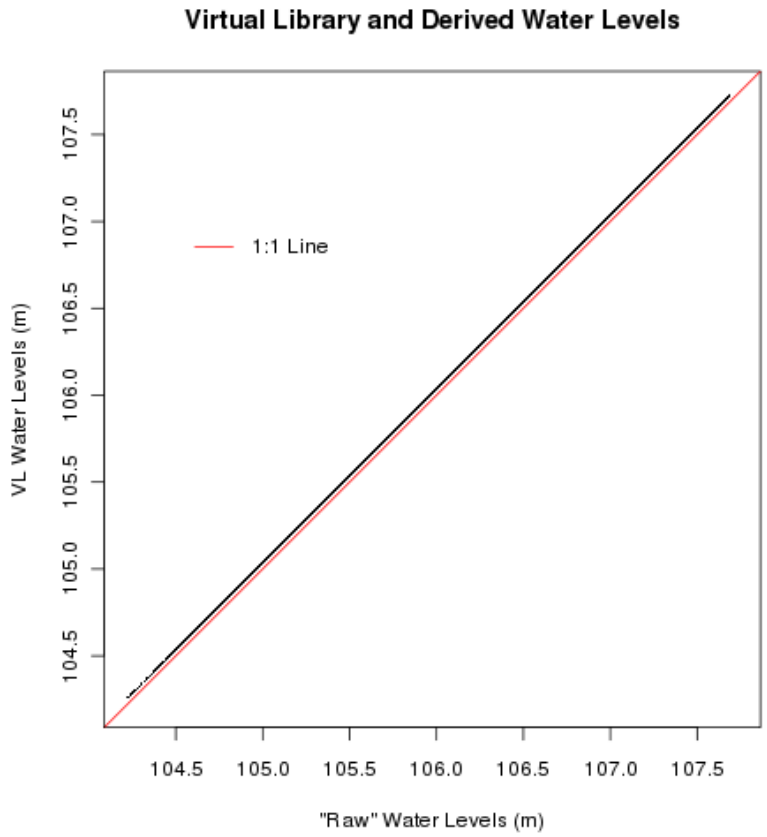

Figure C.2. One-to-one plot of calculated water levels and values in the Hanford Virtual Library. /pic/projects/hanford_300a/QA/scripts/C012/original/output/river_2011-12.png

There are two periods for which water level data at SWS-1 are unavailable because the pressure transducer over-ranged due to high water: late May 2011 to early July 2011, and late June 2012 to late July 2012. To fill in those missing data, output from the physically based Modular Aquatic Simulation System 1D (MASS1) model of the Columbia River was used. MASS1 simulates river stage, discharge, and water temperature at cross sections of the river. Near the 300 Area, the cross-sections or quadrants have an average spacing of 246 m (Figure C.3). Details about the MASS1 quadrants and SWS-1 are listed in Table C.1. Note that the old pressure transducer for the SWS-1 was replaced in FY13 by Pacific Northwest National Laboratory with a new transducer that has a larger range.

Figure C.3. 300 Area vicinity and MASS1 cross-section locations along the Columbia River. Decimal numbers are river mile (RM).
/pic/projects/hanford_300a/QA/fy13_report/figs/waichler_query.png

The MASS1 stage outputs were linearly interpolated between the nearest quadrants to obtain simulated water levels at SWS-1. The MASS1 model uses the NGVD29 datum for elevations, whereas Hanford site elevation data are measured and reported using the NAVD88 datum. MASS1 elevations were converted to NAVD88 (meters) using the shifts listed in Table C.1. Next, the available measured

data from SWS-1 (calculated from mV) were compared to the simulated values (Figure C.4). The time range of these data was 03/17/09 11:00 to 06/30/12 23:00. The regression line through the data (intercept = 1.256, slope = 0.988, R-squared=0.981) is very close to the 1:1 line that represents perfect agreement. To correct the small bias in the MASS1 output as compared to the measured data, the mean difference (data - output) was calculated as -0.00966 m, or approximately 1 cm. For the rest of the study, MASS1 output was first converted to NAVD88 (m) and then the bias correction of -0.00966 m was added to give the bias-corrected river level. Time gaps in the measured dataset for SWS-1 were filled using the corrected MASS1 values to give a complete hourly timeseries of river levels from 01/01/08 00:00 to 06/30/12 23:00. Years 2010 - 2012 are shown in Figure C.5.

Table C.1. MASS1 quadrants (cross section locations) and shifts to convert from meters NGVD29 to NAVD88. /pic/projects/hanford_300a/QA/fy13_report/figs/shoreline_pt.csv

Quad	River Mile	Easting	Northing	Shift
315	345.816	594348.335	117821.654	1.041
316	345.646	594306.055	117594.882	1.041
317	345.476	594309.899	117345.048	1.04
318	345.354	594329.117	117060.621	1.04
319	345.168	594371.396	116795.413	1.04
320	344.969	594405.989	116564.797	1.039
321	344.779	594448.268	116326.493	1.039
322	344.591	594525.14	116061.285	1.039
323	344.293	594578.951	115846.043	1.038
324	344.152	594644.292	115615.427	1.038
325	343.152	594698.102	115384.811	1.037
326	343.842	594755.756	115158.039	1.037
327	343.700	594794.192	114931.266	1.037
328	343.559	594836.472	114689.119	1.036
SWS-1	344.252	594582.44	115779.85	1.038

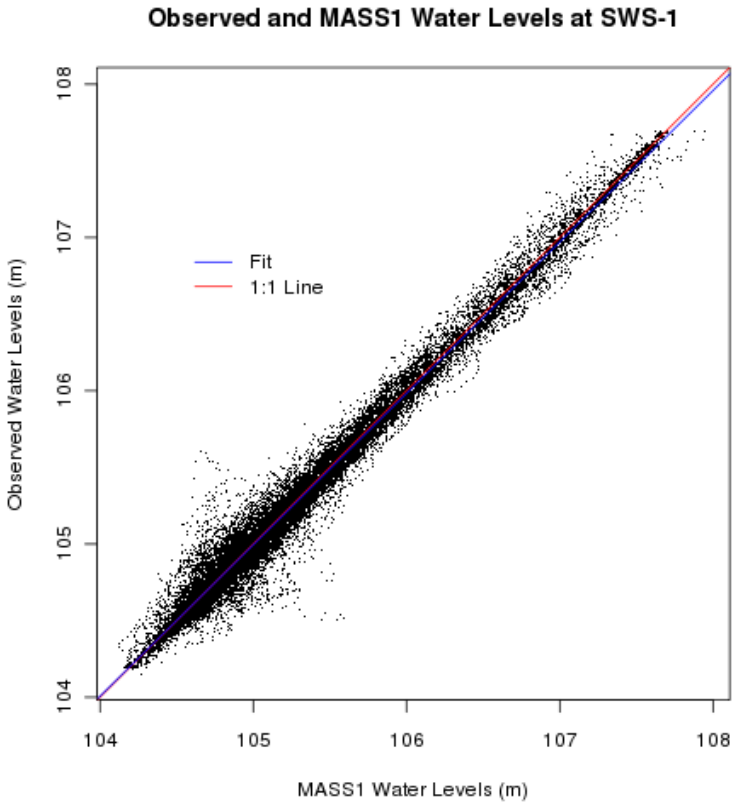

Figure C.4. Observed and adjusted MASS1 water levels at 300 Area gage SWS-1.
/pic/projects/hanford_300a/QA/scripts/C012/original/output/river_obs_mass.png

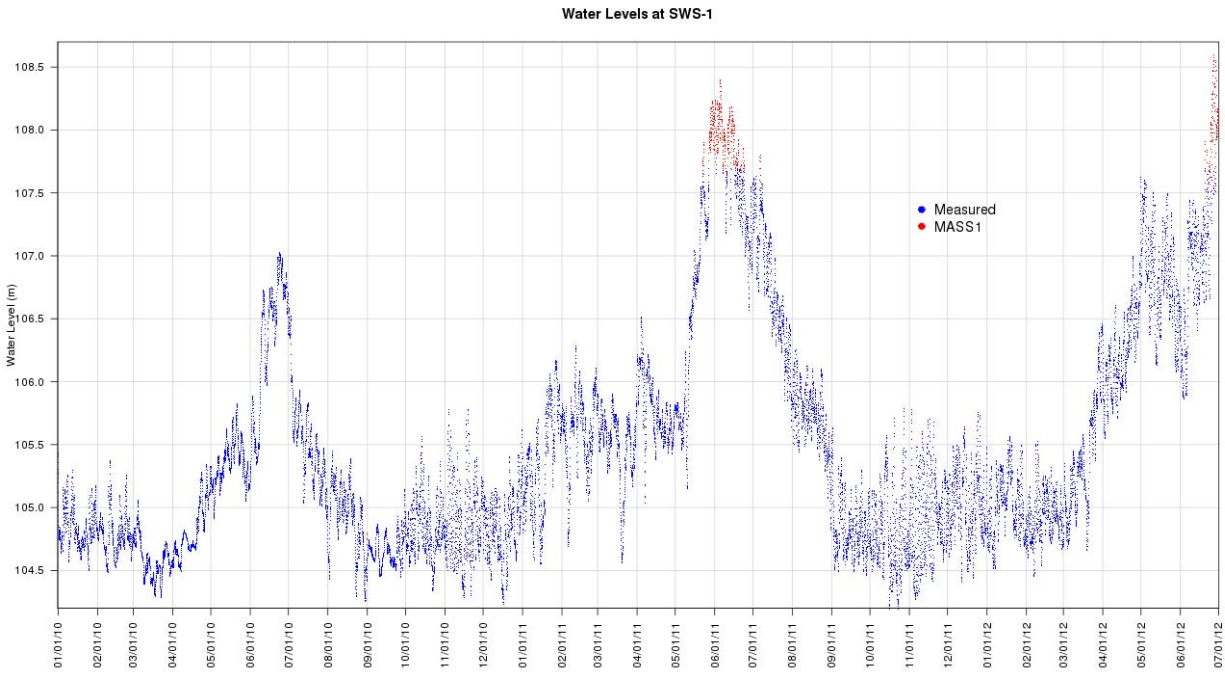

Figure C.5. Observed and adjusted MASS1 water levels vs. time.
/pic/projects/hanford_300a/QA/scripts/C012/original/output/river_obs_mass_timeseries.png

C.2 Groundwater Levels

This section describes the development of statistical models to describe water levels in 42 300 Area wells which have been used for defining initial and boundary conditions for subsurface flow and transport modeling. Hourly groundwater data is available for many 300 Area wells of interest starting in 2011. These data can be used along with the river levels and statistical methods to generate long-term hydraulic head boundary conditions for the groundwater flow and transport models. Groundwater level at a given well and time is highly correlated with other groundwater levels and river levels, at various timescales. The strong correlation between heads at different locations can be seen in Figure C.6. Groundwater levels are clearly related to river stage, except for wells completed in the Ringold Formation (e.g., 699-S29-E11and 699-S27-E9A), which do not have as strong a hydraulic connection to the river.

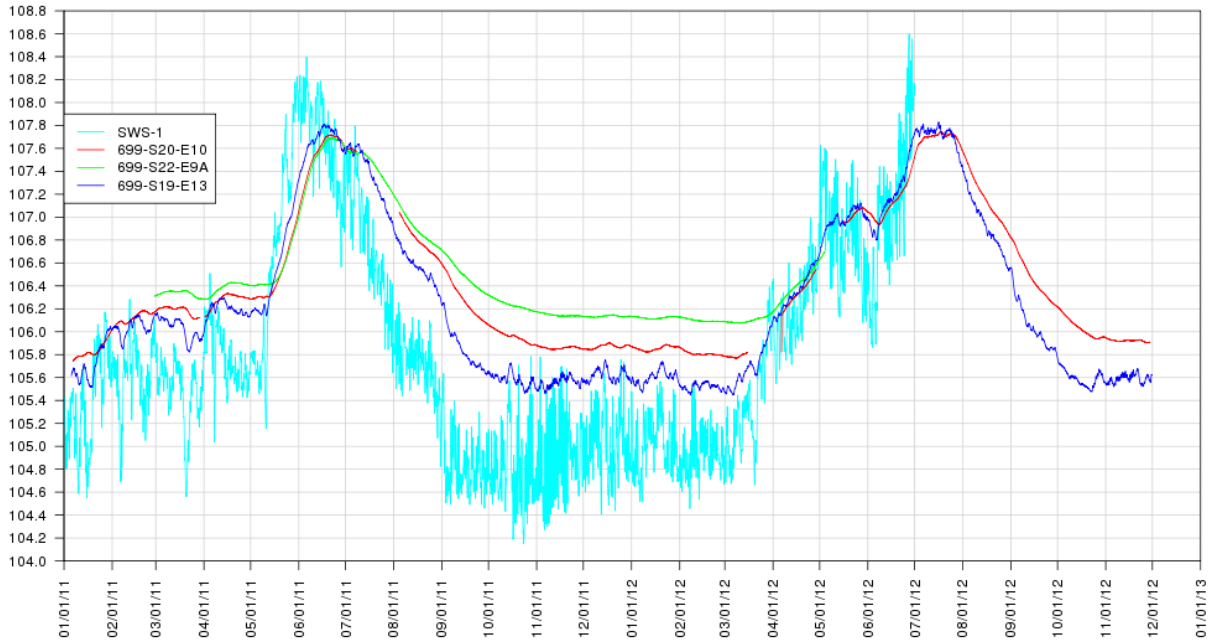

Figure C.6a. Water levels at selected locations vs. time.
/pic/projects/hanford_300a/QA/fy13_report/figs/wells_wl_1.png

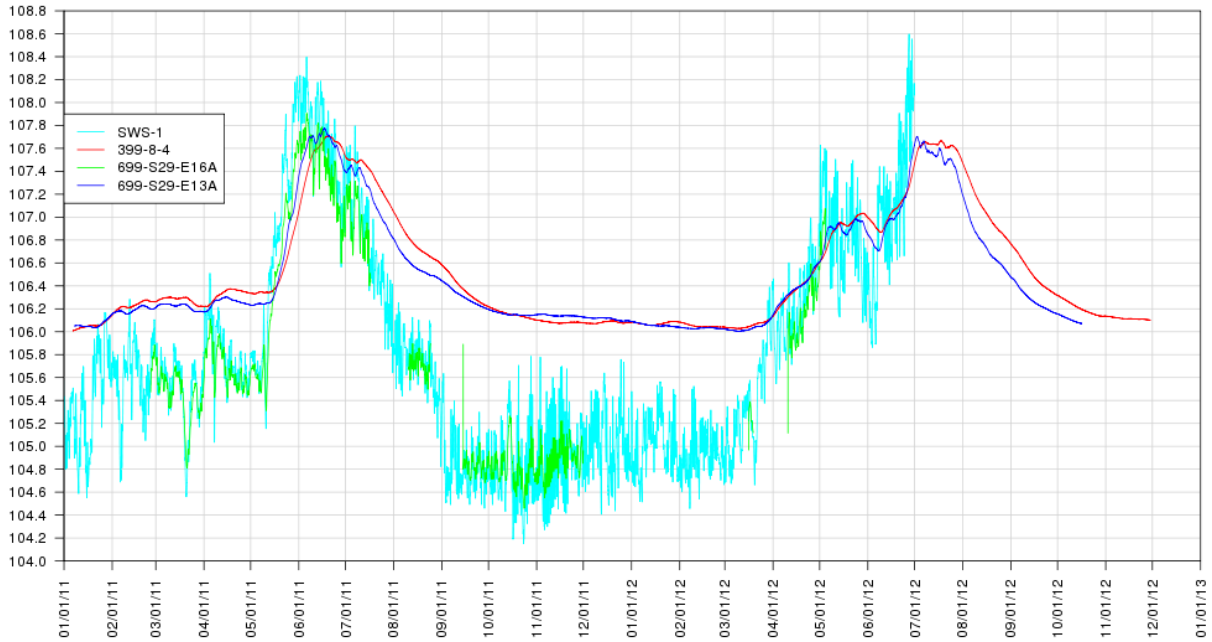

Figure C.6b. Water levels at selected locations vs. time.
/pic/projects/hanford_300a/QA/fy13_report/figs/wells_wl_2.png

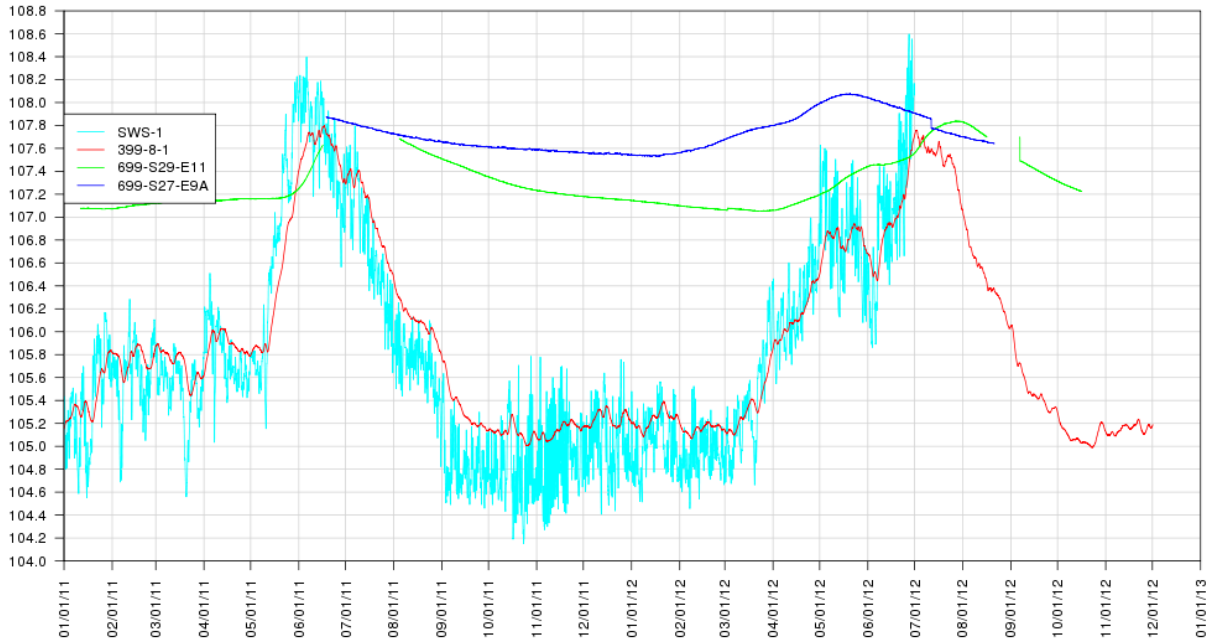

Figure C.6c. Water levels at selected locations vs. time.
/pic/projects/hanford_300a/QA/fy13_report/figs/wells_wl_3.png

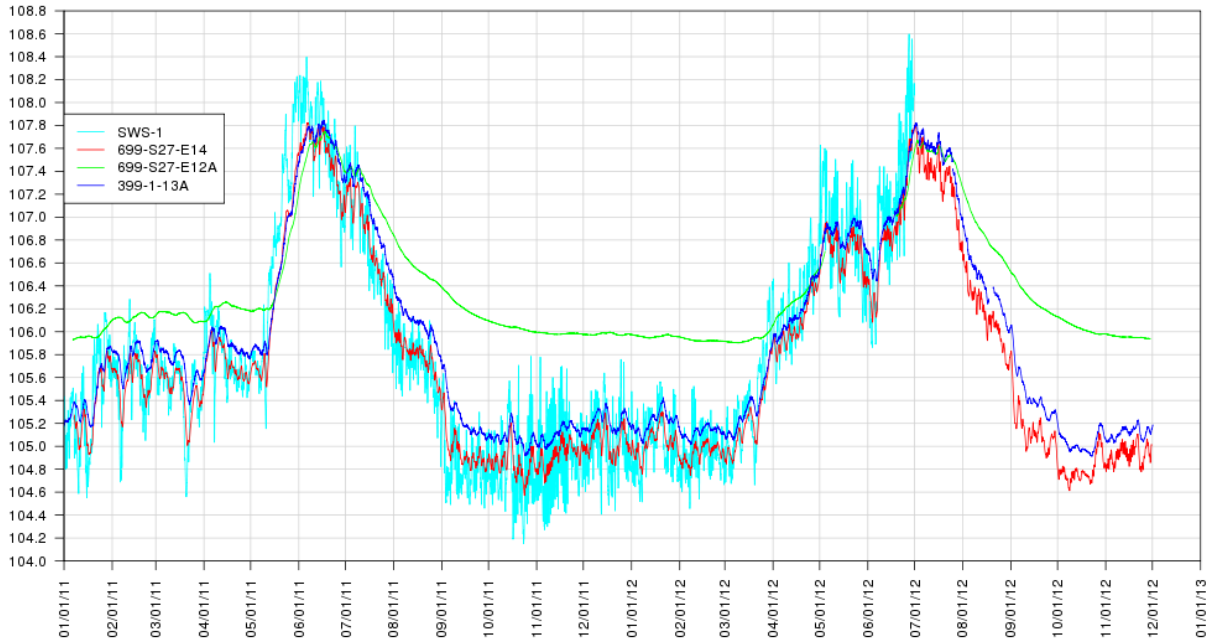

Figure C.6d. Water levels at selected locations vs. time.
/pic/projects/hanford_300a/QA/fy13_report/figs/wells_wl_4.png

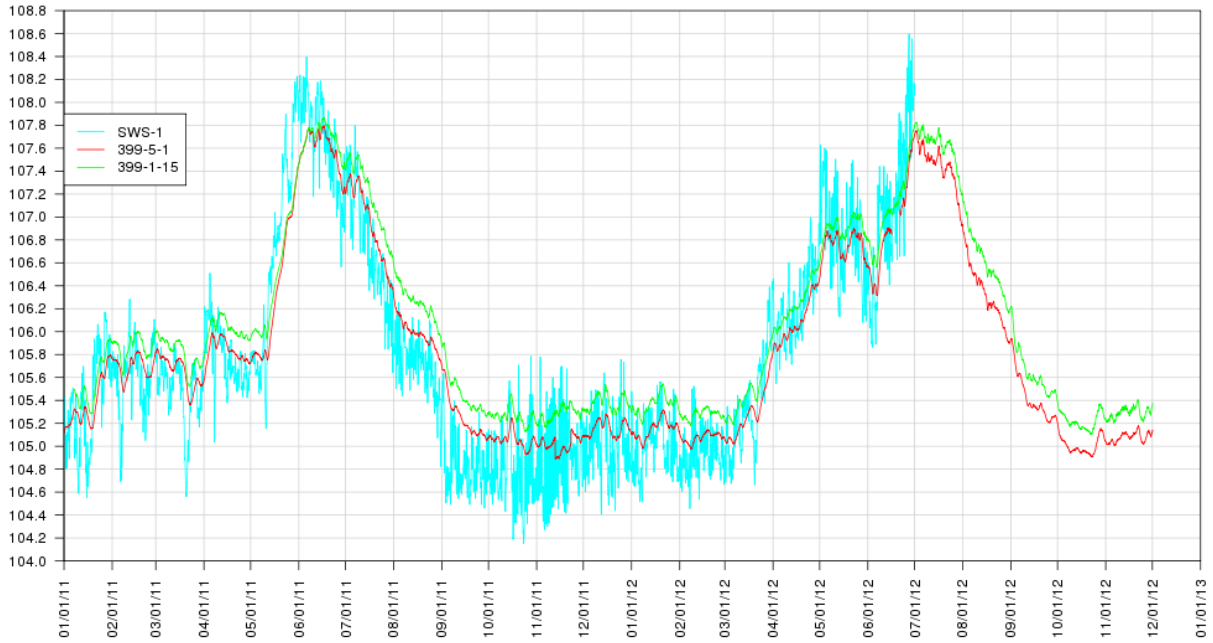

Figure C.6e. Water levels at selected locations vs. time.
/pic/projects/hanford_300a/QA/fy13_report/figs/wells_wl_5.png

After testing various regression model structures, three models were selected for estimating groundwater level at a given well:

$$G\_t = a\ G\_t\text{-}1 + b\ R\_ma + c\ I + d, \quad \text{(C.2)}$$

$$G\_t = b\ R\_ma + c\ I + d, \text{ and} \quad \text{(C.3)}$$

$$G\_t = b\ R\_ma + d \quad \text{(C.4)}$$

where G_t = groundwater level at time t, G_t-1 = groundwater level at the previous hour, R_ma = hourly moving-average of the river level at SWS-1, I = indicator variable for month. a, b, c, d are coefficients fitted by multiple linear regression.

In theory, the first model, Eq. (C.2), should be superior because it includes previous groundwater head, which can be thought of as a measure of storage. How much head can rise or fall in response to inflows and outflows may depend in part on level of storage already in the groundwater reservoir. Also, simply having an additional term in the regression model guarantees a closer fit, although not necessarily better skill for future predictions. Equation (C.2) is also known as a vector auto-regressive (VARX) type of model. Equations (C.3) and (C.4) lack an auto-regressive component and are ordinary linear regression (LS) models.

The second model, Eq. (C.3), wherein groundwater level is dependent only on knowing the river moving average and time of year, has an important advantage of being simpler to apply—no knowledge of prior groundwater levels is required, and water levels can be estimated as long as river data is available. This quality is especially useful for filling long time gaps when no data are available at a well.

The first two equations are multiple linear regression models. The third model, Eq. (C.4), omits the monthly indicator term and is a simple linear regression model, where the river moving average is the only independent variable.

The river moving average term R_ma in the above equations was computed from the hourly river time series at SWS-1 described in the previous section. Moving averages were computed as the mean over a backward-looking window, using 15 different time window lengths: 2, 3, 6, 12, 24 hours, and 2, 3, 5, 7, 10, 14, 21, 30, 45, 60 days. The moving average time series are themselves hourly and were computed for the same period as the hourly river dataset, 1/1/2010 to 6/30/12. Each of the moving averages were used in turn in application of the regression equations, and the final model selected for each well used the moving average that resulted in the lowest mean absolute error (MAE) in the prediction period.

The indicator variable was the same for all models: I = 1 for months January to June, and I = 0 for all other months. This model term was found to be important for capturing the different effects that changing river levels have on groundwater, depending on whether the river is in an overall rising or falling period. Including the indicator term in the models generally improved the fit, reduced bias, and reduced time-dependent trends in the residuals. However, the switch of the indicator value at January 1 and July 1 resulted in spuriously large changes in predicted water levels at those times for certain wells, particularly in 2010. For those wells, the third model, without the month indicator term, Eq. (C.4), was used.

The three forms of linear regression models were each fitted with all available 2011 data. Each of the 15 moving average periods was used for each of the models. The regression models were then used to predict hourly groundwater levels beginning with the first time step after the fitting period, through 6/30/12. If well data were available only before 1/1/12, then the available data were split into equal sized sets for fitting and prediction, with fitting on the earlier period. MAE and bias (bias = mean difference between observed and modeled values) were calculated separately for the fit and prediction periods. In what follows, the default moving average period and corresponding model to be used for a given well was the one having the lowest absolute value of bias for the prediction period. However, for some wells a different moving average period and model were selected after inspecting results. In those instances, a different moving average period provided trend and variability characteristics in the output that more closely matched the data.

Two alternate approaches were used to compile the final, complete groundwater level time series for each of 42 wells. In both, the first preference for sourcing a water level value for a given time step was the available data. Both approaches used the measured values whenever and wherever available. In the first approach, priority for filling in the remaining time steps was given to Eq. (C.2). After using available output from Eq. (C.2), remaining time steps were filled using Eq. (C.3) or Eq. (C.4). Equation (C.3) was used, unless it resulted in significant shifts at January 1 and July 1, in which case Eq. (C.4) was used. In the second approach, filling in the remaining time steps without data was done using Eq. (C.3) or Eq. (C.4). Since there were no groundwater data prior to 2011, Eq. (C.3) or Eq. (C.4) was used in both approaches for all times from 1/1/10 to the start of the data in 2011. Thereafter, output from Eq. (C.2), Eq. (C.3), and Eq. (C.4) was used as just described.

A final step was done to smooth large (> 1 cm) 1-hour changes at transitions between model and data. Changes in water level at the transitions from model to data and data to model were decreased to 1 cm or

less by applying the following algorithm for changing the model values (data were never changed). This smoothing was conducted the same way for both of the final compilation approaches.

1. If the data gap filled by model output was 4 hours or less, the model values were replaced with values linearly interpolated between the data points on either side of the gap.

2. If the gap was 5 hours or longer, then the following was done:

    a) The model values in the data gap were uniformly shifted up or down such that the new water level changes at the transitions are equal in absolute value. This shift typically corrected most of the bias error of the modeled values.

    b) If the new transition changes still exceeded 1 cm, then the model values near the transition were further modified by applying a linear ramp from the transition inward into the model period, until no hourly change in the transition exceeded 1 cm.

The final products were a set of CSV files for each of the two compilation approaches:

- File listing the following summary info for each well: use of multiple or simple linear regression model, moving average period, model coefficient values, times for start and end of fitting and prediction periods, MAE and Bias for fitting and prediction periods (Table C.2 and Table C.3).
- File containing the complete time-series for each well, with time in rows and wells in columns. This file provides a convenient way to access all of the well time series at once (see example snippet in Table C.4).
- File for each well with time in rows, and columns for time, water level, and flag indicating source of each value. Flags were D = data (observed); V = VARX model; M = LR model; I = interpolated. These files tell the user exactly where each hour's water level values come from (example snippet in Table C.5).

Table C.2. Summary information for VARX regression models used for wells. MA=moving average for river levels at SWS-1. a, b, c, d are model coefficients in Eq. (C.2) to Eq. (C.4). Fit refers to period used for fitting the model, Pre refers to period of model prediction. By definition, FitBias was zero at all wells.
/pic/projects/hanford_300a/QA/scripts/C015_rev1/original/output /varx_model_info.csv

Well	River_MA_Period	a	b	c	d	FitBeg	FitEnd	PreBeg	PreEnd	FitMAE	PreMAE	PreBias
399-1-1	24 hours	0.9918094	0.0074668	0.0002446	0.0776908	1/1/2011 1:00	12/31/2011 23:00	1/1/2012 0:00	6/30/2012 23:00	0.0065	0.0903	0.0057
399-1-10A	6 hours	0.9670146	0.0313544	-0.0032532	0.1793504	1/1/2011 1:00	12/31/2011 23:00	1/1/2012 0:00	6/30/2012 23:00	0.0068	0.063	-0.0011
399-1-11	2 days	0.9926019	0.0065316	-0.0001071	0.0932669	1/1/2011 1:00	12/31/2011 23:00	1/1/2012 0:00	6/30/2012 23:00	0.0027	0.0687	0.0065
399-1-12	24 hours	0.9899211	0.0094251	-0.0004721	0.0705651	1/1/2011 2:00	12/31/2011 23:00	1/1/2012 0:00	6/30/2012 23:00	0.0023	0.0385	0.0063
399-1-13A	3 days	0.9916712	0.0074388	-0.000225	0.0955388	1/1/2011 1:00	12/31/2011 23:00	1/1/2012 0:00	6/30/2012 23:00	0.0036	0.0628	0.0002
399-1-15	12 hours	0.9910756	0.0079173	-0.0011694	0.1096065	1/7/2011 8:00	12/31/2011 23:00	1/1/2012 0:00	6/30/2012 23:00	0.0011	0.0438	-0.0004
399-1-17A	3 days	0.9927072	0.006535	0.0002246	0.0806718	1/1/2011 1:00	12/31/2011 23:00	1/1/2012 0:00	6/30/2012 23:00	0.0028	0.0844	0.0007
399-1-18A	2 days	0.9953794	0.0038696	-0.0002501	0.0813345	1/5/2011 8:00	12/31/2011 23:00	1/1/2012 0:00	6/30/2012 23:00	0.0019	0.0593	-0.0015
399-1-2	3 days	0.9931123	0.0062054	4.46E-05	0.0729218	1/1/2011 1:00	12/31/2011 23:00	1/1/2012 0:00	6/30/2012 23:00	0.0046	0.0788	0.001
399-1-21A	3 days	0.9949967	0.0042924	0.0007501	0.0751775	1/1/2011 1:00	12/31/2011 23:00	1/1/2012 0:00	6/30/2012 23:00	0.005	0.1049	-0.0083
399-1-23	3 days	0.9919892	0.0073434	0.0001518	0.0714299	1/1/2011 1:00	12/31/2011 23:00	1/1/2012 0:00	6/30/2012 23:00	0.0027	0.0774	0.0094
399-1-32	3 days	0.993403	0.005923	0.0003898	0.0715707	1/1/2011 1:00	12/31/2011 23:00	1/1/2012 0:00	6/30/2012 23:00	0.0032	0.0958	0.0074
399-1-60	24 hours	0.9879561	0.0111479	-0.000562	0.0955238	4/8/2011 9:00	12/31/2011 23:00	1/1/2012 0:00	6/30/2012 23:00	0.0034	0.0435	-0.0069
399-1-7	2 hours	0.9801322	0.0186487	-0.0016424	0.1320587	1/1/2011 1:00	12/31/2011 23:00	1/1/2012 0:00	6/30/2012 23:00	0.0029	0.0417	0.0002
399-2-10	2 hours	0.9843552	0.0146336	-0.0011022	0.1082753	1/1/2011 1:00	12/31/2011 23:00	1/1/2012 0:00	6/30/2012 23:00	0.0022	0.0333	0.001
399-2-1	24 hours	0.9911751	0.008055	0.0003992	0.0815158	1/1/2011 2:00	12/31/2011 23:00	1/1/2012 0:00	6/30/2012 23:00	0.0071	0.0873	0.0091
399-2-3	2 days	0.9961807	0.0033649	0.0008194	0.0477661	1/1/2011 2:00	12/31/2011 23:00	1/1/2012 0:00	6/30/2012 23:00	0.0058	0.1537	0
399-2-33	24 hours	0.9887674	0.0103464	-0.0001325	0.0941987	4/7/2011 16:00	12/31/2011 23:00	1/1/2012 0:00	6/30/2012 23:00	0.0046	0.0566	0.0045
399-2-5	2 days	0.9923317	0.006989	0.0003812	0.0719187	1/1/2011 1:00	12/31/2011 23:00	1/1/2012 0:00	6/30/2012 23:00	0.0047	0.0927	0.0045
399-3-18	24 hours	0.9892738	0.0098128	0.0002246	0.0967555	1/1/2011 1:00	12/31/2011 23:00	1/1/2012 0:00	6/30/2012 23:00	0.0061	0.0755	0.0034
399-3-20	6 hours	0.9759608	0.0223902	-0.0013029	0.1751436	1/1/2011 1:00	12/31/2011 23:00	1/1/2012 0:00	6/30/2012 23:00	0.0025	0.0286	-0.0025
399-3-22	12 hours	0.9808591	0.0177654	-0.0012076	0.146351	1/1/2011 1:00	12/31/2011 23:00	1/1/2012 0:00	6/30/2012 23:00	0.0027	0.037	-0.0001
399-3-26	2 hours	0.9834467	0.0155487	-0.0011998	0.1074711	12/31/2010 23:00	12/31/2011 23:00	1/1/2012 0:00	6/30/2012 23:00	0.0022	0.0342	0.0011
399-3-34	24 hours	0.9865172	0.0124967	-0.0005682	0.1048323	4/7/2011 18:00	12/31/2011 23:00	1/1/2012 0:00	6/30/2012 23:00	0.0038	0.0327	-0.0058
399-3-37	24 hours	0.9882872	0.0107625	-4.87E-05	0.100873	4/7/2011 17:00	12/31/2011 23:00	1/1/2012 0:00	6/30/2012 23:00	0.0048	0.0586	0.0053
399-4-11	2 hours	0.9855332	0.0134947	-0.0007932	0.1033099	1/7/2011 8:00	12/31/2011 23:00	1/1/2012 0:00	6/30/2012 23:00	0.0022	0.029	0.0009
399-4-14	24 hours	0.9822817	0.0161837	-0.0003297	0.1619664	1/1/2011 1:00	12/31/2011 23:00	1/1/2012 0:00	6/30/2012 23:00	0.0051	0.0542	0.0002
399-4-7	24 hours	0.9930319	0.0062466	0.0008145	0.0755254	1/7/2011 8:00	12/31/2011 23:00	1/1/2012 0:00	6/30/2012 23:00	0.0096	0.1268	0.0095
399-4-9	24 hours	0.9871292	0.011796	0.0003114	0.113378	1/1/2011 1:00	12/31/2011 23:00	1/1/2012 0:00	6/30/2012 23:00	0.0066	0.0918	0.0353
399-5-1	24 hours	0.9913888	0.0077447	-0.0004584	0.092699	1/1/2011 1:00	12/31/2011 23:00	1/1/2012 0:00	6/30/2012 23:00	0.001	0.0429	0.0247
399-8-1	5 days	0.9926317	0.006409	-0.000169	0.1027467	1/1/2011 1:00	12/31/2011 23:00	1/1/2012 0:00	6/30/2012 23:00	0.0014	0.068	0.0034
399-8-4	12 hours	0.9985252	0.0009384	-1.40E-06	0.0578343	1/6/2011 8:00	12/31/2011 23:00	1/1/2012 0:00	6/30/2012 23:00	0.0006	0.0309	0.0025
399-8-5A	5 days	0.9947811	0.0043502	-0.0004073	0.0936173	1/4/2011 8:00	12/31/2011 23:00	1/1/2012 0:00	6/30/2012 23:00	0.0008	0.0467	0.0031
699-S19-E13	5 days	0.9973586	0.0020645	0.0001681	0.0622372	1/5/2011 8:00	12/31/2011 23:00	1/1/2012 0:00	6/30/2012 23:00	0.0019	0.0977	-0.0012
699-S19-E14	24 hours	0.996805	0.002594	0.0001576	0.0649323	1/4/2011 8:00	12/31/2011 23:00	1/1/2012 0:00	6/30/2012 23:00	0.0049	0.0971	0.0048
699-S20-E10	24 hours	0.9984036	0.0012576	-0.0001241	0.0369968	1/6/2011 8:00	12/31/2011 23:00	1/1/2012 0:00	6/30/2012 23:00	0.0006	0.0152	-0.0044
699-S22-E9A	2 days	0.9983307	0.0010717	-0.000142	0.0646484	2/28/2011 2:00	12/31/2011 23:00	1/1/2012 0:00	6/30/2012 23:00	0.0006	0.0404	0.0006
699-S27-E12A	2 hours	0.9982112	0.0011375	-6.13E-05	0.0700558	1/6/2011 8:00	12/31/2011 23:00	1/1/2012 0:00	6/30/2012 23:00	0.0008	0.0365	-0.007
699-S27-E14	2 days	0.9895512	0.0094323	0.0002986	0.1069861	1/7/2011 8:00	12/31/2011 23:00	1/1/2012 0:00	6/30/2012 23:00	0.005	0.0892	-0.0031
699-S27-E9A	60 days	0.9993302	0.0001874	3.98E-05	0.0523137	1/1/2011 9:00	12/31/2011 23:00	1/1/2012 0:00	6/30/2012 23:00	0.0005	0.0106	0.0007
699-S29-E11	45 days	0.9991626	0.0003567	1.32E-05	0.0521782	1/1/2011 8:00	12/31/2011 23:00	1/1/2012 0:00	6/30/2012 23:00	0.0004	0.0155	0.0058
699-S29-E13A	2 hours	0.9982744	0.0010317	-6.09E-05	0.074654	1/7/2011 8:00	12/31/2011 23:00	1/1/2012 0:00	6/30/2012 23:00	0.0007	0.0415	-0.004
699-S29-E16A	6 hours	0.9194397	0.0722237	-0.0015173	0.8752821	2/25/2011 8:00	12/1/2011 10:00	12/1/2011 1:00	6/30/2012 23:00	0.008	0.0452	0.0127

Table C.3. Summary information for regular linear regression models used for wells. MA=moving average for river levels at SWS-1. b, c, d are model coefficients in Eq. (C.2) and Eq. (C.3). Fit refers to period used for fitting the model, Pre refers to period of model prediction. By definition, FitBias was zero at all wells. /pic/projects/hanford_300a/QA/scripts/C015_rev1/original/output/mlr_model_info.csv

Well	ModelForm	River_MA_Period	b	c	d	FitBeg	FitEnd	PreBeg	PreEnd	FitMAE	PreMAE	PreBias
399-1-1	MLR	7 days	0.9235713	-0.0277489	8.252831	1/1/2011 0:00	12/31/2011 23:00	1/1/2012 0:00	6/30/2012 23:00	0.0898	0.0859	0.0054
399-1-10A	MLR	10 days	0.9311896	0.0047331	7.437237	1/1/2011 0:00	12/31/2011 23:00	1/1/2012 0:00	6/30/2012 23:00	0.0905	0.1103	-0.0027
399-1-11	MLR	7 days	0.8841879	-0.0912134	12.5078986	1/1/2011 0:00	12/31/2011 23:00	1/1/2012 0:00	6/30/2012 23:00	0.0792	0.065	0.0065
399-1-12	MLR	7 days	0.9228999	-0.0715588	8.3049946	1/1/2011 2:00	12/31/2011 23:00	1/1/2012 0:00	6/30/2012 23:00	0.0866	0.0579	0.0027
399-1-13A	MLR	7 days	0.8954563	-0.1013583	11.2625619	1/1/2011 0:00	12/31/2011 23:00	1/1/2012 0:00	6/30/2012 23:00	0.0761	0.0574	-0.0009
399-1-15	MLR	7 days	0.8597618	-0.1486499	15.187398	1/7/2011 18:00	12/31/2011 23:00	1/1/2012 0:00	6/30/2012 23:00	0.0904	0.0656	0.0002
399-1-17A	MLR	7 days	0.908372	-0.0657755	9.8129146	1/1/2011 0:00	12/31/2011 23:00	1/1/2012 0:00	6/30/2012 23:00	0.0669	0.0584	0.0003
399-1-18A	MLR	5 days	0.8155622	-0.2101281	19.9971478	1/5/2011 18:00	12/31/2011 23:00	1/1/2012 0:00	6/30/2012 23:00	0.1294	0.084	0.0004
399-1-2	MLR	2 days	0.9021416	-0.1521994	10.5370755	1/1/2011 0:00	12/31/2011 23:00	1/1/2012 0:00	6/30/2012 23:00	0.1189	0.1099	0.0014
399-1-21A	SLR	5 days	0.8765769	NA	13.1245087	1/1/2011 0:00	12/31/2011 23:00	1/1/2012 0:00	6/30/2012 23:00	0.0902	0.0795	0.0037
399-1-23	MLR	2 days	0.8701618	-0.0861986	13.8685533	1/1/2011 0:00	12/31/2011 23:00	1/1/2012 0:00	6/30/2012 23:00	0.1122	0.0931	0.004
399-1-32	MLR	7 days	0.9153391	-0.0407441	9.042193	1/1/2011 0:00	12/31/2011 23:00	1/1/2012 0:00	6/30/2012 23:00	0.0684	0.0613	0.0072
399-1-60	MLR	5 days	0.9277784	-0.0947047	7.7199054	4/8/2011 19:00	12/31/2011 23:00	1/1/2012 0:00	6/30/2012 23:00	0.0736	0.0624	-0.0189
399-1-7	MLR	14 days	0.9106442	0.0506739	9.5412283	1/1/2011 0:00	12/31/2011 23:00	1/1/2012 0:00	6/30/2012 23:00	0.1	0.1203	-0.0023
399-2-10	MLR	14 days	0.9055567	0.0488081	10.0146624	1/1/2011 0:00	12/31/2011 23:00	1/1/2012 0:00	6/30/2012 23:00	0.0943	0.1147	0.0003
399-2-1	MLR	7 days	0.9280103	-0.0080519	7.6535613	1/1/2011 2:00	12/31/2011 23:00	1/1/2012 0:00	6/30/2012 23:00	0.0824	0.0833	0.006
399-2-3	MLR	14 days	0.9113006	0.0720869	9.3866568	1/1/2011 2:00	12/31/2011 23:00	1/1/2012 0:00	6/30/2012 23:00	0.1097	0.1283	0.0003
399-2-33	MLR	10 days	0.9172696	0.0040556	8.7833801	4/7/2011 16:00	12/31/2011 23:00	1/1/2012 0:00	6/30/2012 23:00	0.0673	0.091	-0.0006
399-2-5	MLR	10 days	0.9185829	0.0065423	8.6431655	1/1/2011 0:00	12/31/2011 23:00	1/1/2012 0:00	6/30/2012 23:00	0.0799	0.0928	0.0022
399-3-18	MLR	7 days	0.9237991	-0.0056673	8.0878447	1/1/2011 0:00	12/31/2011 23:00	1/1/2012 0:00	6/30/2012 23:00	0.0802	0.0826	0.0019
399-3-20	MLR	3 days	0.9158209	-0.0501039	8.9307862	1/1/2011 0:00	12/31/2011 23:00	1/1/2012 0:00	6/30/2012 23:00	0.0767	0.0506	0.0111
399-3-22	MLR	14 days	0.9036803	0.0598085	10.1719177	1/1/2011 0:00	12/31/2011 23:00	1/1/2012 0:00	6/30/2012 23:00	0.1015	0.1201	-0.0017
399-3-26	MLR	5 days	0.9223608	-0.0627215	8.2797846	12/31/2010 23:00	12/31/2011 23:00	1/1/2012 0:00	6/30/2012 23:00	0.0705	0.0604	0.0003
399-3-34	MLR	5 days	0.9293418	-0.0798341	7.5265224	4/7/2011 18:00	12/31/2011 23:00	1/1/2012 0:00	6/30/2012 23:00	0.0693	0.0508	-0.0306
399-3-37	MLR	10 days	0.9159543	0.0136909	8.9105709	4/7/2011 17:00	12/31/2011 23:00	1/1/2012 0:00	6/30/2012 23:00	0.0699	0.0941	-0.001
399-4-11	MLR	14 days	0.9029631	0.0595954	10.2398865	1/7/2011 18:00	12/31/2011 23:00	1/1/2012 0:00	6/30/2012 23:00	0.0999	0.1181	0.001
399-4-14	MLR	5 days	0.9152343	-0.0268988	8.950866	1/1/2011 0:00	12/31/2011 23:00	1/1/2012 0:00	6/30/2012 23:00	0.075	0.0688	-0.0011
399-4-7	MLR	7 days	0.9338938	0.0196448	6.9288297	1/7/2011 18:00	12/31/2011 23:00	1/1/2012 0:00	6/30/2012 23:00	0.1075	0.1033	0.0019
399-4-9	MLR	7 days	0.923265	0.014573	8.0872014	1/1/2011 0:00	12/31/2011 23:00	1/1/2012 0:00	6/30/2012 23:00	0.0865	0.1021	0.0305
399-5-1	MLR	10 days	0.8830723	-0.0539464	12.4886783	1/1/2011 0:00	12/31/2011 23:00	1/1/2012 0:00	6/30/2012 23:00	0.0612	0.066	0.0224
399-8-1	MLR	10 days	0.8732307	-0.1000158	13.6207449	1/1/2011 0:00	12/31/2011 23:00	1/1/2012 0:00	6/30/2012 23:00	0.0622	0.0546	0.0016
399-8-4	MLR	45 days	0.5593465	-0.0421515	47.3682711	1/6/2011 18:00	12/31/2011 23:00	1/1/2012 0:00	6/30/2012 23:00	0.1011	0.0339	0.0033
399-8-5A	MLR	5 days	0.8104068	-0.2389971	20.4632453	1/4/2011 18:00	12/31/2011 23:00	1/1/2012 0:00	6/30/2012 23:00	0.1399	0.1032	0.0025
699-S19-E13	MLR	24 hours	0.7377491	-0.2809637	28.3701506	1/5/2011 18:00	12/31/2011 23:00	1/1/2012 0:00	6/30/2012 23:00	0.1934	0.1355	0.0019
699-S19-E14	MLR	3 days	0.8086618	-0.2214113	20.7997623	1/4/2011 18:00	12/31/2011 23:00	1/1/2012 0:00	6/30/2012 23:00	0.1466	0.099	0.0008
699-S20-E10	SLR	30 days	0.6314647	NA	39.627548	1/6/2011 18:00	12/31/2011 23:00	1/1/2012 0:00	6/30/2012 23:00	0.1082	0.1055	0.0669
699-S22-E9A	SLR	45 days	0.5474724	NA	48.6826833	2/28/2011 12:00	12/31/2011 23:00	1/1/2012 0:00	6/30/2012 23:00	0.1009	0.0763	0.0763
699-S27-E12A	SLR	21days	0.5559789	NA	47.5932142	1/6/2011 18:00	12/31/2011 23:00	1/1/2012 0:00	6/30/2012 23:00	0.115	0.095	0.0718
699-S27-E14	MLR	5 days	0.9147458	-0.0344208	9.00034	1/7/2011 18:00	12/31/2011 23:00	1/1/2012 0:00	6/30/2012 23:00	0.0728	0.0658	0.0009
699-S27-E9A	SLR	3 days	0.0319743	NA	104.3126824	1/11/2011 9:00	12/31/2011 23:00	1/1/2012 0:00	6/30/2012 23:00	0.1419	0.0994	0.0797
699-S29-E11	SLR	45 days	0.1523635	NA	91.1726824	1/11/2011 18:00	12/31/2011 23:00	1/1/2012 0:00	6/30/2012 23:00	0.1189	0.0837	0.0714
699-S29-E13A	MLR	30 days	0.533396	-0.1200669	50.1141261	1/7/2011 18:00	12/31/2011 23:00	1/1/2012 0:00	6/30/2012 23:00	0.1194	0.0653	-0.0145
699-S29-E16A	MLR	2 days	0.8945275	-0.0110806	11.0745211	2/25/2011 18:00	12/1/2011 0:00	12/1/2011 1:00	6/30/2012 23:00	0.0834	0.0832	-0.0009

Table C.4. Portion of a file containing the complete timeseries for all wells, with time in rows and wells in columns.
/pic/projects/hanford_300a/QA/scripts/C015_rev1/original/output/mlr_all_hourly.csv

Datetime	SWS-1	399-1-1	399-1-10A	399-1-11	399-1-12	399-1-13A	399-1-15	399-1-17A	399-1-18A	...other wells
1/1/2010 0:00	105.107	105.246	105.245	105.301	105.184	105.229	105.357	105.172	105.543	...
1/1/2010 1:00	105.165	105.246	105.245	105.301	105.184	105.229	105.357	105.172	105.543	...
1/1/2010 2:00	105.215	105.246	105.245	105.301	105.184	105.229	105.357	105.172	105.535	...
1/1/2010 3:00	105.231	105.246	105.245	105.301	105.184	105.229	105.357	105.172	105.535	...
1/1/2010 4:00	105.264	105.246	105.254	105.301	105.184	105.229	105.357	105.172	105.535	...
1/1/2010 5:00	105.307	105.246	105.254	105.301	105.184	105.229	105.357	105.172	105.535	...
1/1/2010 6:00	105.36	105.246	105.254	105.301	105.184	105.229	105.357	105.172	105.543	...
1/1/2010 7:00	105.406	105.255	105.254	105.31	105.193	105.238	105.365	105.181	105.543	...
1/1/2010 8:00	105.431	105.255	105.254	105.31	105.193	105.238	105.365	105.181	105.543	...
1/1/2010 9:00	105.422	105.255	105.263	105.31	105.193	105.238	105.365	105.181	105.552	...
1/1/2010 10:00	105.359	105.255	105.263	105.31	105.193	105.238	105.365	105.181	105.552	...
...	...	...	...	...	...	...	...	...	...	...

Table C.5. Portion of a file for each well with time in rows, and water level and flag indicating source of each value in columns. Flag D = data (observed); V = VARX model; M = LR model. These files tell the user exactly where each hour's water level come. (Made-up example).

Datetime	WaterLevel	Flag
1/1/2010 0:00	105.223	M
1/1/2010 1:00	105.223	M
1/1/2010 2:00	105.223	M
1/1/2010 3:00	105.223	M
1/1/2010 4:00	105.223	D
1/1/2010 5:00	105.223	D
1/1/2010 6:00	105.223	V
1/1/2010 7:00	105.233	V
1/1/2010 8:00	105.233	V
1/1/2010 9:00	105.233	V
1/1/2010 10:00	105.233	V
1/1/2010 11:00	105.242	D
1/1/2010 12:00	105.242	D
1/1/2010 13:00	105.242	D
1/1/2010 14:00	105.242	V

Water levels for each well were also plotted with color-coding of the source, with some examples given in Figure C.7a, b, and c.

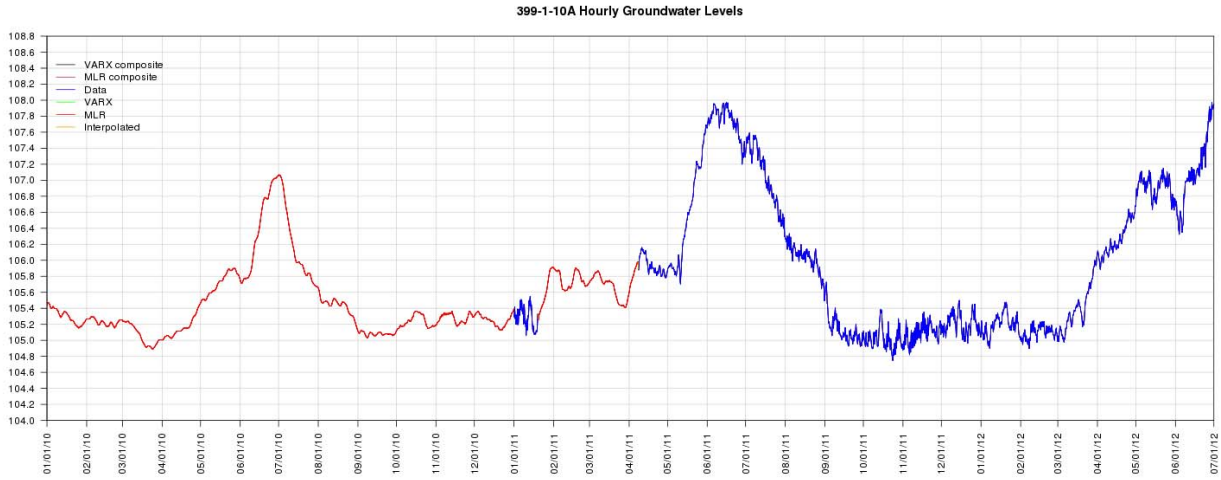

Figure C.7a. Composite hourly groundwater level at 399-1-10A, with line color indicating source of values.
/pic/projects/hanford_300a/QA/scripts/C016_rev1/original/unused/comp2_smooth_399-1-10A.png

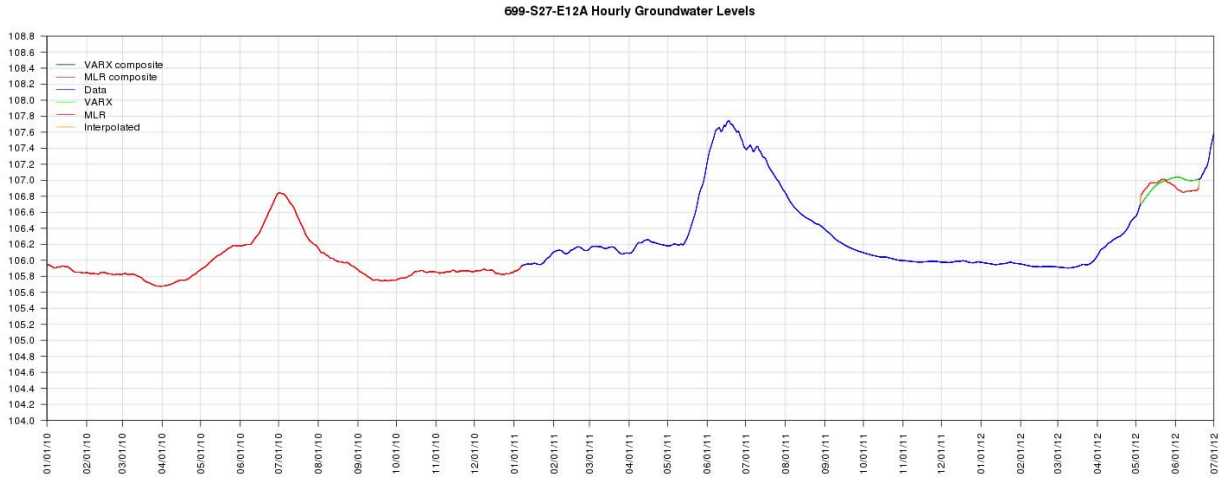

Figure C.7b. Composite hourly groundwater level at 699-S27-E12A, with line color indicating source of values.
/pic/projects/hanford_300a/QA/scripts/C016_rev1/original/unused/comp2_smooth_699-S27-E12A.png

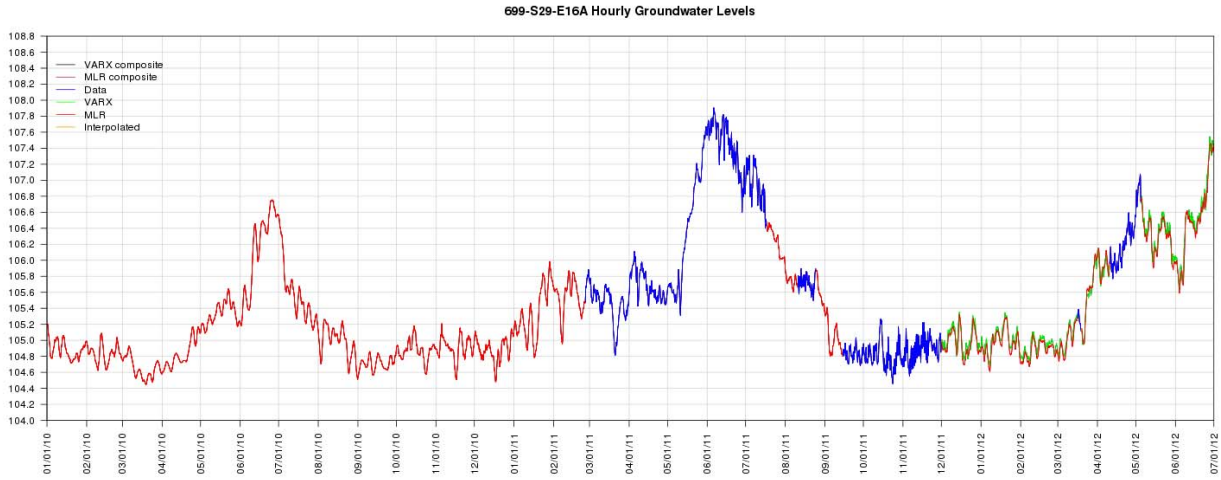

Figure C.7c. Composite hourly groundwater level at 699-S29-E16A, with line color indicating source of values. /pic/projects/hanford_300a/QA/scripts/C016_rev1/original/unused/comp2_smooth_699-S29-E16A.png

Pacific Northwest
NATIONAL LABORATORY

Proudly Operated by **Battelle** *Since 1965*

U.S. DEPARTMENT OF
ENERGY

902 Battelle Boulevard
P.O. Box 999
Richland, WA 99352
1-888-375-PNNL (7665)
www.pnnl.gov